10. TAG-4 AREA[1]

Shipboard Scientific Party[2]

HOLE 957I

Date occupied: 30 October 1994

Date departed: 31 October 1994

Time on hole: 18 hr

Position: 26°8.195′N, 44°49.585′W

Bottom felt (drill-pipe measurement from rig floor, m): 3645.0

Distance between rig floor and sea level (m): 11.72

Water depth (drill-pipe measurement from sea level, m): 3633.3

Total depth (from rig floor, m): 3658.5

Penetration (m): 13.5

Number of cores (including cores having no recovery): 1

Total length of cored section (m): 4.5

Total core recovered (m): 0.77

Core recovery (%): 17.1

Hard rock:
Depth (mbsf): 13.5
Nature: Massive sulfide

Comments: Drilled from 0.0 to 9.0 mbsf

HOLE 957J

Date occupied: 31 October 1994

Date departed: 1 November 1994

Time on hole: 17 hr, 15 min

Position: 26°8.238′N, 44°49.590′W

Bottom felt (drill-pipe measurement from rig floor, m): 3647.0

Distance between rig floor and sea level (m): 11.72

Water depth (drill-pipe measurement from sea level, m): 3635.3

Total depth (from rig floor, m): 3656.0

Penetration (m): 9.0

Number of cores (including cores having no recovery): 1

Total length of cored section (m): 9.0

Total core recovered (m): 0.08

Core recovery (%): 0.9

Hard rock:
Depth (mbsf): 9.0
Nature: Chert

HOLE 957K

Date occupied: 1 November 1994

Date departed: 2 November 1994

Time on hole: 1 day, 8 hr, 30 min

Position: 26°8.239′N, 44°49.583′W

Bottom felt (drill-pipe measurement from rig floor, m): 3644.0

Distance between rig floor and sea level (m): 11.75

Water depth (drill-pipe measurement from sea level, m): 3632.3

Total depth (from rig floor, m): 3664.0

Penetration (m): 20.0

Number of cores (including cores having no recovery): 3

Total length of cored section (m): 20.0

Total core recovered (m): 0.99

Core recovery (%): 5.0

Hard rock:
Depth (mbsf): 20.00
Nature: Massive sulfide

HOLE 957M

Date occupied: 8 November 1994

Date departed: 10 November 1994

Time on hole: 2 days, 7 hr

Position: 26°8.222′N, 44°49.588′W

Bottom felt (drill-pipe measurement from rig floor, m): 3648.0

Distance between rig floor and sea level (m): 11.81

Water depth (drill-pipe measurement from sea level, m): 3636.2

Total depth (from rig floor, m): 3699.2

Penetration (m): 51.2

Number of cores (including cores having no recovery): 10

Total length of cored section (m): 51.2

Total core recovered (m): 6.95

Core recovery (%): 13.6

Hard rock:
Depth (mbsf): 42.3

---

[1]Humphris, S.E., Herzig, P.M., Miller, D.J., et al., 1996. *Proc. ODP, Init. Repts.*, 158: College Station, TX (Ocean Drilling Program).

[2]Shipboard Scientific Party is as given in the list of participants in the contents.

Nature: Massive sulfide, pyrite-silica breccia, and silicified wallrock breccia

Basement:

Depth (mbsf): 51.2

Nature: Sparsely olivine phyric basalt

Principal results: Holes 957I, 957J, 957K, and 957M were drilled on the upper terrace on the western side of the mound (TAG-4). The objectives of drilling at this location were (1) to recover a section through the sulfides and into the stockwork zone in an area of low conductive heat flow (<20 mW/m^2), and (2) to determine the extent of the sulfides and the stockwork on the western side of the deposit. Holes 957I, 957K, and 957M were drilled about 20 m west of the Black Smoker Complex in a water depth of 3645 m. The most complete section was cored at Hole 957M (from 9.3 to 51.2 mbsf) with recovery of 13.6%. Hole 957K was drilled approximately 5–8 m north of Hole 957M; the section down to 20 mbsf was sampled, with recovery of 5.0%. Hole 957I was located 10–15 m west of Hole 957K and drilled to 9 m before coring to 13.5 m with 17% recovery. Hole 957J was located 25 m northeast of Hole 957I in a water depth of 3647 m; only one core was retrieved with 1.0% recovery.

Core recovered from the TAG-4 area indicates that the western side of the upper terrace consists mainly of massive sulfide crusts and sulfide-cemented breccias. In addition, significantly higher amounts of sphalerite, marcasite, and amorphous silica were found in this area than in samples drilled elsewhere on the mound. Anhydrite is virtually absent from the TAG-4 cores. The upper 10 m of the mound consists of porous colloform pyrite + marcasite with red and gray chert; a 10-m-thick zone of massive pyrite and massive pyrite breccia with minor sphalerite and a few altered basalt clasts occurs below this. Between 20 and 30 mbsf, massive pyrite grades downward into pyrite-silica breccia, in which larger, silicified wallrock fragments (up to 10 cm) are abundant. Silicified wallrock breccias are the dominant lithology between 30 and 42 mbsf, followed by an abrupt transition into slightly to moderately altered basalt, which was drilled down to 51.2 mbsf.

In the top of Hole 957M, fine- to coarse-grained, red-brown and orange Fe-oxides and minor pyrite and silica were recovered as drill cuttings. Geochemical analyses of this material indicate high Fe contents (up to 52.4 wt%), but low S (4.7 wt%), Cu (up to 0.29 wt%), and Zn (0.28 wt%) concentrations compared with near-surface drill cuttings recovered from the TAG-2 area, indicative of the higher abundance of Fe-oxides and Fe-oxyhydroxides at the TAG-4 location.

The dominant rock type in the upper 10 m of the section is porous massive pyrite, which consists of variable proportions of pyrite + marcasite with colloform-banded textures and a coarse vuggy porosity. The colloform texture commonly encloses zones of massive fine-grained pyrite and marcasite, or grades into dark gray pyrite-silica. Minor chalcopyrite occurs as 1- to 3-mm aggregates associated with silica-rich zones. Minor amounts of sphalerite are intergrown with pyrite and marcasite and are also present as overgrowths on the colloform pyrite. Geochemical analyses of four samples indicate high Fe (38.4–45.7 wt%) and S (41.0–50.8 wt%) contents. Concentrations of Zn range from 3.0 to 3.7 wt%, among the highest values determined, whereas Cu contents are only 0.05–0.13 wt%. The upper 10 m of core from Holes 957J, 957K, and 957M also contain clasts of red and gray chert, which consist of dark red Fe-oxides intimately intergrown with silica. These clasts are similar to those observed in the uppermost hard layer at the TAG-2 and TAG-3 areas.

Between 10 and 20 mbsf, porous massive pyrite and massive granular pyrite occur in Hole 957K and 957M. Massive granular pyrite consists almost entirely of granular aggregates of fine-grained pyrite with abundant colloform texture. Chalcopyrite is rare; sphalerite occurs as a vug lining. This rock type may have formed by recrystallization of the porous massive marcasite + pyrite, but it also incorporates pyritized silicified wallrock fragments.

The lithology in the TAG-4 area grades down into pyrite-silica breccia containing numerous silicified wallrock fragments, which increase in abundance and size between 30 and 40 mbsf until they comprise more than 50 vol% of the rock. The pyrite-silica breccias are matrix supported and consist of assemblages of different clasts derived from surface hydrothermal processes (e.g., cherts) and subsurface alteration processes (e.g., silicified wallrock) in a dark gray pyrite-silica matrix. Two textural subtypes of pyrite-silica breccias, which occur over similar depth intervals, can be distinguished. Fine-grained pyrite-silica breccias are composed of well-sorted, rounded to subrounded, fine-grained (<10 mm) pyrite; light gray silicified wallrock; and gray quartz clasts in a dark gray silica-pyrite matrix. Pyrite clasts are often brecciated. Quartz clasts contain disseminated euhedral pyrite. Fine-grained chalcopyrite aggregates (up to 3 mm in diameter) occur. In general, fine-grained pyrite-silica breccias have a low porosity (<5%) and resemble those recovered from Holes 957C, 957F, and 957H on the eastern side of the mound. Coarse-grained pyrite-silica breccias contain clasts of the fine-grained pyrite-silica breccia intergrown with massive pyrite clasts (3–15 mm) and pale gray pyrite-silica clasts (as large as 2.5 cm), both commonly rimmed by pyrite. Late marcasite and pyrite line vugs. The dominant clast type in these samples consists of pale gray silica with disseminated pyrite, which appears to have been derived from silicified wallrock material. Coarse-grained pyrite-silica breccias commonly have a higher, vuggy porosity (10%–20%).

Between 30 and 42 mbsf, silicified wallrock breccias resemble those in the upper part of the quartz-rich stockwork in the TAG-1 and TAG-2 areas, but these are generally softer, have greater porosity, lack significant quartz veining, and contain greater quantities of massive pyrite. The breccias consist of angular to subrounded clasts of variably silicified and highly altered basalt enclosed in a matrix of pyrite-silica breccia or porous massive pyrite. The clasts are generally hard and silicified, and contain abundant pyrite disseminated in the matrix. The buff to gray color of the groundmass suggests replacement by chlorite. The siliceous wallrock breccias are cut by several generations of quartz and pyrite veins. A few pieces of chloritized basalt breccia occur below 34 mbsf, where they are gradational from the silicified wallrock breccias, and where silicification of the altered basalt material is less intensive.

Below 42 mbsf, the silicified wallrock and chloritized basalt breccias are underlain by slightly to moderately altered (~20%) basalts having chloritized alteration halos. These basalts are mostly dark gray, but some have <1-mm red Fe-oxide/oxyhydroxide coatings on their outer surfaces or display various combinations of 1- to 5-mm-wide red, black, or green chloritized alteration halos around central portions of dark gray basalt. Veins of quartz, chlorite, and pyrite are also present in these rocks. These sparsely olivine phyric basalts are fragments of pillow basalts, as several of the pieces are rimmed with glassy rinds or are holohyaline. Textures range from intergranular to subvariolitic and variolitic. Olivine is partly altered to colorless to pale green to tan smectite, rarely with small amounts of accompanying red iron oxyhydroxide. The groundmass is composed of microcrystalline to cryptocrystalline plagioclase, clinopyroxene, small interstices of variably altered glass, and granular fine-grained titanomagnetite. Vesicles are filled with a light green smectite. Small (10 µm) veinlets of tan smectite are also present in some samples. Disseminated pyrite is common, and chalcopyrite rare, both occurring as 1- to 20-µm grains and rare globules in interstitial areas, along micrometer-sized fractures, and rarely lining vesicles. The XRF analyses of one sample indicate that it is virtually identical to the basalt analyzed from Hole 957B; it has a Mg# of 60.8 and contains 1.67 wt% TiO_2 and 2.42 wt% Na_2O.

Physical properties measurements on sulfides from the TAG-5 area indicate that the porous massive pyrites exhibit a narrow range of high values of bulk density (4.34–4.50 g/cm^3), combined with high values of porosity (8.22–11.53%). Pyrite-silica breccias have lower bulk densities (3.46–4.38 g/cm^3), which are similar to those of silicified wallrock breccias (3.51–4.65 g/cm^3). Porosities for these two rock types range from 2.86 to 9.09%. The slightly altered basalts have typical bulk densities of 2.88–2.90 g/cm^3, porosities of <2%, and compressional (*P*-wave) velocities of 6.09–6.13 km/s.

Paleomagnetic measurements were conducted on two basalt samples and indicated NRM intensities (~4×10^3 mA/m) much stronger than those typical of oceanic basalts. Based on the magnetic behavior during AF demagnetization, the magnetic carrier is speculated to be titanomagnetite. The stable component of magnetization for both samples has a much shal-

Table 1. Distribution of dominant lithologies in core from the TAG-4 area..

Dominant lithology	Intervals recovered		Approximate location: Top (mbsf)	Approximate location: Bottom (mbsf)	Estimated total thickness (m)
Porous, massive pyrite (Type 5) with red and gray chert	158-957J-1X-1	(0–0.2 m)	0	0.2	1
	158-957K-1X-1	(0–0.5 m)	0	0.5	
	158-957M-1R-1	(0–0.5 m)	0	0.9	
Massive, porous pyrite ± sphalerite (Type 5)	158-957I-1N-1	(0–0.7 m)	9.0	9.7	10
	158-957K-1N-1	(0–0.5 m)	10.0	10.5	
	158-957M-2R-1	(0–0.5 m)	9.3	9.8	
Massive pyrite breccias (Type 6), pyrite-silica breccias (Type 9), and silicified basalt clasts	158-957K-3X-1	(0–0.4 m)	14.5	14.9	10
	158-957M-3R-1	(0–1.5 m)	14.3	15.8	
	158-957M-3R-2	(0–0.2 m)	15.8	16.0	
	158-957M-4R-1	(0–0.6 m)	19.3	19.9	
Pyrite-silica breccias (Type 9) with coarse wallrock fragments	158-957M-5R-1	(0–1.1 m)	24.3	25.4	10
	158-957M-6R-1	(0–0.4 m)	29.3	29.7	
Silicified wallrock breccias (Type 10a) with porous pyrite	158-957M-7R-1	(0–0.3 m)	34.3	34.6	12
	158-957M-8R-1	(0–0.4 m)	38.3	38.7	
	158-957M-9R-1	(0–0.2 m)	42.3	42.5	
Moderately altered basalt with chloritized halos	158-957M-9R-1	(0.2–1.2 m)	42.5	43.5	—
	158-957M-10R-1	(0–1.5 m)	43.5	46.2	
	158-957M-10R-2	(0–0.4 m)	46.2	46.6	

lower inclination (14°) compared with the expected inclination (55°) at this site, suggesting that the magnetization is unlikely to have been acquired during cooling of the basalt but may be related to the pervasive hydrothermal alteration that has affected the TAG hydrothermal mound.

STRATIGRAPHY

Introduction

In the TAG-4 area, Holes 957I, 957J, 957K, and 957M are located at a water depth of 3645–3655 m on the upper terrace of the mound about 5–25 m west of the Black Smoker Complex. Hole 957I is at the edge of the mound, and Holes 957K and 957M are about 10 m closer to the Black Smoker Complex. Hole 957J is located about 25 m to the northeast of Hole 957K. The most complete section of stratigraphy through this part of the mound was cored in Hole 957M (0–51 mbsf), with a recovery of 13.6%. Core 158-957J-1X was a surface core, and Holes 957I and 957K were cored to depths of 10 and 15 m with recoveries of 17% and 5%, respectively. A combined graphic log of the most complete core sections is shown in Figure 1, and Table 1 lists the different rock types and their distribution in each core. For more detailed descriptions of the rock types in the TAG-4 area, see the "Sulfide Petrology and Geochemistry" section (this chapter).

Distribution of Lithologies

The upper 10 m of the mound in the TAG-4 area consists of porous, colloform, massive pyrite + marcasite with red and gray chert. This material overlies a 10-m-thick zone of massive pyrite and massive pyrite breccias, with minor sphalerite, to a depth of 20 mbsf. Massive pyrite grades downward into pyrite-silica breccia between about 20 and 30 mbsf. A few altered basalt clasts occur in the massive pyrite breccias between 0 and 20 mbsf, and larger, silicified wallrock fragments (up to 10 cm) are abundant in the pyrite-silica breccias below about 20 mbsf. Silicified wallrock breccias are the dominant lithology between 30 and 42 mbsf; these rocks may be in contact with relatively fresh basalt recovered between 42 and 51 mbsf. In general, the breccias in the TAG-4 area are more heterogeneous and coarse grained than similar breccias from the TAG-2 area on the east side of the mound. Colloform massive pyrite is common as cement within the TAG-4 breccias, but anhydrite is notably absent.

Drill cuttings from the top of the mound in Section 158-957M-1R-1 contain abundant Fe-oxides, resembling the surface material recovered in the TAG-2 area (see Section 158-957B-1R-1). The first

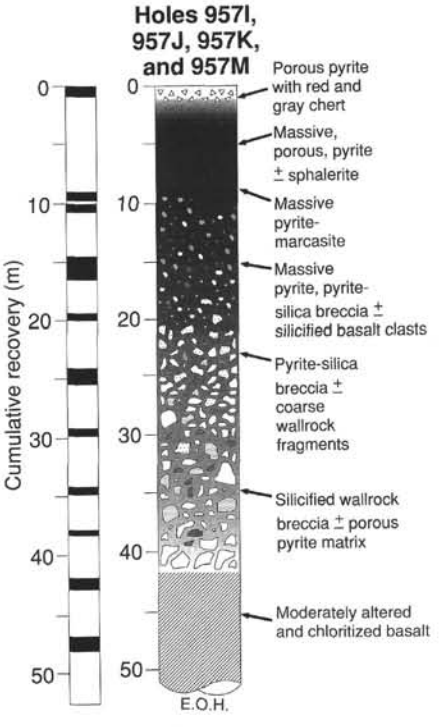

Figure 1. Schematic stratigraphic section of the mound in the TAG-4 area, showing the distribution of principal rock types in cores from Holes 957I, 957J, 957K, and 957M.

few meters of core from Holes 957J, 957K, and 957M also contain abundant clasts of red and gray chert, similar to those observed in the uppermost hard layer of the TAG-2 area. However, chert clasts are less common at depth in the TAG-4 area than in the TAG-2 and TAG-3 areas of the mound. The massive sulfides, which make up the upper 10 m of the mound, consist of colloform-banded, pyrite-marcasite crusts, exhibiting primary depositional textures and high porosity. Fine- to medium-grained, colloform pyrite is locally replaced by chalcopyrite but shows limited recrystallization. Sphalerite is present as overgrowths on the colloform pyrite and filling late cavities, and also occurs with marcasite in network-like veins (up to 0.5 cm wide)

cutting through the massive pyrite. Below about 10 mbsf, wallrock fragments and patches of pyrite-silica breccia occur within the massive pyrite; between 10 and 20 mbsf, the bulk of the massive sulfide section consists of pyrite-silica breccias cemented by porous pyrite. Below 20 mbsf, the breccias contain numerous silicified wallrock fragments, and these clasts increase in size and abundance between 30 and 40 mbsf, where they make up more than 50% of the rock by volume. Chloritized basalt fragments are also present locally in the core between 35 and 40 mbsf. The lowermost portion of Hole 957M (43–51.2 mbsf) consists of moderately altered basalt having chloritized alteration halos and containing veins of quartz + sulfides.

The coarse, silicified wallrock breccias in this part of the mound resemble the upper part of the quartz-rich stockwork in the TAG-1 area, but they have substantially greater porosity, lack significant quartz veining, and contain greater quantities of massive pyrite. Large open cavities or vugs (up to 1 cm) between the clasts are commonly lined by coarse, euhedral pyrite, and porous massive pyrite typically cements the coarser wallrock fragments. In general, the breccias are framework supported, and neighboring clasts cannot be pieced together, suggesting that the brecciation did not occur in situ.

Porous, colloform pyrite, semi-massive pyrite, and quartz-pyrite veins are abundant in the silicified wallrock breccias, and account for 30%–40% of the rock by volume to a depth of at least 42 mbsf. In Hole 957M, massive porous and granular pyrite was recovered from immediately above the basaltic basement. Numerous fragments of red chert and quartz also occur in the lowermost part of the core, from about 35 to 46 mbsf, in the silicified wallrock breccias as well as in the underlying basalt breccias. These may be discrete clasts or partially replaced remnants of interpillow chert.

Veining

Quartz-pyrite veining occurs only locally at depth, mainly below 25 mbsf and primarily in the silicified wallrock breccias. Pyrite-only veins are common higher up in the core and within large wallrock fragments in the underlying breccias. Anhydrite is virtually absent in both the matrix and as veins, suggesting that high-temperature upflow has not occurred recently in the TAG-4 area.

Mineralization

Pyrite is abundant throughout the entire cored section in the TAG-4 area. The upper 10–15 m of the mound consists of 80–100 vol% pyrite-marcasite, decreasing to about 50–60 vol% in the pyrite-silica breccias, and to 30–40 vol% in the silicified wallrock breccias. Chalcopyrite occurs locally in the upper 15 m of the mound, replacing early-formed colloform pyrite-marcasite. Sphalerite occurs mainly in the upper 5–10 m, but it also is present locally down to 15 mbsf. In contrast to the massive sulfide sections in the TAG-1 and TAG-2 areas, where most of the pyrite occurs as breccias, much of the pyrite at TAG-4 appears to have been precipitated in situ as massive crusts in the uppermost 10 m or as cement in the underlying wallrock breccias. On average, the core from this section of the mound contains almost twice as much pyrite as core from the same interval in the nearby TAG-1 area.

Drill cuttings from the surface in the TAG-4 area are distinctly metal poor in comparison to similar cores from the TAG-2 area (see Core 957B-1R-1). Samples of porous and colloform, massive pyrite from the upper 15 m of the mound average close to 3 wt% Zn, but have low Cu contents (<0.05 wt%). Samples of pyrite-silica breccias between 15 and 25 mbsf average close to 1 wt% Zn, but these breccias contain somewhat higher Cu (1.3 wt%) than in the massive pyrite higher up in the core. A sample of massive pyrite cement in the silicified wallrock breccias near the base of the mound contains nearly 2 wt% Cu and 1 wt% Zn (see "Sulfide Petrology and Geochemistry" section, this chapter).

Interpretation

Core recovered from the TAG-4 area indicates that the western side of the upper terrace consists mainly of massive sulfide crusts and sulfide-cemented breccias. Although abundant wallrock clasts were recovered, the framework-supported nature of the breccias, the absence of pervasive quartz and anhydrite cement, and the presence of relatively unaltered basaltic basement at the bottom of Hole 957M suggest that this is not part of the high-temperature stockwork. Measured from the basalt basement, breccias containing abundant silicified wallrock fragments are at least 20 m thick and are capped by a 10- to 15-m-thick carapace of massive pyrite. The fact that altered basalt clasts occur 20 m shallower at TAG-4 than elsewhere on the mound is puzzling, but it may indicate that there could have been a local basement high. The massive sulfide carapace on top of the breccias may either be an in situ hydrothermal precipitate, composed mainly of porous and colloform pyrite-marcasite crusts, or primary precipitates that originate from the Black Smoker Complex. This is in contrast to the uppermost part of the mound in the TAG-2 area, which is composed mainly of sulfide debris. In addition, the breccias in the TAG-4 area are generally more heterogeneous and coarser grained than similar breccias from the TAG-2 area, suggesting a more complex history at TAG-4.

Thus, the outer margin of the stockwork zone on the western side of the mound is somewhere between Hole 957M and the Black Smoker Complex, and within about 5–10 m of the present high-temperature upflow. Despite their proximity to the present Black Smoker Complex, the wallrock breccias in the TAG-4 area are less extensively veined by quartz and lack anhydrite veins. Abundant colloform pyrite and late-stage sphalerite in cavities and veins suggest that low-temperature upflow, possibly originating from beneath the present Black Smoker Complex, has occurred through the flanks of the mound and was likely responsible for cementing breccias in the TAG-4 area and for deposition of the carapace of massive sulfide on top of the breccias. The low Cu contents of the sulfides are also consistent with little or no high-temperature venting through the talus pile at the edge of the mound.

The recovery of massive pyrite and slightly altered basalt in the same section suggests that a sharp contact is present between hydrothermally altered and mineralized material and the underlying basement. The large, rounded clasts of silicified wallrock at the base of the cored section appear to sit directly on top of slightly altered basalt, suggesting that alteration of the breccias occurred before their emplacement. This altered talus may have been derived from preexisting altered and mineralized pillows beneath the present mound or could have been eroded from an exposed part of the stockwork during an earlier stage in its development. The presence of chloritized alteration halos and quartz + pyrite veins in otherwise slightly altered basalt below 43 mbsf, however, indicates that hydrothermal fluids ($T > 200°C$) circulated beneath the margins of the mound. The current position of the high-temperature upflow zone suggests that the Black Smoker Complex may have developed either at the margins of a brecciated massive flow or at the top of a partially eroded fault scarp. The presence of mineralized clasts with different degrees of alteration in the same section (e.g., chloritized fragments together with quartz-rich, mineralized clasts) is consistent with derivation of the talus breccias from a faulted portion of the stockwork.

SULFIDE PETROLOGY AND GEOCHEMISTRY

Introduction

Holes 957I, 957J, 957K and 957M were drilled on the western side of the mound (TAG-4 area; see Fig. 3, Chapter 1, this volume). Hole 957I is located 30 m west of the Black Smoker Complex at a water depth of 3645 m; it was drilled to a depth of 9 mbsf and then

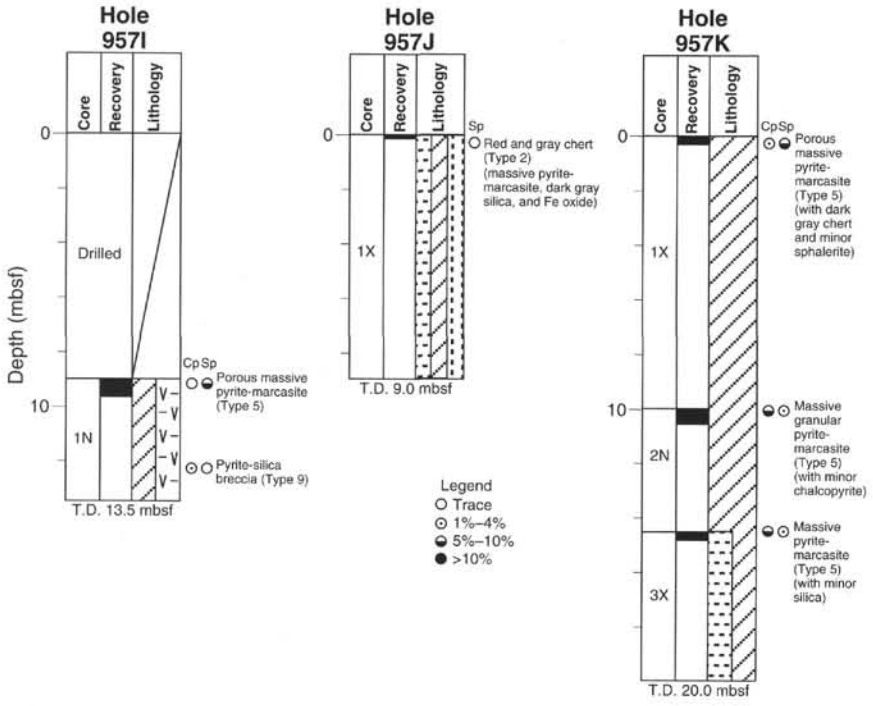

Figure 2. Schematic stratigraphic section through Holes 957I, 957J, and 957K. Cp = chalcopyrite, and Sp = sphalerite. T.D. = total depth.

cored to 13.5 mbsf. One core was recovered. Hole 957J is located 25 m northeast of Hole 957I between Markers C and F at a water depth of 3647 m; it was cored to 9 mbsf. Hole 957K is located approximately 10 m east of Hole 957I closer to the Black Smoker Complex at a water depth of 3644 m. Three cores (0–10, 10–14.5, and 14.5–20 mbsf) were recovered from Hole 957K. Hole 957M is located approximately 5 m south of Hole 957K in a water depth of 3648 m and was cored to a depth of 51.2 mbsf. Ten RCB cores were recovered.

Holes 957I, 957J, and 957K

Visual Core Description

A listing of the visual core descriptions for all three holes is given in Table 2 (in back pocket), and a schematic section of the holes is illustrated in Figure 2. The rock types recovered in these holes are gray and red chert (Type 2), massive pyrite (Type 5), porous massive pyrite (Type 5a), massive granular pyrite (Type 5c), and pyrite-silica breccia (Type 9a).

Pieces of gray and red chert were recovered in Section 158-957J-1N-1 (0–9 mbsf), together with very small rollers of more pyrite-rich material. Porous massive pyrite dominates from 0 to 10 mbsf in core from Hole 957K (Section 158-957K-1X-1) and from 9 to 13.5 mbsf in core from Hole 957I (Section 158-957I-1N-1). Three pieces of pyrite-silica breccia were recovered in Section 158-957I-1N-1. Massive granular pyrite and massive pyrite were recovered from 10 to 20 mbsf in Hole 957K (Sections 158-957K-2N-1 and 3X-1).

Gray and Red Chert (Type 2)

One sample of this type was recovered from 0 to 9 mbsf in Core 158-957J-1N (Fig. 3). It consists of massive Fe-oxide-bearing silica (red chert) surrounded by gray cherty material. The contacts between red and gray chert are irregular, sharp, or gradational. Pyrite is rare in the red chert, but it is more abundant in the gray chert. Pyrite occurs as fine-grained, disseminated, euhedral grains and as colloform layers in cavities. In general, areas of red chert are less porous than gray chert. In thin section, the red chert consists of Fe-oxides, minor chalcedony, and a bright yellow fibrous clay mineral. Hematite is fine

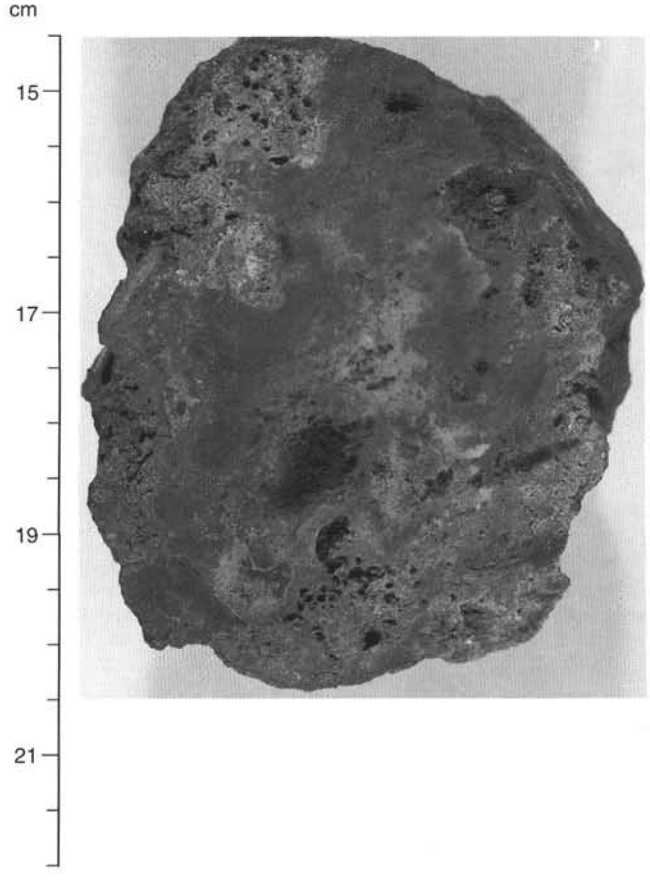

Figure 3. Red and gray chert (Type 2) composed of very fine-grained, low-porosity, red chert with gradational to sharp contacts to more porous gray chert. Pyrite is disseminated in the gray chert or lines cavities in the red and gray chert. Sample 158-957J-1X-1 (Piece 3, 14.5–22.0 cm).

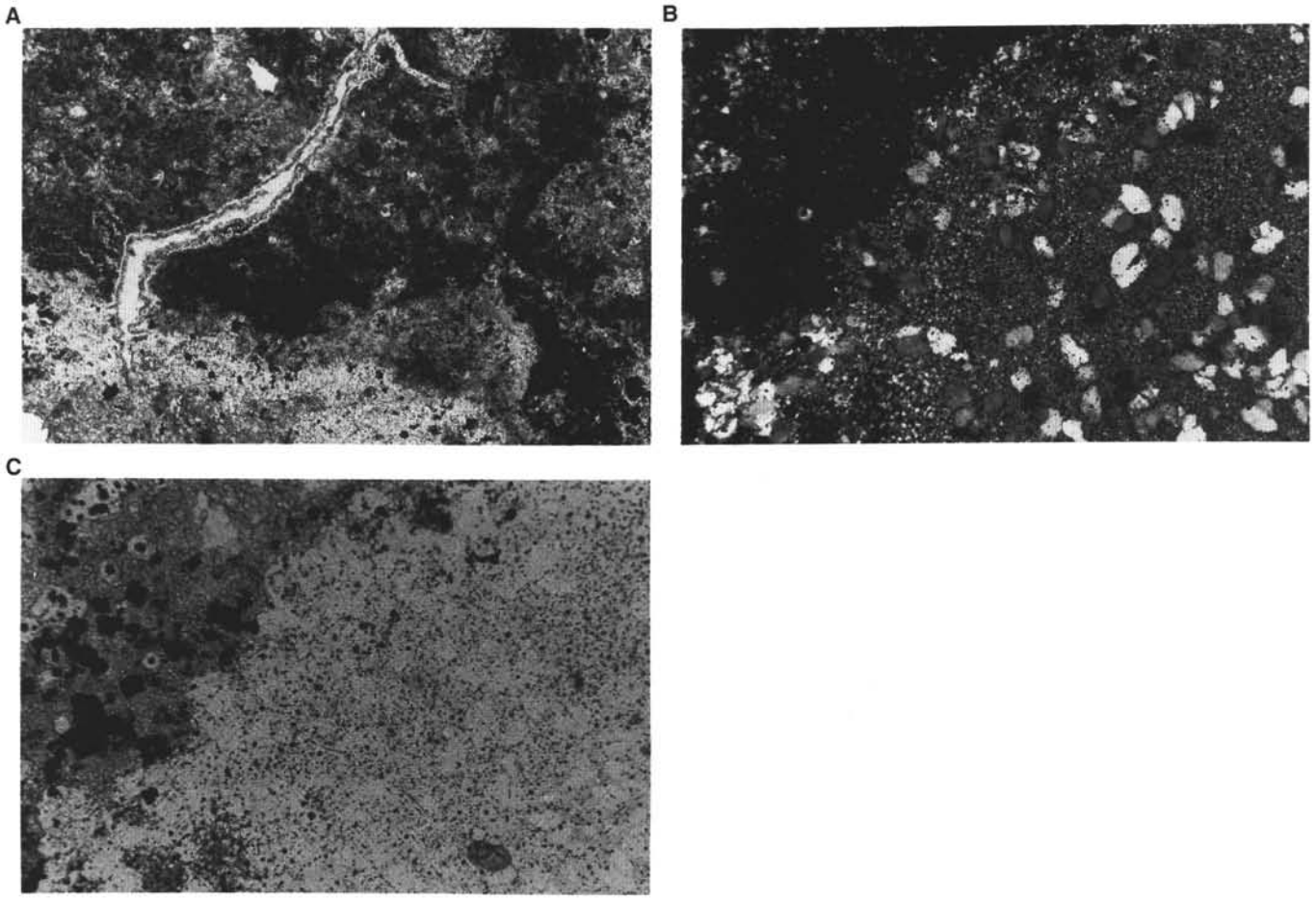

Figure 4. Photomicrographs of red and gray chert. Sample 158-957J-1X-1 (Piece 3, thin section from 15.0 to 17.0 cm). **A.** Chalcedony with disseminated pyrite (black) and Fe-oxides (gray, mottled), cut by a fracture lined by late amorphous silica (white). Transmitted light, field of view = 6 mm. **B.** Chalcedony, with subhedral quartz grains. The dark zone (left) is dominantly amorphous silica. Transmitted light (crossed nicols), field of view = 1.5 mm. **C.** Same view in plane polarized light, showing fine disseminated pyrite, with coarser pyrite associated with globular amorphous silica (darker gray). Transmitted light (crossed nicols), field of view = 1.5 mm.

grained or occurs as aggregates disseminated in red chert and could represent the product of amorphous Fe-oxide recrystallization. Small fractures that are lined with amorphous silica cut the red chert, but they are not well developed in the gray chert (Fig. 4A). Chalcedony and quartz were observed in the gray chert, and the preservation of spheroidal textures in chalcedony suggests recrystallization of amorphous silica to chalcedony. Coarse-grained euhedral quartz is disseminated in a very fine-grained matrix of chalcedony (Fig. 4B, C). Pyrite occurs as disseminated euhedral grains in areas of gray chert or as polycrystalline aggregates at contacts between red and gray chert. Fine-grained pyrite grains are dominantly euhedral, whereas larger grains are often corroded and partly replaced by silica. Anhedral marcasite inclusions occur in the pyrite. Trace sphalerite occurs as inclusions in the pyrite and as euhedral crystals in the gray chert. Late, amorphous silica is overgrowing chalcedony and quartz in the gray chert. Quartz and chalcedony contain inclusions of Fe-oxides and/or euhedral pyrite.

Massive Pyrite (Type 5)

Three different types of massive pyrite were distinguished according to their textural appearance. Pyrite textures are either porous, granular, or massive. In most samples, the porosity is similar (10% or higher by visual estimate).

Porous massive pyrite (Type 5a) is abundant from 9 to 13.5 mbsf in Hole 957I and consists almost entirely of pyrite and marcasite, often with colloform textures and with only traces of chalcopyrite. The samples are partly coated by a thin layer of yellow-orange Fe-oxides and/or Fe-oxyhydroxides. Sample 158-957I-1N-1 (Piece 1) exhibits a network of massive pyrite veins in a porous pyritic matrix, suggesting fluid channelways (Fig. 5). Porous massive pyrite samples from Hole 957K contain disseminated siliceous material and dark gray to black chert cut by pyrite and marcasite veins (Fig. 6). The silica content for all material recovered in Core 158-957K-1X was averaged visually to be 10 vol%, but locally runs as high as 65 vol% in Sample 158-957K-1X-1 (Piece 2). A light to dark brown sphalerite vein (2 mm wide) also occurs in this sample (Fig. 7). Microscopically, porous pyrite samples show multiple generations of pyrite and marcasite intergrowths. Early assemblages consist of several generations of colloform porous pyrite often separated by fine-grained sphalerite (Fig. 8). The colloform pyrite in Sample 158-957K-1X-1 (Piece 4) forms regular, inclusion-rich spherules in a coarser grained marcasite and pyrite matrix. Early pyrite is overgrown by fine-grained, banded marcasite and pyrite in which marcasite is dominant. Late, coarse-grained marcasite and pyrite bands line the fine-grained assemblage. Repeated, alternating overgrowths of coarse- and fine-grained pyrite and marcasite assemblages are present. The grain size and pyrite content seem to increase with time within each successive cycle. The

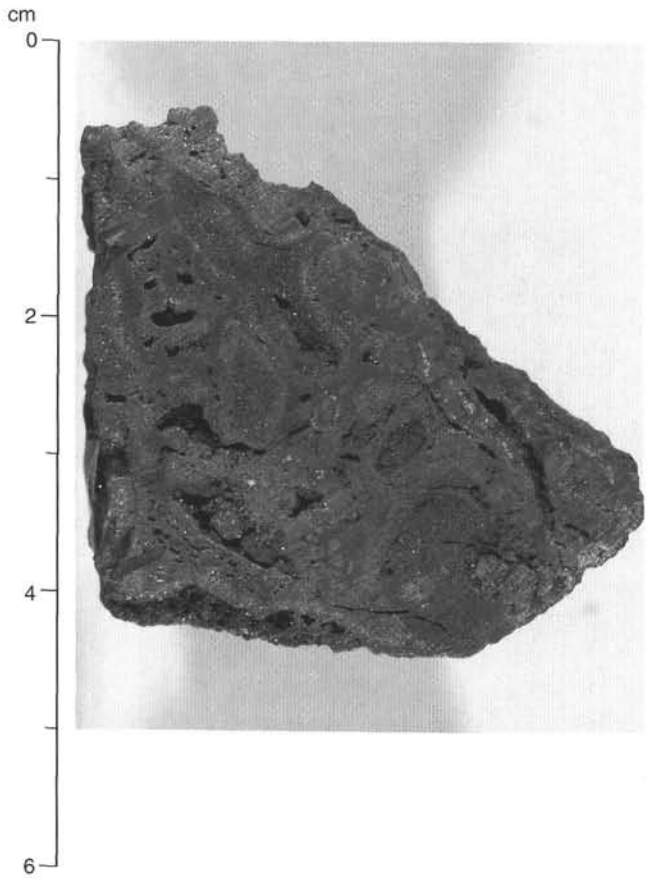

Figure 5. Porous massive pyrite (Type 5a) with massive colloform pyrite and marcasite veinlets that cut across more porous pyrite + marcasite. Vugs are lined by euhedral pyrite. Marcasite, identified in thin section, comprises up to 50% of the sample. Sample 158-957I-1N-1 (Piece 1, 0–6 cm).

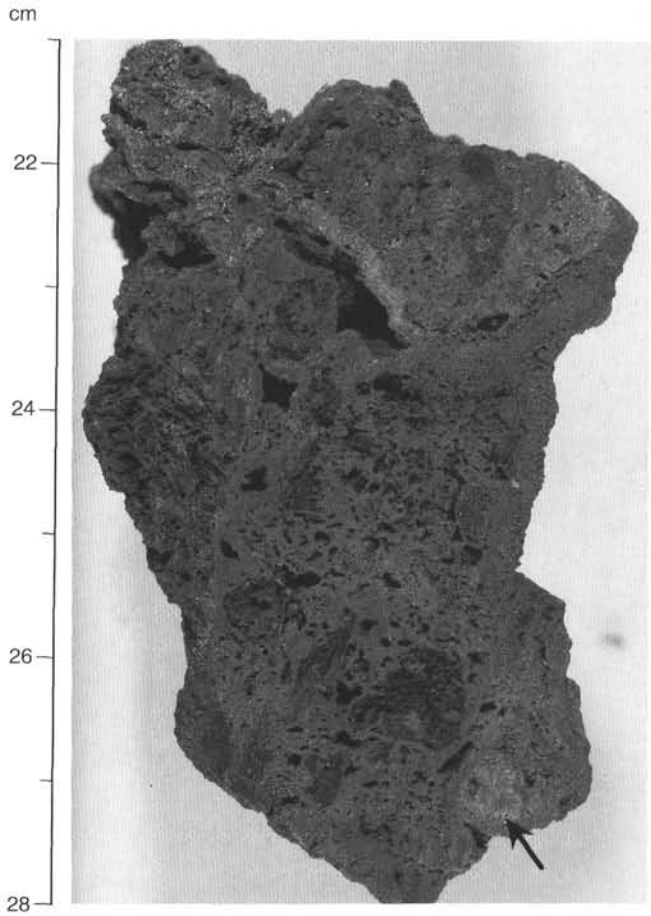

Figure 6. Porous massive pyrite (Type 5a) typical for the upper part of Hole 957K (0–9 mbsf). This porous massive pyrite sample consists of porous pyrite clasts (dark) and gray chert (arrow) cut by more massive pyrite and marcasite veins. Sample 158-957K-1X-1 (Piece 4, 21–28 cm).

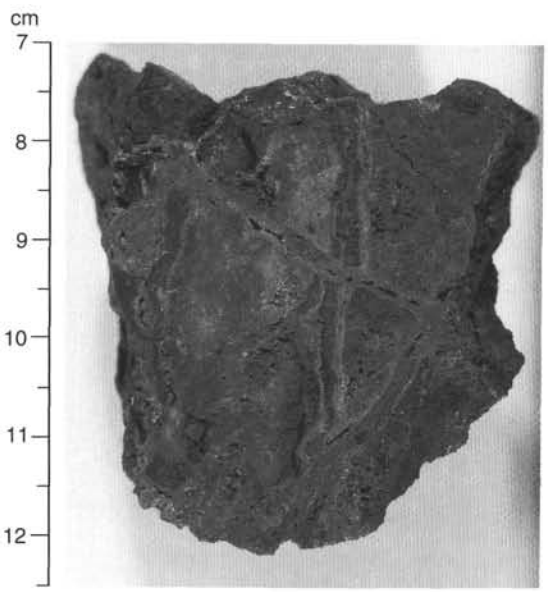

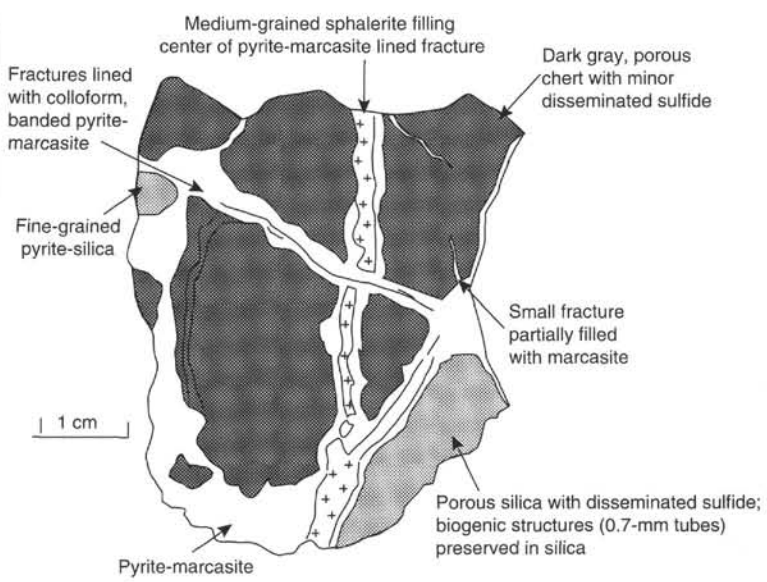

Figure 7. Photograph and sketch of a chert-rich sample of porous massive pyrite (Type 5a) with black chert clasts cut by a sphalerite vein and later by pyrite and marcasite veins. Sample 158-957K-1X-1 (Piece 2, 7–10 cm).

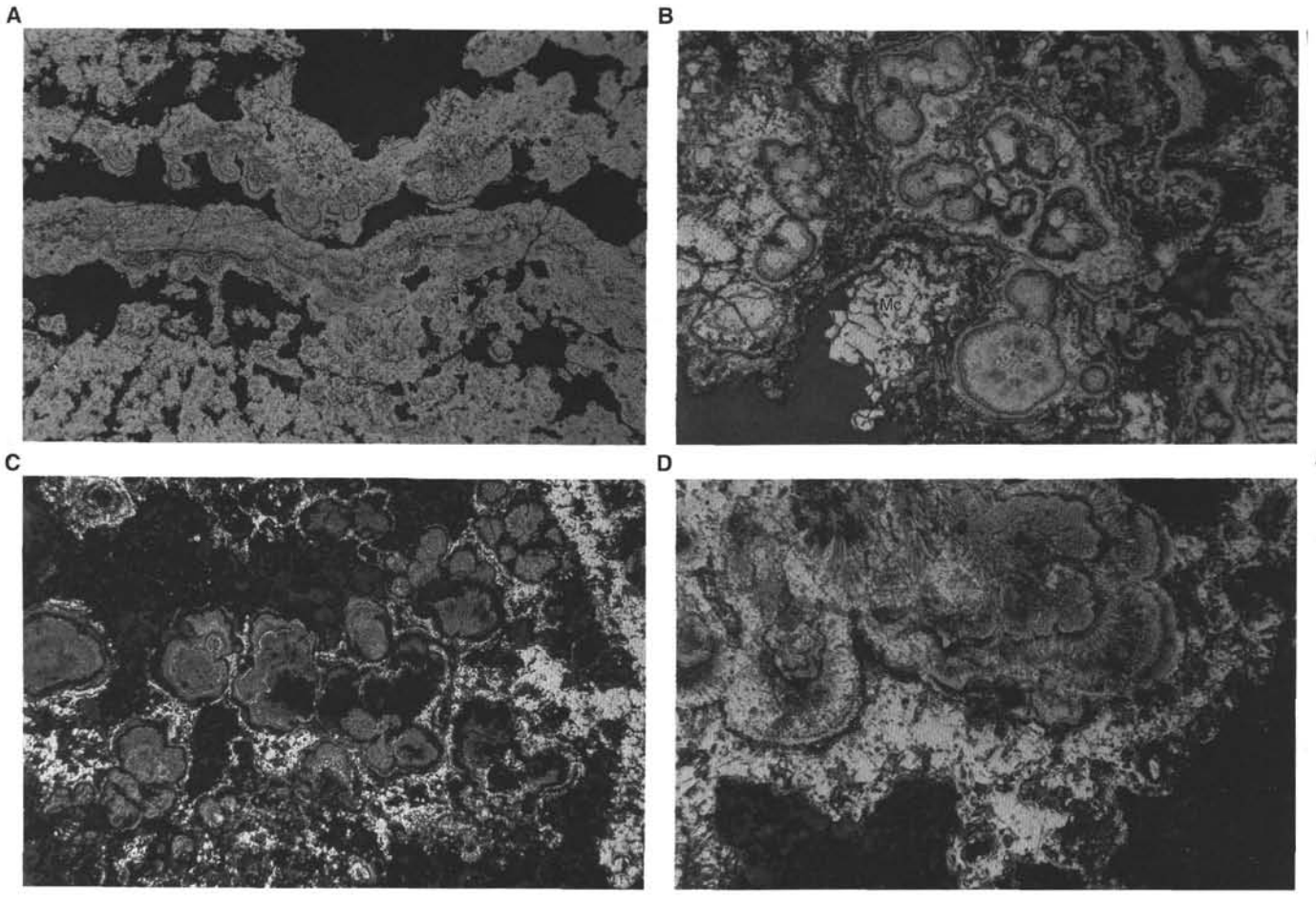

Figure 8. Thin-section photomicrographs of porous massive pyrite and marcasite. **A.** Porous, colloform-banded pyrite-marcasite. Silica and sphalerite typically occur between colloform bands. Reflected light, field of view = 6 mm. Sample 158-957I-1X-1 (Piece 8, thin section from 49 to 52 cm). **B.** Multiple growth layers of porous, fine-grained pyrite and marcasite showing colloform and spheroidal textures. Note the euhedral pyrite grains (white) in the core of spheroids. Late, coarse marcasite (Mc) grows into void spaces. Reflected light, field of view = 1.5 mm. Sample 158-957K-1X-1 (Piece 4, thin section from 21 to 23 cm). **C.** Colloform textures (cauliflower texture) in porous pyrite caused by abundant mineral inclusions (silica?) in pyrite. As a result, the reflectivity of this material is very low. Reflected light, field of view = 1.5 mm. Sample 158-957K-1X-1 (Piece 4, thin section from 21 to 23 cm). **D.** Close-up photograph of colloform textures with multiple banding and dendritic textures. Reflected light, field of view = 750 µm. Sample 158-957K-1X-1 (Piece 4, thin section from 21-23 cm).

later, coarser generations are associated with sphalerite and chalcopyrite, with chalcopyrite replacing sphalerite. Remnants of framboidal pyrite were found in more massive pyrite. Small, late, marcasite veins (100 µm thick) cut an early pyrite and marcasite assemblage. Samples from core from Hole 957K contain abundant dark gray to black angular chert clasts in a pyrite and marcasite matrix (Fig. 9A). The angular clasts consist of amorphous silica with abundant, very fine-grained, dusty, dark inclusions (Mn-oxides?) and minor disseminated pyrite (Fig. 9B). The chert clasts contain dendritic textures, as well as rounded textures with pyritized walls (0.2–1.5 mm in diameter), similar to fossil worm tubes (Figs. 9C, D). Some of the amorphous silica is filamentous, which may be the result of biological precipitation. The chert was later brecciated and cemented by colloform pyrite. Coarse-grained marcasite veins cut the chert clasts and the colloform pyrite. Late, colorless, amorphous silica fills open space and fractures.

Massive granular pyrite (Type 5c) (Fig. 10) was recovered from 10 to 14.5 mbsf in Hole 957K; it consists almost entirely of granular aggregates of very fine-grained to fine-grained pyrite with abundant colloform texture. Chalcopyrite is rare. Dark sphalerite occurs lining vugs. A silica phase occurs as pore-space filling between pyrite in Sample 158-957K-2N-1 (Piece 6). Dark blue crystals with a metallic luster were observed in several hand specimens, suggesting the presence of secondary Cu-sulfides (e.g., covellite). Porous pyrite aggregates are the major constituent of these samples and are overgrown by banded pyrite and marcasite (Fig. 11). The porous pyrite aggregates sometimes preserve colloform textures. Chalcopyrite is concentrated in these aggregates and occurs interstitial to the porous pyrite aggregates or as small inclusions in pyrite. Sphalerite inclusions in pyrite are usually associated with chalcopyrite. The early assemblage of pyrite, sphalerite, and chalcopyrite is overgrown by coarse-grained marcasite with minor coarse-grained pyrite. Chalcopyrite grains that are in contact with marcasite develop a thin (<5 µm) rim of digenite, bornite, and covellite. Chalcopyrite grains in contact with pyrite rarely exhibit similar oxidation. The outer part of the sample consists of a thick, banded zone of alternating pyrite and marcasite, with characteristics ranging from coarse-grained and euhedral to fine-grained and colloform. Pyrite-rich layers contain rare marcasite, sphalerite, and chalcopyrite inclusions.

Massive pyrite (Type 5) was recovered from 14.5 to 20 mbsf in Hole 957K and is composed of fine- to medium-grained pyrite and marcasite with abundant colloform textures similar to porous massive pyrite. Massive pyrite samples, however, are less granular than porous pyrite samples (Fig. 12). The massive pyrite samples consist of almost equal amounts of pyrite and marcasite, with minor sphalerite and quartz and traces of chalcopyrite and amorphous silica. In thin

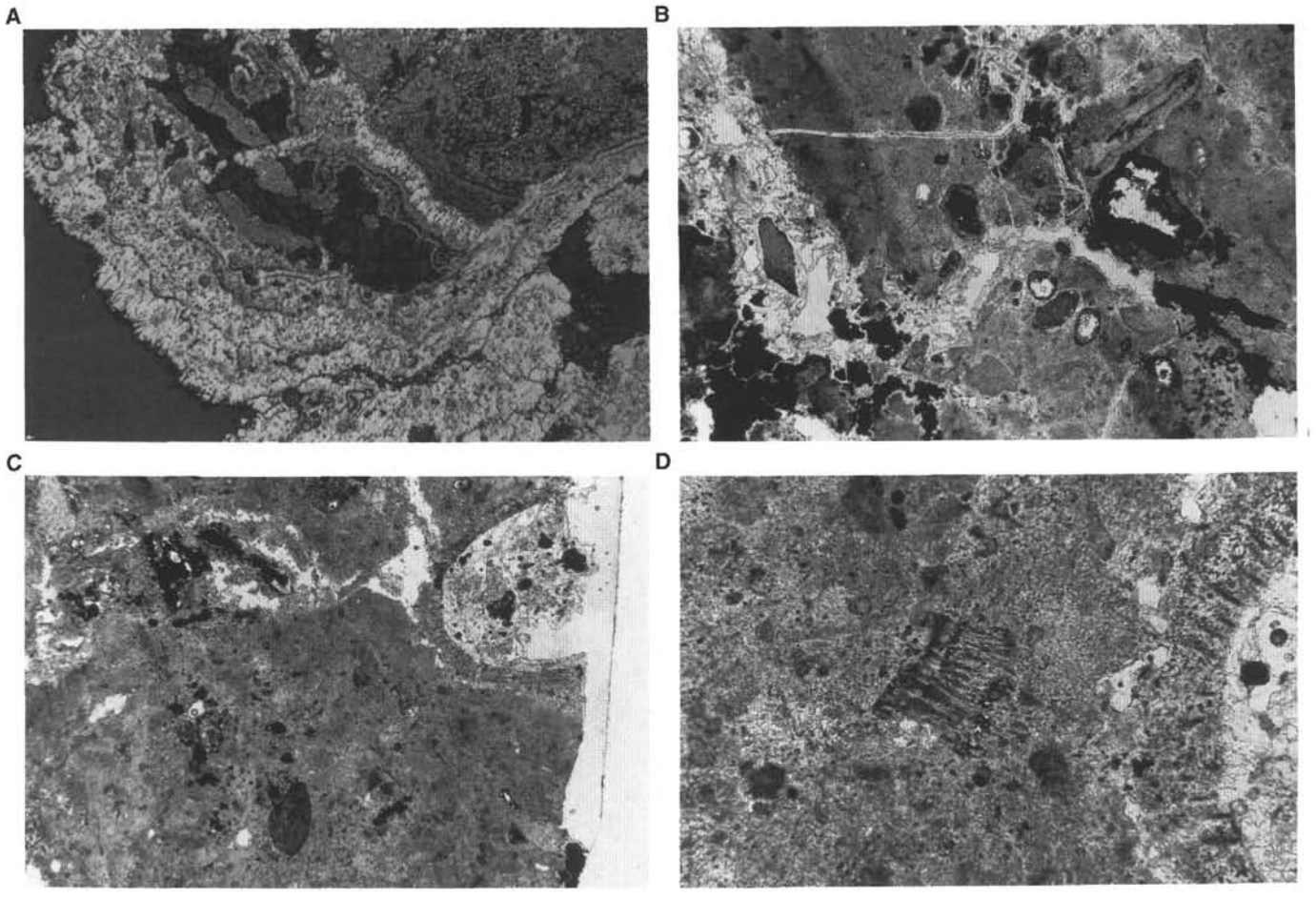

Figure 9. Thin-section photomicrographs of textural features in dark gray to black chert clasts enclosed in porous massive pyrite. Sample 158-957K-1X-1 (Piece 2, thin section from 10-12 cm). **A.** Clasts of chert (black) overgrown by colloform pyrite and cut by late marcasite veins. Reflected light, field of view = 6 mm. **B.** Fractured and porous dark gray chert, with pyrite-marcasite (black) and amorphous silica variously distributed in vugs and fractures. Transmitted light, field of view = 6 mm. **C.** Chert, mottled gray as a result of very fine mineral inclusions (Mn-oxides?). The chert contains minor disseminated pyrite (black) and colorless amorphous silica lines voids and fractures (white). The circular texture on the edge appears to be a section through a tubular structure of biological origin. Transmitted light, field of view = 6 mm. **D.** Detailed view of the tube wall shown in Figure 9C, now silicified and containing pyrite inclusions. Another structure of possible biological origin is embedded in the dusty chert (center). Transmitted light, field of view = 1.5 mm.

section, porous pyrite and marcasite, sometimes preserving colloform or framboidal textures, with minor amounts of silica and rare sphalerite, form the substrate. This substrate was then overgrown by coarse-grained sphalerite and later by coarse-grained marcasite. Traces of chalcopyrite are associated with coarse-grained sphalerite. Complex multistage layers of alternating pyrite and marcasite overgrow this early stage. Amorphous silica and chalcedony are found occasionally lining voids in colloform pyrite and marcasite.

Pyrite-Silica Breccia (Type 9a)

Three samples of pyrite-silica breccia that resemble those recovered in deeper parts of cores from the eastern side of the mound were found in Section 158-957I-1N-1 (Fig. 13). Sample 158-957I-1N-1 (Piece 11) is a light gray pyrite-silica clast (70% quartz and 30% pyrite), with a few small patches of red chert (1 mm in diameter), surrounded by dark gray quartz with disseminated pyrite. This piece is partly rimmed by pyrite (2–6 mm thick). The other samples consist of equal amounts of dark gray quartz and disseminated pyrite with only minor chalcopyrite and represent the matrix to the above-described light gray pyrite-silica clasts (see Fig. 14). Euhedral pyrite crystals, as well as polycrystalline aggregates of euhedral pyrite and porous pyrite, were observed microscopically in a matrix of fine-grained quartz and chalcedony (Fig. 14A). Remnants of "clast"-like textures are visible because of the different grain sizes of quartz in different areas of the section, as well as because of the presence of pyrite rims surrounding sulfide-poor quartz (Fig. 14B). Chalcedony is present only in the matrix and not in the clasts. Single, large (200–400 μm), euhedral crystals of quartz were observed in the matrix and within clasts. A few polycrystalline chalcopyrite aggregates occur in the matrix. Pyrite is variably intergrown (replaced?) with chalcopyrite. At least two generations of pyrite formed before and after chalcopyrite deposition. The later generation of pyrite forms thin (<100 μm) rims on euhedral and porous pyrite aggregates. One aggregate, composed of pyrite, brown clay with a faint sheaf-like texture and quartz, is thought to be an altered basalt clast.

Hole 957M

Visual Core Description

A listing of the visual core descriptions for sulfide and Fe-oxide-bearing rocks from this hole is given in Table 2 (see back pocket) and a schematic section of the hole is illustrated in Figure 15. The rock types recovered in Hole 957M include Fe-oxides (Type 1), red and gray chert and quartz (Type 2), porous massive pyrite (Type 5a), massive granular pyrite (Type 5c), pyrite-silica breccia (Type 9a), si-

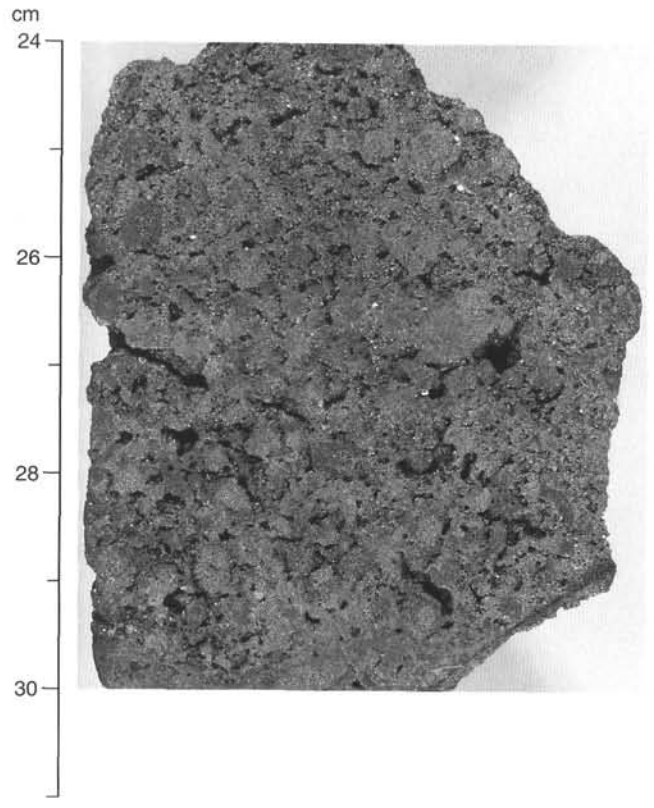

Figure 10. Massive granular pyrite (Type 5c) comprised of granular aggregates of pyrite and overgrown by colloform pyrite and marcasite. Sample 158-957K-2N-1 (Piece 7, 24–31 cm).

licified wallrock breccia (Type 10a), chloritized basalt breccia (Type 10b), and variably altered, sparsely olivine-phyric basalt.

Fe-oxides were encountered only as drill cuttings at the top of Section 158-957M-1R-1 and in the upper part of Section 158-957M-1R-2 (<9.3 mbsf). Red cherts occur above 9.3 mbsf, and as clasts in pyrite-silica breccias farther downcore. Three pieces of gray and red quartz were recovered below 34.3 mbsf. Porous massive pyrite was mainly found between 9.3 and 24.3 mbsf, whereas massive granular pyrite was observed between 24.3 and 42.3 mbsf, with a single piece found in the interval from 0.0 to 9.3 mbsf. Massive pyrite types occur together with pyrite-silica breccia, which is the dominant rock type from 9.3 to 42.3 mbsf. Silicified wallrock material was first encountered as clasts in pyrite-silica breccias between 0.0 and 9.3 mbsf, but these clasts occur mainly below 24.3 mbsf. Small pieces of chloritized basalt breccia were found below 34.3 mbsf. From 42.3 to 51.2 mbsf (E.O.H.), slightly altered, sparsely olivine-phyric basalt was the dominant rock type.

Fe-oxides (Type 1)

The first cored section in Hole 957M recovered 55 cm of fine- to coarse-grained, red-brown and orange, Fe-oxide sediment (Fig. 16). The grading observed in the core is probably drilling induced. Fine-grained pyrite and several dark gray grains (silica?) were also observed. Larger Fe-oxide grains are platy or tabular and some show layering. A similar morphology was observed in Sample 158-957M-1R-2 (Piece 4). The layering is pronounced, with dark and bright orange laminations.

Red and Gray Chert (Type 2)

Red cherts were observed as discrete pieces in the first cored interval, between 0 and 9.3 mbsf (Sample 158-957M-1R-1, Pieces 1 and 3), and consist of dark red Fe-oxides intimately intergrown with silica. They are similar to material recovered from Hole 957J. Sample 158-957M-1R-2 (Piece 3), however, consists of several angular red

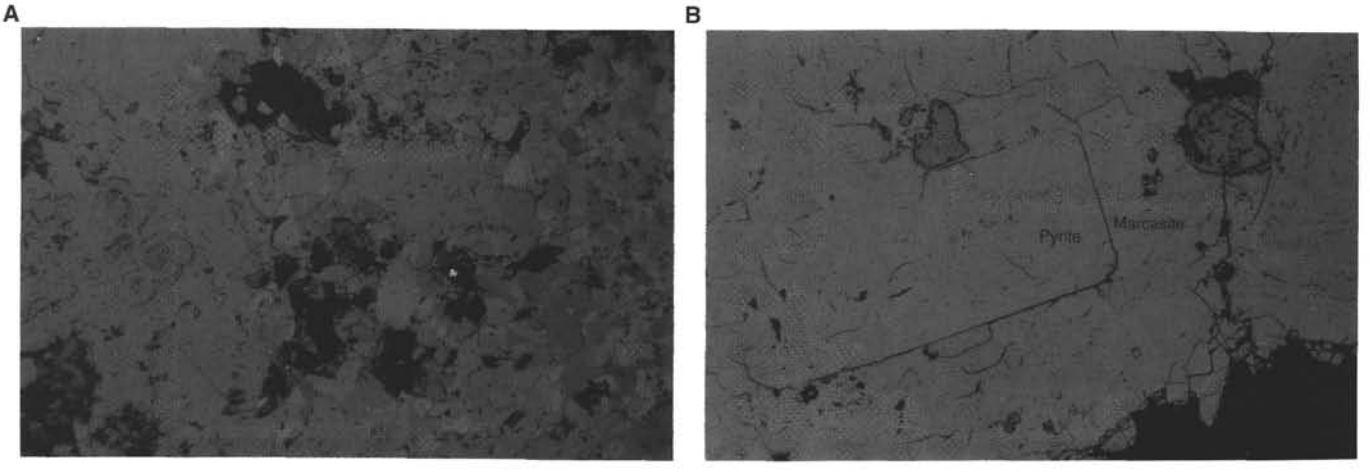

Figure 11. Thin-section photomicrographs of typical textures observed in granular pyrite. Sample 158-957K-2N-1 (Piece 9, thin section from 37 to 38 cm). **A.** Multiple generations of pyrite and marcasite, with local recrystallization. Colloform pyrite, overgrown by polycrystalline pyrite with chalcopyrite and sphalerite inclusions. This passes to intergrowths of pyrite and marcasite (anisotropy visible as shades of gray). Reflected light, partly uncrossed nicols, field of view = 1.5 mm. **B.** Euhedral pyrite lath (white, center) is enclosed in polycrystalline marcasite. Corroded chalcopyrite inclusions (gray) are rimmed by bornite-digenite-covellite intergrowths (dark). Reflected light, field of view = 1.5 mm.

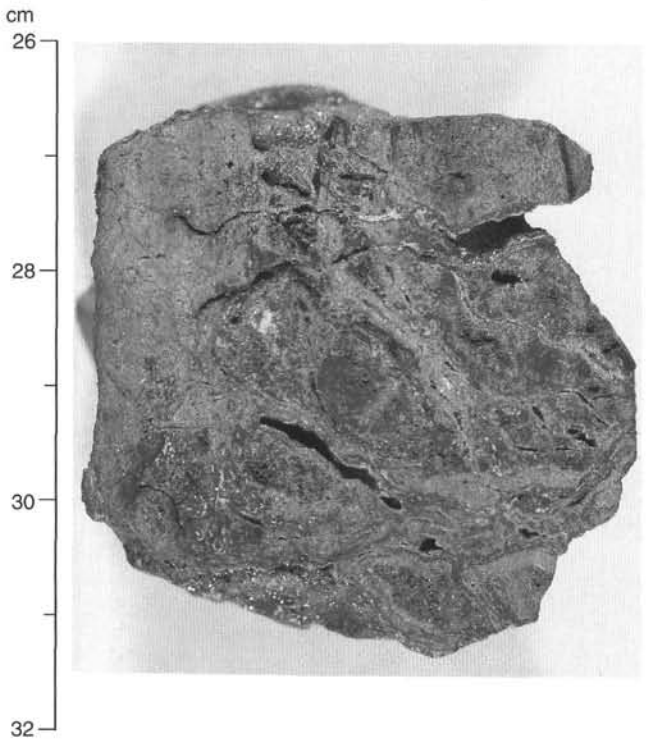

Figure 12. Typical massive pyrite sample (Type 5) comprised of multiple generations of pyrite and marcasite veins. Gray quartz veins (<1 mm wide) cut through the sample, and euhedral white quartz lines the open space in these fractures. Sample 158-957K-3X-1 (Piece 6, 26–32 cm).

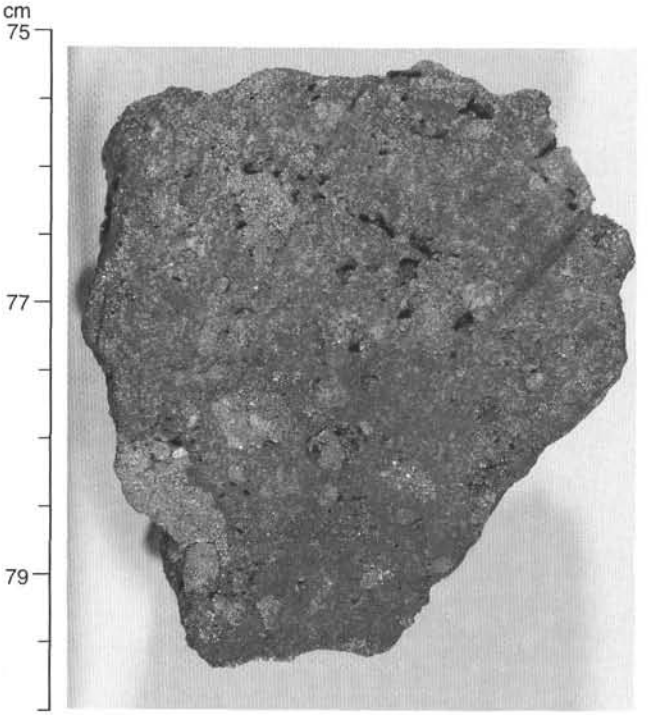

Figure 13. Dark gray pyrite-silica breccia (Type 9a) with pyrite aggregates in a matrix of dark gray quartz and disseminated pyrite. Sample 158-957I-1N-1 (Piece 12, 75–80 cm).

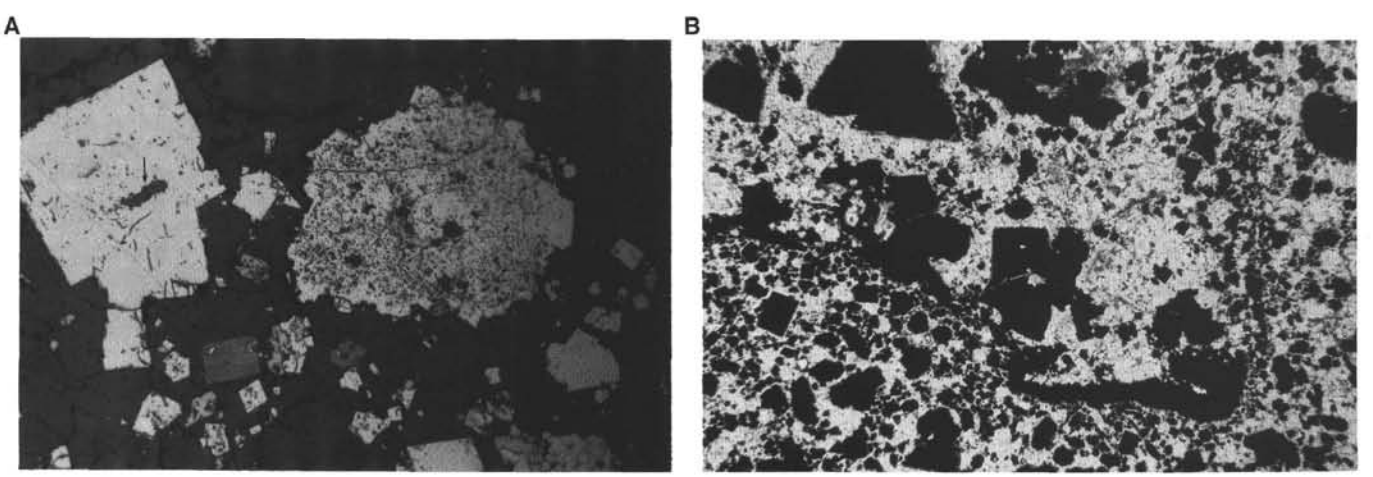

Figure 14. Thin-section photomicrographs of pyrite-silica breccia. Sample 158-957I-1N-1 (Piece 12, thin section from 75 to 76 cm). **A.** Porous pyrite clast (light gray) with abundant chalcopyrite (medium gray) inclusions and coarse-grained euhedral pyrite in a matrix of fine-grained quartz (dark gray) and euhedral pyrite. Chalcopyrite in the matrix is interstitial to quartz and pyrite. Note the Fe-oxide inclusion in the euhedral pyrite grain (arrow). Reflected light, field of view = 1.5 mm. **B.** Pyrite-silica clast with coarse-grained quartz matrix and coarse-grained euhedral pyrite (black). The outline of a replaced clast is visible because of the partial rim of pyrite. The clast is enclosed in a matrix of fine-grained quartz and disseminated pyrite. Transmitted light, field of view = 6 mm.

chert clasts in a matrix of more porous red chert with large (1–8 mm), rounded voids (Fig. 17). These voids are lined by very fine-grained quartz. Gray silica occurs in small quantities in fractures and vugs. Colloform marcasite forms a very fine-grained crust around the outside of the piece. Red chert, with disseminated euhedral pyrite, occurs as a clast (1.5 cm in diameter) in fine-grained, pyrite-silica breccias with nodular pyrite and gray pyrite-silica clasts (Fig. 18). Pyrite is replacing the Fe-oxides around the rim of the clast and possibly along laminations. Smaller red chert clasts occur within pyrite-silica breccias throughout the core, but the main occurrences are between 9.3 and 24.3 mbsf, and between 38.3 and 42.3 mbsf. No red chert clasts were observed in samples from Cores 158-957M-5R to

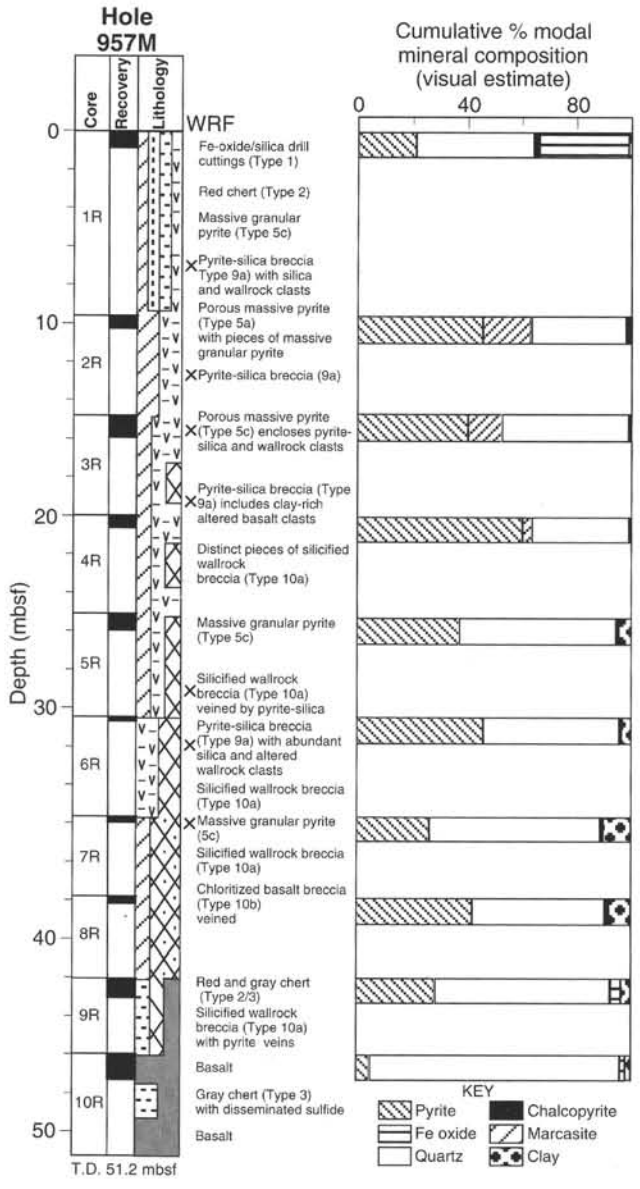

Figure 15. Schematic stratigraphic section through Hole 957M. WRF = wallrock fragment, shown by a small ×. T.D. = total depth.

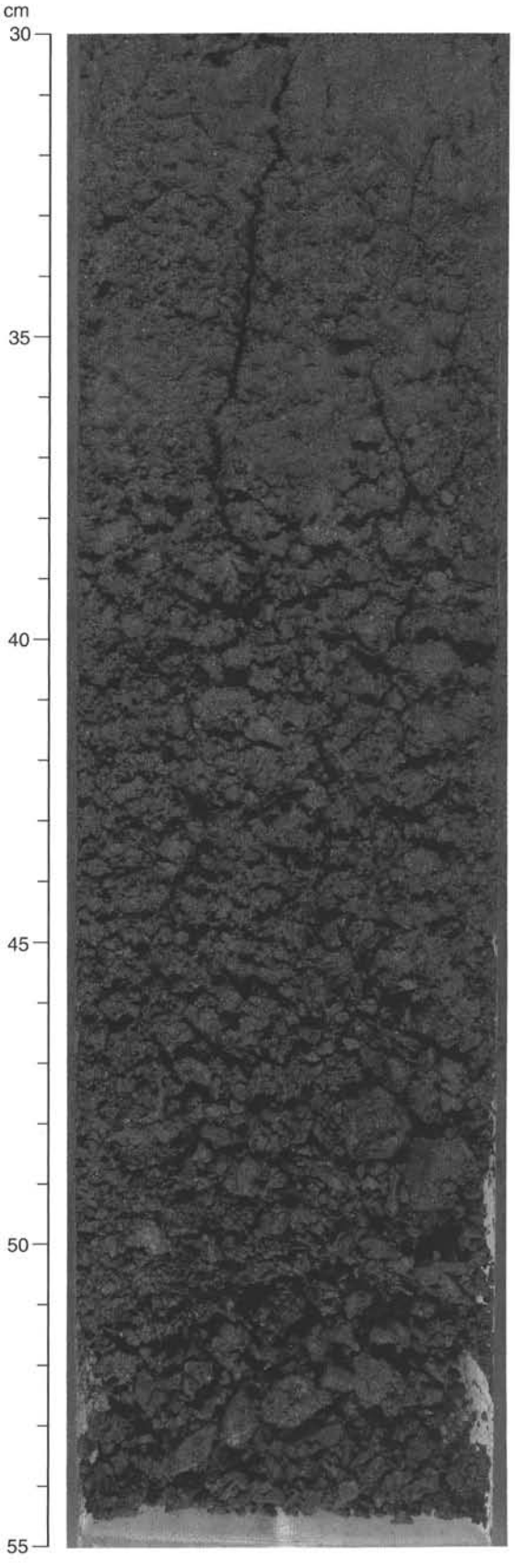

Figure 16. Fe-oxide-rich drill cuttings with angular Fe-oxide (up to 1.5 cm) and minor silica pieces. The apparent grading in the cuttings is drilling induced. Sample 158-957M-1R-1 (Piece 1, 30–55 cm).

7R. Some red chert clasts occur also in porous massive pyrite (Sample 158-957M-2R-1, Pieces 4 and 5) and in clay-rich siliceous wallrock breccia (Sample 158-957M-8R-1, Piece 5).

Three pieces of red and gray quartz were recovered below 34.3 mbsf. Two pieces were found in the sequence of silicified wallrock and chloritized basalt breccias from 34.3 to 42.3 mbsf. They are composed of massive, medium-grained, light gray to gray quartz aggregates with variable red Fe-oxide coloration (Fig. 19). Minor euhedral to subhedral pyrite is disseminated throughout the sample and also lines cavities within the quartz. One piece occurred in the basaltic unit below 42.3 mbsf (Sample 158-957M-10R-1, Piece 17) and contains abundant, angular hyaloclastite fragments, now altered to chlorite(?). All pieces are rimmed by massive pyrite, which suggests that they occur as clasts. However, gray and red quartz observed as a minor component on the outside of a piece of silicified wallrock breccia appears to have a banded, veinlike morphology (Sample 158-957M-7R-1, Piece 3). The sample from immediately above the basaltic unit (Sam-

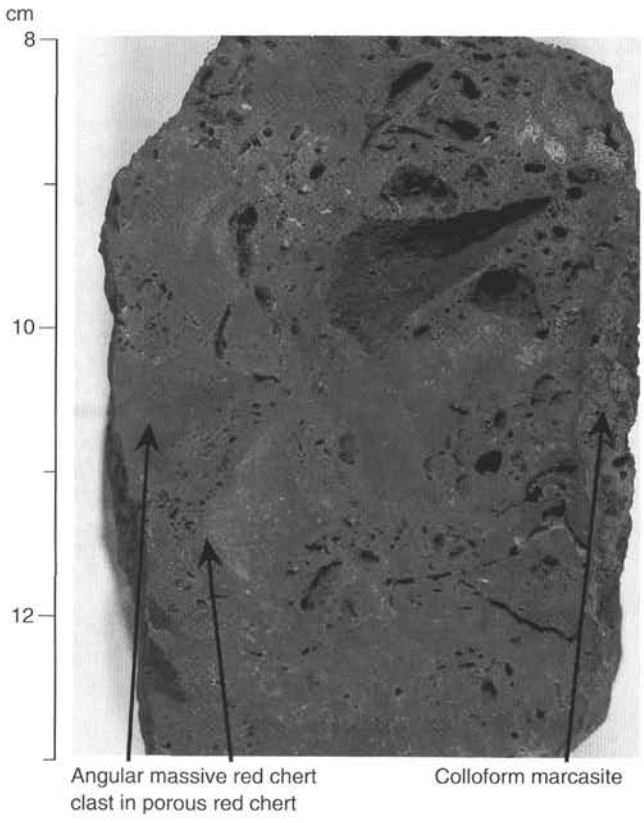

Figure 17. Massive red chert consisting of Fe-oxide-bearing silica with rare disseminated pyrite. Clasts of massive red chert (labeled) are enclosed in a matrix of less porous red chert. The sample is partly rimmed by colloform marcasite (labeled). Sample 158-957M-1R-2 (Piece 3, 8–13 cm).

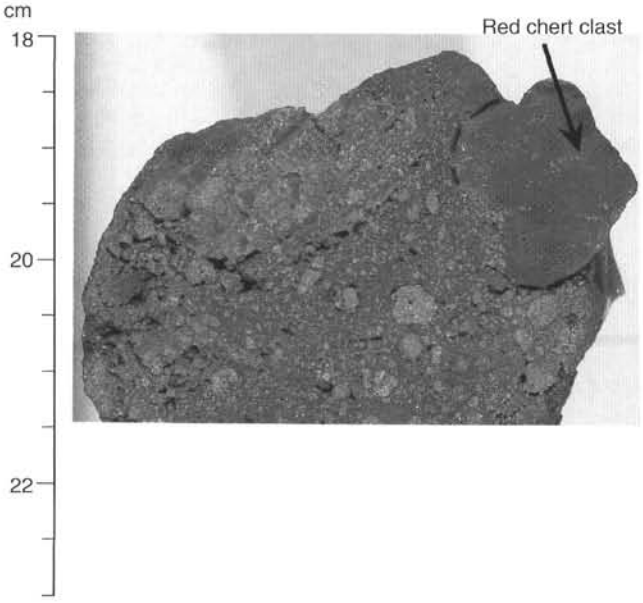

Figure 18. Red chert clast with disseminated euhedral pyrite in fine-grained pyrite-silica breccia (Type 9a). Pyrite is replacing the Fe-oxides along grain boundaries. Sample 158-957M-4R-1 (Piece 5, 18–23 cm).

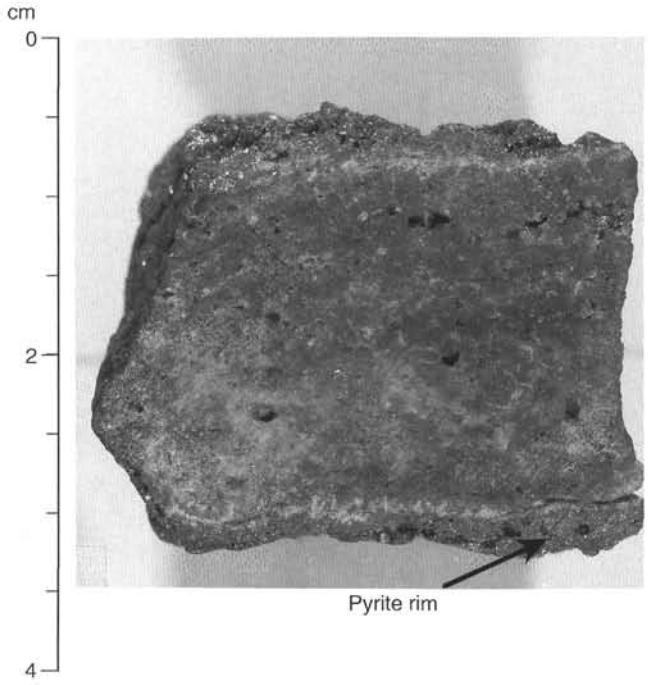

Figure 19. Gray clast consisting of massive medium- to coarse-grained quartz. The quartz is colored by various amounts of Fe-oxides. Pyrite occurs as euhedral grains disseminated in the quartz and as small euhedral grains lining vugs. The sample is rimmed by massive pyrite (labeled). Sample 158-957M-7R-1 (Piece 1, 0–4 cm).

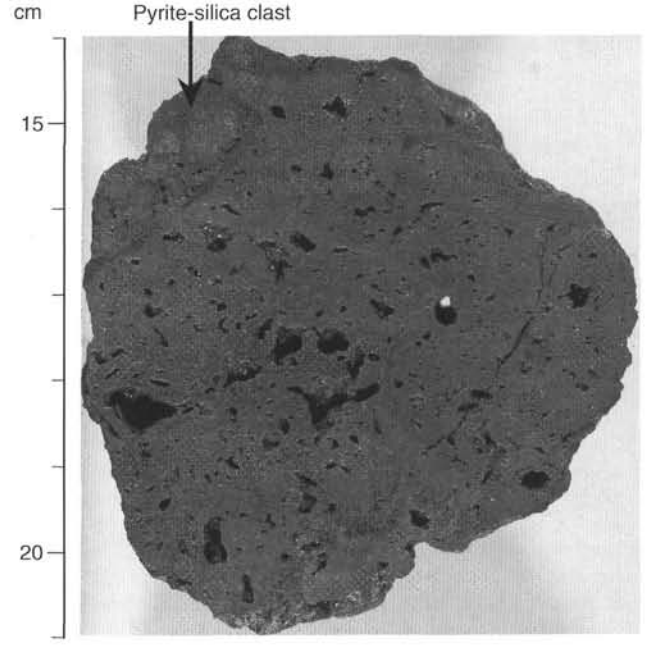

Figure 20. Porous massive pyrite (Type 5a) with colloform-banded textures. In thin section, similar samples were observed to be composed of up to 50% marcasite. The porous sulfide encloses dark gray pyrite-silica clasts (labeled). Sample 158-957M-2R-1 (Piece 4, 14–21 cm).

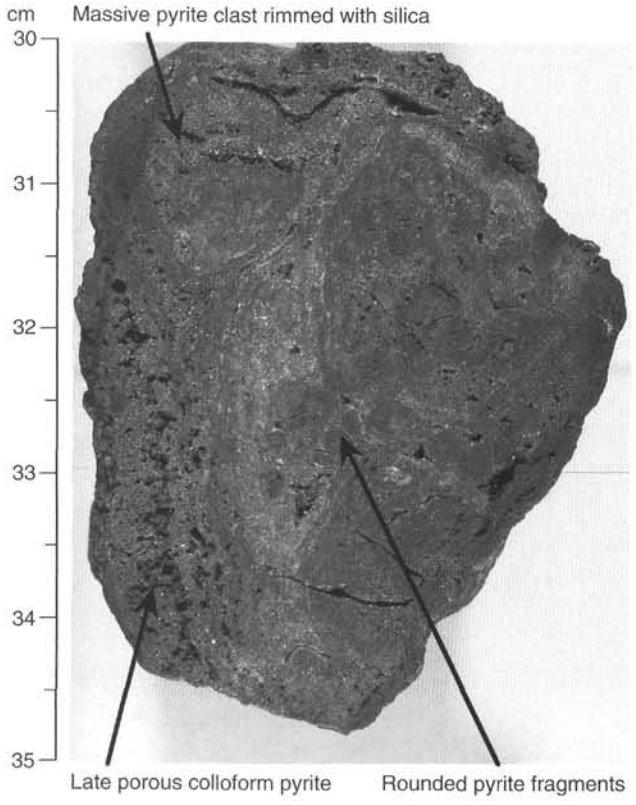

Figure 21. Porous massive pyrite (Type 5a) with colloform pyrite and marcasite overgrowing massive, angular to subrounded pyrite clasts. Amorphous silica occurs lining the clasts. A late porous massive pyrite encloses the sample. Sample 158-957M-3R-1 (Piece 8, 30–35 cm).

ple 158-957M-9R-1, Piece 1) is transitional in texture and composition between gray quartz and red chert.

Massive Pyrite (Type 5)

Massive pyrite is abundant throughout the cores: as discrete samples, and overgrowing chert, pyrite-silica breccias, and silicified wallrock breccias. Porous massive pyrite (Type 5a) is present from 9.3 to 24.3 mbsf; it consists of variable proportions of pyrite and marcasite with colloform-banded textures and a coarse (1–5 mm) vuggy porosity (up to 20 vol%) (Fig. 20). The colloform texture commonly encloses zones of massive fine-grained pyrite and marcasite (Fig. 21) or grades into dark gray pyrite-silica. Samples from Sections 158-957M-2R-1, 3R-1, and 4R-1 record a complete range of intergrowths: from porous massive pyrite with minor silica inclusions, to pyrite-silica breccias with minor porous pyrite overgrowths. Minor chalcopyrite occurs as 1- to 3-mm aggregates associated with silica-rich zones, and euhedral fine-grained sphalerite is lining vugs. Microscopically, multiple generations of colloform, polycrystalline and/or euhedral pyrite and marcasite (in approximately equal proportions) form massive millimeter-growth layers on cores of porous, colloform pyrite (Fig. 22A). Coarse euhedral marcasite and, in places, late pyrite line voids (Fig. 22B). Traces of euhedral to subhedral sphalerite (characteristically yellow and orange in transmitted light) are intergrown with pyrite and marcasite. Zones of very fine-grained sphalerite are often associated with coarse-grained marcasite (Fig. 22C). Chalcopyrite is a trace phase. These samples are composed of significant amounts of marcasite and sphalerite; in this respect, they are different from the porous pyrite recovered from the other parts of the mound.

Massive granular pyrite (Type 5c) occurs between 0 and 9.3 mbsf (Sample 158-957M-1R-2, Piece 2) and between 24.3 and 42.3 mbsf. This massive granular pyrite consists almost entirely of granular aggregates of fine-grained pyrite, often incorporating pyrite-silica breccia clasts (Fig. 23). Some of these clasts show gradational contacts with the surrounding massive pyrite. Subrounded clasts of very-fine grained, massive pyrite were observed in the upper part of the core (Fig. 24). The pyrite aggregates commonly contain subrounded to rounded clasts of silicified wallrock material, with disseminated clay and pyrite, or clasts of pale gray silica (with disseminated pyrite) (Fig. 25). It is possible that the fine-grained, subrounded pyrite clasts in the massive granular pyrite near the top of the core developed by complete pyritization of silicified wallrock clasts. In some cases, the intermediate stages in this process are still preserved (e.g., Samples 158-957M-6R-1, Piece 5, and 7R-1, Piece 2). Traces of chalcopyrite occur as disseminated fine-grained aggregates in the pyrite. Massive granular pyrite pieces from 24.3 to 42.3 mbsf are texturally distinct from the samples above 9.3 mbsf. These samples of recrystallized, colloform-banded pyrite preserve a coarse, vuggy porosity and appear transitional between porous massive and granular pyrite types.

Pyrite-Silica Breccia (Type 9a)

Pyrite-silica breccias occur between 0.0 and 34.3 mbsf, and are most abundant from 9.3 to 24.3 mbsf. They are matrix supported and consist of a assemblage of different clasts in a dark gray pyrite-silica matrix. Pyrite (commonly brecciated), pyrite-silica, light gray silicified wallrock, and gray quartz clasts occur. Two textural subtypes of pyrite-silica breccia, which occur over similar depth intervals, can be distinguished. Fine-grained pyrite-silica breccias are composed of well-sorted, rounded to subrounded, fine-grained (<10 mm) pyrite, light gray silicified wallrock, and gray quartz clasts in a dark gray silica-pyrite matrix (Fig. 26). Pyrite clasts are often brecciated. Quartz clasts contain disseminated euhedral pyrite. Fine-grained chalcopyrite aggregates (up to 3 mm in diameter) occur. In general, fine-grained pyrite-silica breccias have a low porosity (<5%). Coarse-grained pyrite-silica breccias contain clasts of the fine-grained pyrite-silica breccia intergrown with massive pyrite clasts (3–15 mm) and pale gray pyrite-silica clasts (as large as 2.5 cm), both commonly rimmed by pyrite. Late marcasite and pyrite line vugs, especially in samples from Section 158-957M-3R-1 (Fig. 27). The dominant clast type in these samples consists of pale gray silica with disseminated pyrite, which appears to have been derived from silicified wallrock material (Fig. 28). Coarse-grained pyrite-silica breccias commonly have a higher, vuggy porosity (10%–20%).

Several pyrite-silica breccia pieces exhibit textures transitional between both types. Some of the silicified wallrock fragments in Sample 158-957M-1R-2 (Piece 31) show a distinct rim, several millimeters in width, enriched in chalcopyrite. Several small angular pieces of altered hyaloclastite occur in Sample 158-957M-3R-1 (Piece 31) (Fig. 29). Microscopically, these breccias consist of polycrystalline pyrite aggregates and euhedral to subhedral pyrite (20–45 vol% combined pyrite) in a quartz matrix with minor interstitial chalcopyrite (Fig. 30A). Marcasite and pyrite intergrowths line vugs and pores with, generally, pyrite forming euhedral overgrowths on marcasite. Pyrite clasts have inclusions of anhedral chalcopyrite and euhedral to subhedral quartz and are often fractured. Locally, these fractures are filled with quartz. Several growth stages occur in pyrite grains (Fig. 30B), and porous colloform cores are common. Locally, pyrite grain boundaries indicate dissolution. In some cases, chalcopyrite replaces pyrite (Fig. 30C), but overgrowths of pyrite on chalcopyrite also occur. Brown clay in quartz-rich pyrite-silica clasts (2 mm to 1 cm in diameter) suggest the presence of silicified basalt clasts.

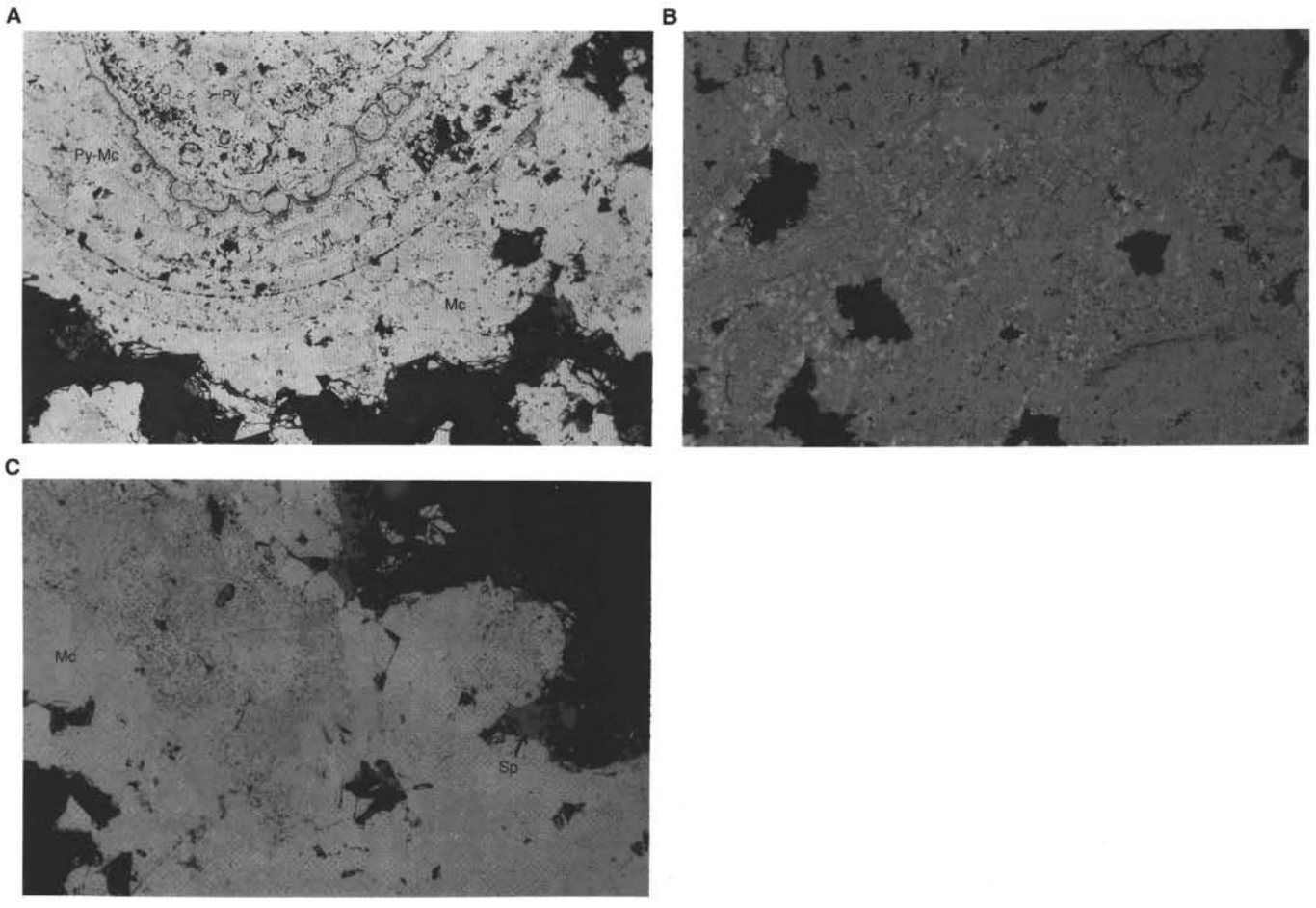

Figure 22. Thin-section photomicrographs of porous massive pyrite and marcasite. Sample 158-957M-2R-1 (Piece 4, thin section from 18 to 20 cm). **A.** Colloform porous pyrite (Py) is rimmed by multiple layers of intimately intergrown pyrite and marcasite (Py-Mc). The vugs (black) are lined by coarse-grained euhedral marcasite (Mc). Reflected light, field of view = 1.5 mm. **B.** Porous pyrite is overgrown by coarse-grained marcasite (anisotropy is visible as shades of gray). Late euhedral pyrite overgrows marcasite in some pore spaces. Reflected light, partly uncrossed nicols, field of view = 6 mm. **C.** Fine dusting of sphalerite (gray) in coarse-grained marcasite (Mc). A late, euhedral sphalerite (Sp) is present in the open space (black). Reflected light, field of view = 750 µm.

Some clasts are rimmed by a 0.2- to 1-mm-wide chalcopyrite rim. Covellite is observed with chalcopyrite near the contact of chalcopyrite and quartz. The matrix consists of anhedral to euhedral quartz, microcrystalline quartz, and chalcedony, as well as subhedral aggregates of pyrite and chalcopyrite (Fig. 30D). Multiple generations of silica precipitation occur. Banded chalcedony and microcrystalline quartz, with decreasing band widths, overgrows zoned euhedral quartz, and the remaining pore space is filled with massive chalcedony (Fig. 30E). Several anhedral inclusions (of a colorless mineral with high birefringence and weak 90° cleavage [anhydrite?]) were found in coarse-grained quartz (Fig. 30F).

Silicified Wallrock Breccia (Type 10a)

Pieces of silicified wallrock material are present in the first section of the core (interval 158-957M-1R-2, Pieces 5–7), but silicified wallrock breccias first appear as isolated pieces at 14.3 mbsf (Sample 158-957M-3R-1, Pieces 2, 3, and 5). The breccias consist of angular to subrounded clasts of variably silicified and highly altered basalt; these are enclosed in a matrix of pyrite-silica breccia or porous massive pyrite and are cut by pyrite and quartz veins (see "Hydrothermal Alteration" section, this chapter). The altered basalts are recognized by the presence of tan clays and fine-grained disseminated pyrite and the preservation of basaltic textures (Sample 158-957M-8R-1, Piece 5) (Fig. 31; see "Hydrothermal Alteration" section, this chapter). This sample also contains an angular fragment of dark red chert.

Chloritized Basalt Breccia (Type 10b)

A few pieces of chloritized basalt breccia occur below 34.3 mbsf (e.g., Sample 158-957M-7R-1, Pieces 5 and 6), where they are gradational from the silicified wallrock breccias, and where less intensive silicification of the altered basalt material occurs. Below 42.3 mbsf, the silicified wallrock and chloritized basalt breccias are underlain by slightly altered basalts, which contain disseminated pyrite and rare chalcopyrite. The basalt samples are cut by rare, ≤0.5 mm pyrite-silica-chlorite veins (see "Hydrothermal Alteration" section, this chapter).

Sulfide Geochemistry

Nine samples from cores recovered from Holes 957I, 957K and 957M in the TAG-4 area west of the Black Smoker Complex were analyzed by AAS and CHNS. The data are summarized in Table 3.

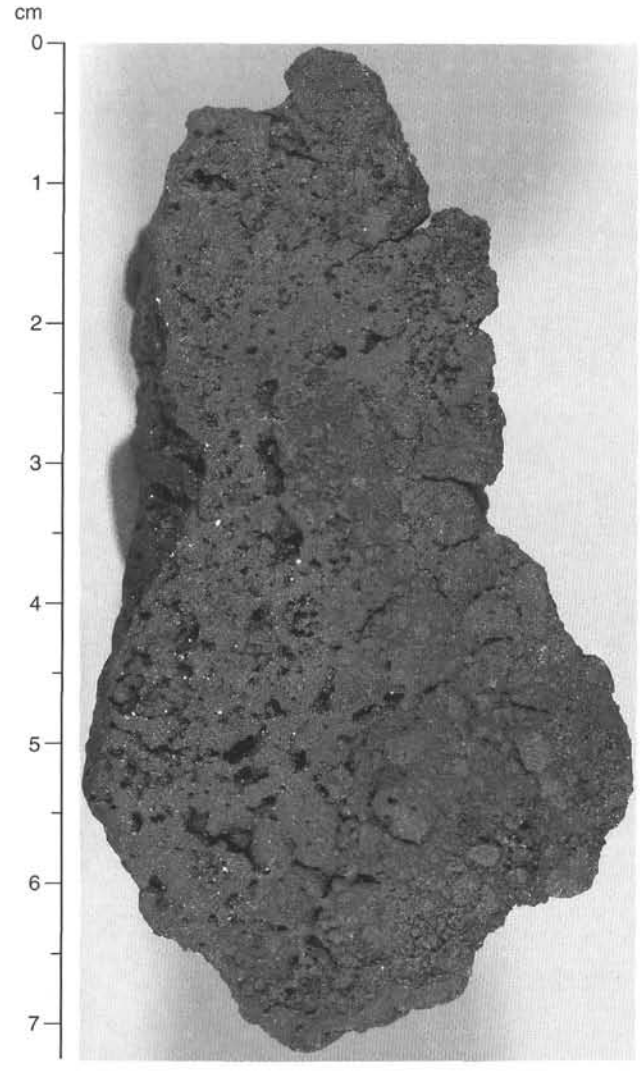

Figure 23. Massive granular pyrite (Type 5c) with abundant inclusions of pyrite-silica breccia. The contacts between massive pyrite and breccia are often gradational. Sample 158-957M-8R-1 (Piece 1, 0–7 cm).

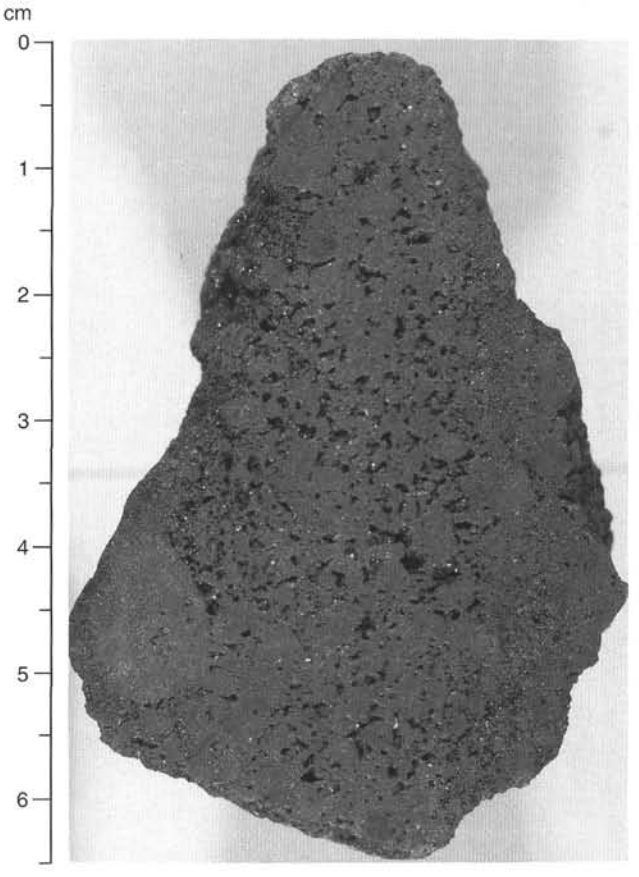

Figure 24. Subrounded clasts of massive fine-grained pyrite (up to 1 cm in diameter) in massive granular pyrite. The presence of pyrite grains and aggregates of varying size gives the sample a clastic brecciated appearance. Sample 158-957M-2R-1 (Piece 1, 0–5 cm).

The samples comprise Fe-oxide-rich rocks from the upper part of the sulfide mound, massive pyrite from depths of 0.2–14.8 mbsf as well as 38.3 mbsf, and pyrite-silica breccia from 14.9 to 25.2 mbsf.

Composition of Rock Types Analyzed in the TAG-4 Area

Fe-oxides (Type 1)

The surface layer of Hole 957M consists of Fe-oxides; their composition was determined on a composite sample of drill cuttings from the interval between 16 and 47 cm of Section 158-957M-1R-1. The cuttings were sifted into three grain-size fractions that were analyzed separately: >420 µm, 420–63 µm and <63 µm. This oxidized surface layer contains less than 4.7 wt% S but up to 52.4 wt% Fe. The finest (<63 µm) of the three grain-size fractions has the highest S (4.7 wt%), Cu (0.29 wt%), Zn (0.28 wt%), Pb (132 ppm), Ag (12 ppm), and Cd (5 ppm) contents. This indicates that the fine-grained fraction contains a higher amount of sulfide minerals than the remaining fractions.

Massive Pyrite (Types 5, 5a, and 5c)

Four samples of massive and porous massive pyrite from the upper part of the sulfide mound beneath the Fe-oxide cap in the TAG-4 area (0.24–14.82 mbsf) and one sample from 38.30 mbsf were analyzed (Table 3). Their high Fe (38.4–45.7 wt%) and S (41.0–50.8 wt%) contents confirm that this rock type mainly consists of pyrite/marcasite. Three samples (158-957I-1N-1, Piece 6; 158-957K-1X-1, Piece 4; and 158-957K-3X-1, Piece 7) have high Zn contents of 3.0–3.7 wt%, which are among the highest values determined during Leg 158. These data indicate that the proportion of sphalerite is on the order of 5 wt% in these samples. However, these samples have low Cu contents of only 0.05 to 0.13 wt%. Samples 158-957K-2N-1 (Piece 9) and 158-957M-8R-1 (Piece 1) differ from the others in that they contain significantly lower Zn (0.76 and 0.71 wt%) but higher Cu concentrations (1.11 and 1.84 wt%). In the top 15 m of the TAG-4 area, concentrations of trace metals in the massive pyrite range from 107 to 218 ppm for Pb, from 17 to 21 ppm for Ag, and from 14 to 167 ppm for Cd. The sample of massive granular pyrite from 38.3 mbsf (Sample 158-957M-8R-1, Piece 1) has much lower trace element concentrations, similar to those observed in the TAG-1 and TAG-2 areas.

Pyrite-Silica Breccia (Type 9a)

The composition of the pyrite-silica breccia has been determined on two samples recovered from Core 158-957M-3R at depths of 14.9 and 15.5 mbsf and from Core 158-957M-5R at 25.2 mbsf. Sample 158-957M-3R-1 (Piece 14) has a composition similar to that of the Zn-rich massive pyrite described above, in that S, Fe, and Zn contents are high (49.8, 40.5, and 4.3 wt%, respectively), but the Cu concentration is low (0.37 wt%). The other samples (Samples 158-957M-3R-1, Piece 28; and 5R-1, Piece 15) are lower in S (40.2 and 26.1

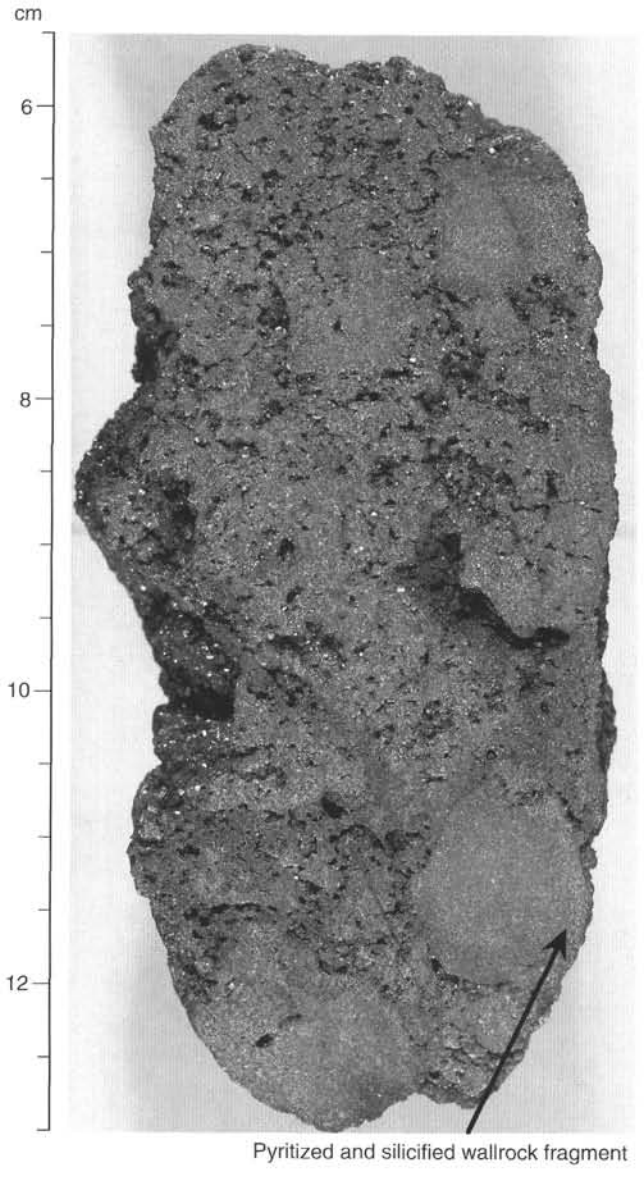

Figure 25. Massive granular pyrite (Type 5c) containing subrounded clasts of pyritized siliceous wallrock fragments. Sample 158-957M-7R-1 (Piece 2, 5–13 cm).

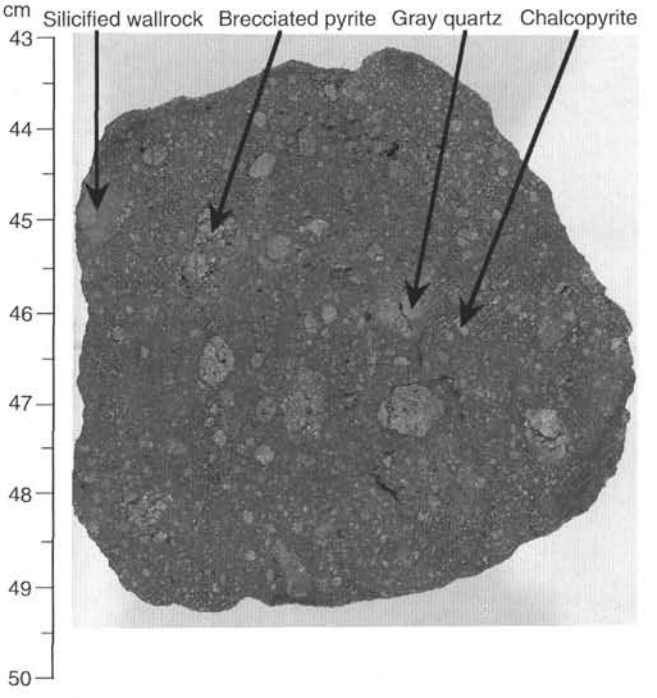

Figure 26. Fine-grained, pyrite-silica breccia (Type 9a) dominated by subrounded to rounded pyrite clasts (commonly fractured) in a matrix of fine sandy pyrite and silica. Silicified wallrock clasts and chalcopyrite aggregates (labeled) occur. Sample 158-957M-2R-1 (Piece 10, 43–50 cm).

wt%) and Fe (34.0 and 23.7 wt%), respectively. This indicates that these samples contain lower amounts of pyrite, but larger proportions of silica. They also have lower Zn (0.87 and 0.04 wt%) but higher Cu (1.6 and 1.4 wt%) concentrations. Sample 158-957M-3R-1 (Pieces 14 and 28) has the highest Ag concentrations observed in the sulfide-rich rocks from the TAG-4 area, ranging from 26 to 47 ppm.

Chemical Variations Along a Stratigraphic Profile of the TAG-4 Area

In general, samples from the TAG-4 have significantly higher concentrations of Zn, Pb, Ag, and Cd than those of the TAG-1 area. Furthermore, compared to Fe-Cu-Zn-rich sulfides from the Kremlin (TAG-2) area, the rocks from the TAG-4 area are generally Fe- and Zn-rich, but Cu-poor. The chemical variation down a stratigraphic profile of the TAG-4 area is shown in Figure 32. One feature is the increasing Ag content from the surface down to intermediate depths of about 15 mbsf. The highest Ag concentration at TAG-4 was determined in the pyrite-silica breccia at 15.5 mbsf (Sample 158-957M-3R-1, Piece 28). Further down the stratigraphic column, the pyrite-silica breccia grades into massive granular pyrite and the Ag concentration decreases to the low values (<14 ppm) found in the rocks of other areas of the TAG hydrothermal mound. The massive pyrite zone from 0.24 to 14.8 mbsf has high Pb contents (123–218 ppm); however, below 15 mbsf, Pb concentrations again decrease to low levels of 61 to 14 ppm. Zn and Cd display a similar pattern, but the variation is more erratic in the massive pyrite zone. In contrast, the highest Cu concentrations (1.35–1.84 wt%) occur in the lower part of the stratigraphic column, that is, below 15 mbsf. Sulfur and Fe concentrations do not show a systematic variation with depth.

Summary

Samples recovered from the TAG-4 area show significantly higher amounts of sphalerite, marcasite, and amorphous silica and lower amounts of anhydrite than samples drilled elsewhere on the mound. Marcasite, sphalerite, and pyrite-rich samples that exhibit probable flow channels are similar in texture and mineralogy to marcasite-rich sulfide crust samples recovered by submersible from the surface of the Black Smoker Complex (Tivey et al., 1995). The presence of significant amounts of amorphous silica could indicate conductive cooling of black smoker fluid. Textural and mineralogical similarities between red and gray cherts and red and gray quartz samples suggest that they are genetically related. The difference in grain size might be explained by recrystallization. Moreover, the recrystallized cherts (now quartz) occur only at depth. The red cherts form near the surface, either on the mound (explaining their distribution in the upper mound section), or as interpillow precipitates (now recrystallized and associated with silicified wallrock fragments). There are clear parallels with the distribution of chert in Hole 957B in the TAG-2 area,

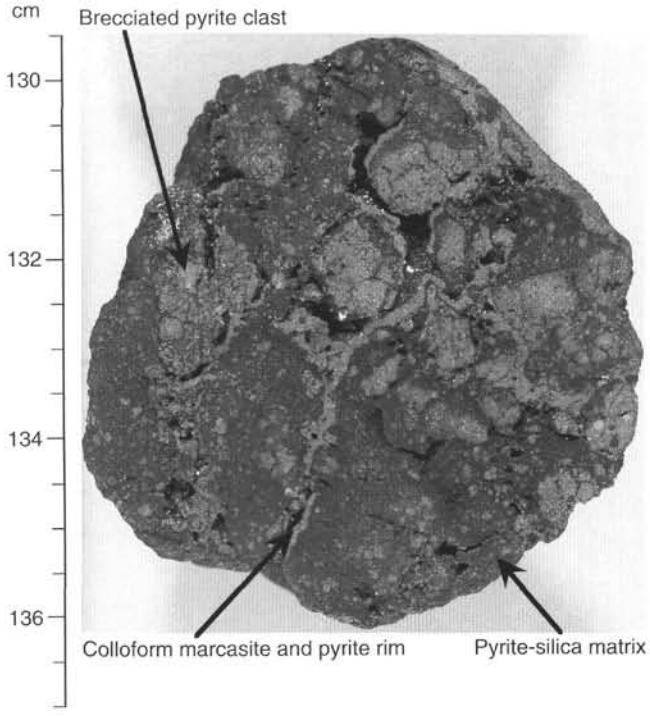

Figure 27. Coarse-grained pyrite-silica breccia (Type 9a) with abundant massive pyrite clasts (locally fractured) in a vuggy, dark gray, silica matrix. Vugs are lined by coarse-grained marcasite (labeled) and in places by later euhedral pyrite. Sample 158-957M-3R-1 (Piece 30, 129.5–137 cm).

where cherts occur close to the mound surface and also within the basalt sequence (see "Sulfide Petrology and Geochemistry" section, Chapter 8, this volume).

The other major lithologies present in cores taken from the TAG-4 area are massive pyrite, pyrite-silica breccia, silicified wallrock breccias, chloritized basalt breccias, and basalt. Massive granular pyrite seems to have formed by recrystallization of the porous massive marcasite and pyrite, but it also incorporates pyritized silicified wallrock fragments. Pyrite-silica breccias from the TAG-4 area contain clasts derived from both surface hydrothermal processes (e.g., cherts) and subsurface alteration processes (e.g., silicified wallrock). The fine-grained pyrite-silica breccias in samples from the TAG-4 area resemble those recovered from Holes 957C, 957F (TAG-1), and 957H (TAG-2). Pyrite-silica breccias in the TAG-1 and TAG-2 areas, however, are overlain by pyrite-anhydrite breccias and underlain by silicified wallrock and chlorite basalt breccias. In the TAG-4 area, a late phase of mound mineralization appears to have been superimposed on the breccia assemblage, with the deposition of silica and colloform marcasite and pyrite. Sphalerite and traces of chalcopyrite are related to this process. This mineral assemblage was sampled near the surface of the mound in cores from Holes 957I, 957J, and 957K. In the TAG-4 area the sicilified wallrock breccias grade down into chloritized basalt breccias from approximately 30 to 40 mbsf. Weakly altered basalt occurs below the chloritized basalt beccias. Quartz-pyrite stockwork veining is not as well developed in the TAG-4 area as compared with the TAG-1 area.

The absence of anhydrite in samples recovered from the TAG-4 area could be explained by several processes (e.g., a lack of seawater being entrained into the mound at this location, thus preventing the high sulfate concentrations needed for the deposition of anhydrite). Alternatively, the temperature at which the mixing of seawater and

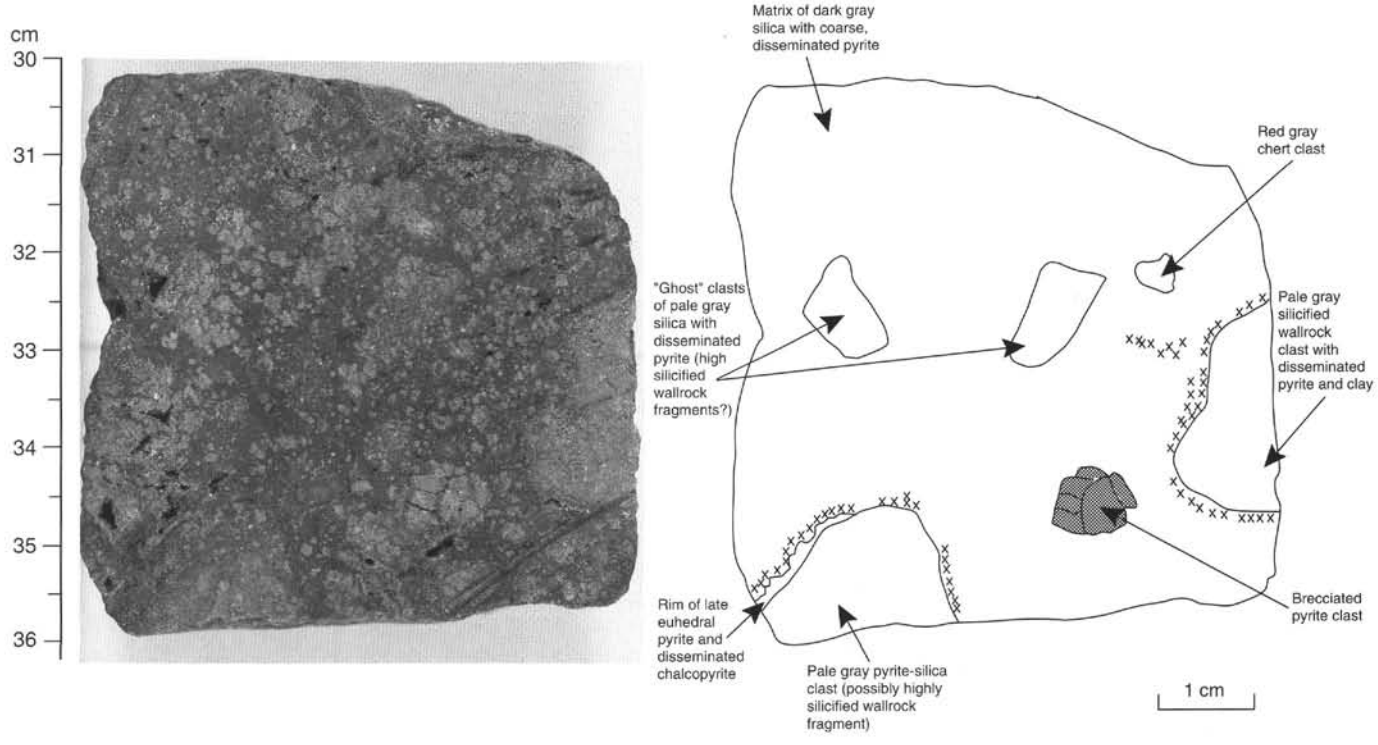

Figure 28. Photograph and sketch of fine-grained pyrite-silica breccia (Type 9a) with abundant silicified wallrock fragments. Chalcopyrite is enriched near the silicified wallrock fragments. Some vugs are lined with late marcasite. Sample 158-957M-1R-2 (Piece 7, 30–36 cm). Cross-hatching indicates chalcopyrite distribution.

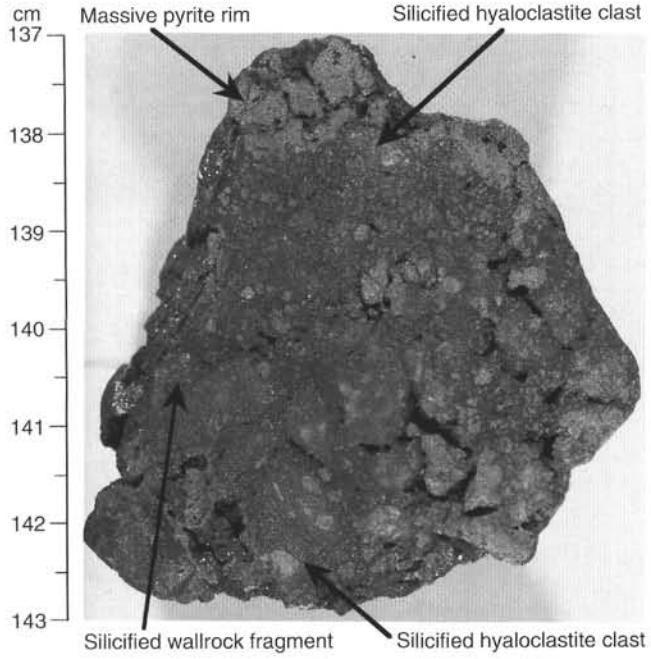

Figure 29. Pyrite-silica breccia (Type 9a) with large silicified wallrock clasts containing angular pieces of altered, silicified hyaloclastite (labeled). Sample 158-957M-3R-1 (Piece 31, 137–143 cm).

hydrothermal fluid occurs is not high enough to precipitate anhydrite (<150°C). This would suggest that conductive cooling of the hydrothermal fluids took place before they were mixed. It is also possible that previously abundant anhydrite has been dissolved during the later history of this part of the mound. However, only traces of chalcopyrite, which can be an abundant constituent of the anhydrite-vein selvages in the other areas and is not affected by dissolution, are found in material recovered from the TAG-4 area. A final possibility is that anhydrite is present but that it was selectively not recovered (recovery for the TAG-4 area is 9.2%). However, in other areas drilled on the mound, with similar low recovery (TAG-1 area, 14.5% recovery; TAG-2 area, 5.9% recovery), anhydrite is always present in at least small amounts.

HYDROTHERMAL ALTERATION

Basaltic material was recovered in Holes 957I and 957M in the TAG-4 area on the eastern side of the Black Smoker Complex (see Fig. 3, Chapter 1, this volume). Only vestiges of extremely altered basalt were observed in a thin section from near the top of Hole 957I. In Hole 957M, silicified basaltic clasts are common in the pyrite-silica breccias throughout the hole, in silicified wallrock breccias below 20 mbsf, and as moderately altered basalt with totally chloritized alteration halos along fractures from 43 mbsf to the bottom of the hole at 51.2 mbsf (Cores 158-957M-9R and 10R).

In Hole 957I, which was cored only from 9.0 to 13.5 mbsf (Fig. 2), evidence for the presence of basaltic material comes from a single thin section from near the top of the core (Sample 158-957I-1N-1, Piece 12, 75–76 cm). This sample contains a 5-mm clast, which consists of 0.01- to 1-mm subhedral grains and aggregates of pyrite intergrown with 10- to 200-µm anhedral quartz (Fig. 33). A brown phyllosilicate occurs in the interstices of the pyrite grains and aggregates, and in 10- to 100-µm patches intergrown with pyrite and "dirty" quartz, filled with micrometer-sized inclusions (of fluid?, clays?, or leucoxene?) (Fig. 34). The textures observed in this clast are identical to those interpreted to be the result of total alteration and silicification of basalt clasts in other drill core from the TAG mound (see "Hydrothermal Alteration" sections, Chapters 7 and 8, this volume).

Silicified basalt fragments are common in the pyrite-silica breccias throughout Hole 957M, beginning in Core 158-957M-1N-1 (from <9.3 mbsf; see Table 2, in back pocket, and Fig. 2). Although some of the pieces of pyrite-silica breccia in Hole 957M consist of up to 50% or more silicified basalt fragments, these pieces differ from siliceous wallrock breccias in other holes from the TAG mound because the clasts in the pyrite-silica breccias from Hole 957M are rounded and may be reworked, rather than angular to rounded and commonly brecciated in situ, as observed in the other cores (see "Hydrothermal Alteration" sections, Chapters 7 and 8, this volume). The silicified clasts in the pyrite-silica breccias of Hole 957M are 0.1–3 cm across, gray to buff, rounded and hard, in a matrix of dark gray, fine-grained quartz and 0.1- to 1.5-cm-diameter grains and aggregates of pyrite (see Fig. 28). The basalt is totally replaced by quartz, fine-grained pyrite, and buff to tan phyllosilicate (chlorite?) (Fig. 35). Fine-grained pyrite occurs disseminated in the clasts and replacing plagioclase microlites; it is commonly surrounded by quartz. Many clasts are totally replaced by quartz and pyrite, with or without millimeter-sized patches of tan clay, but with no relict basaltic texture observable in hand specimen. The various clasts are identical to those observed in cores drilled from other holes in the TAG mound. Many of the silicified basalt clasts in Hole 957M have 1- to 3-mm-thick rims of pyrite, which may be in part replacements of the clast margins by pyrite, but may also be remnants of pyrite veins. The clasts are commonly cut by <1-mm-thick pyrite and 1- to 3-mm-thick quartz + pyrite veins. No clear relationship between veins and matrix material was observed.

In thin section (Sample 158-957M-1R-2, Piece 7, 34–36 cm), the clasts are intensively silicified, with 10-µm to 5-mm, subhedral, pyrite grains and aggregates intergrown with 20- to 500-µm quartz. The quartz appears dirty and contains abundant micrometer-sized inclusions (of fluid?, leucoxene?, and/or clays?). Also present are 10- to 100-µm-diameter patches of brown clay (chlorite?, illite?, or mixed layer phases?) intergrown with the dirty quartz. The clasts are rimmed by a 0.2- to 1-mm-thick layer of pyrite with or without an outer 0.1- to 0.5-mm-thick layer of chalcopyrite. The matrix consists of 10- to 400-µm anhedral to subhedral quartz intergrown with 0.01- to 1-mm subhedral grains and aggregates of pyrite, plus small amounts of 0.05- to 2-mm subhedral to euhedral grains and aggregates of chalcopyrite. Veins of chalcopyrite (100–200 µm thick) cut the pyrite rims on basalt clasts.

Silicified wallrock breccias occur in Hole 957M, interspersed with intervals of pyrite-silica breccia, from ~24 to ~42 mbsf (Section 158-957M-4R-1 through Sample 158-957M-9R-1, Piece 4; see Fig. 2; Table 2 [in back pocket]). The silicified wallrock breccias in Hole 957M are generally similar to those recovered from the TAG-1 and TAG-2 areas, but those from Hole 957M are softer and less intensively silicified. Angular, gray clasts, 1–5 mm across, occur in a matrix of gray to white quartz and pyrite (Figs. 36, 37). The matrix is generally more pyrite rich than in similar breccias from elsewhere in the TAG mound. The clasts are generally hard and silicified, and contain abundant pyrite disseminated in the matrix. The buff to gray color of the groundmass suggests replacement by chlorite, as observed in thin sections of core from elsewhere on the mound (see "Hydrothermal Alteration" sections, Chapters 7 and 8, this volume). Some round vesicles are filled with gray quartz. Locally, a white phyllosilicate is present in samples containing chloritized and silicified glass fragments (e.g., Samples 158-957M-5R-1, Piece 6, and 9R-1, Piece 3). Below 38 mbsf, basalt clasts are generally less intensively silicified, and several pieces are classified as chloritized basalt (Samples 158-957M-7R-1, Pieces 5 and 6; 8R-1, Piece 3; and 9R-1, Piece 3).

Altered basalt clasts also occur rarely in massive pyrite in Hole 957M. Several 1-cm-diameter, rounded, silicified basalt clasts, intensively replaced by pyrite, occur in a piece of massive granular pyrite

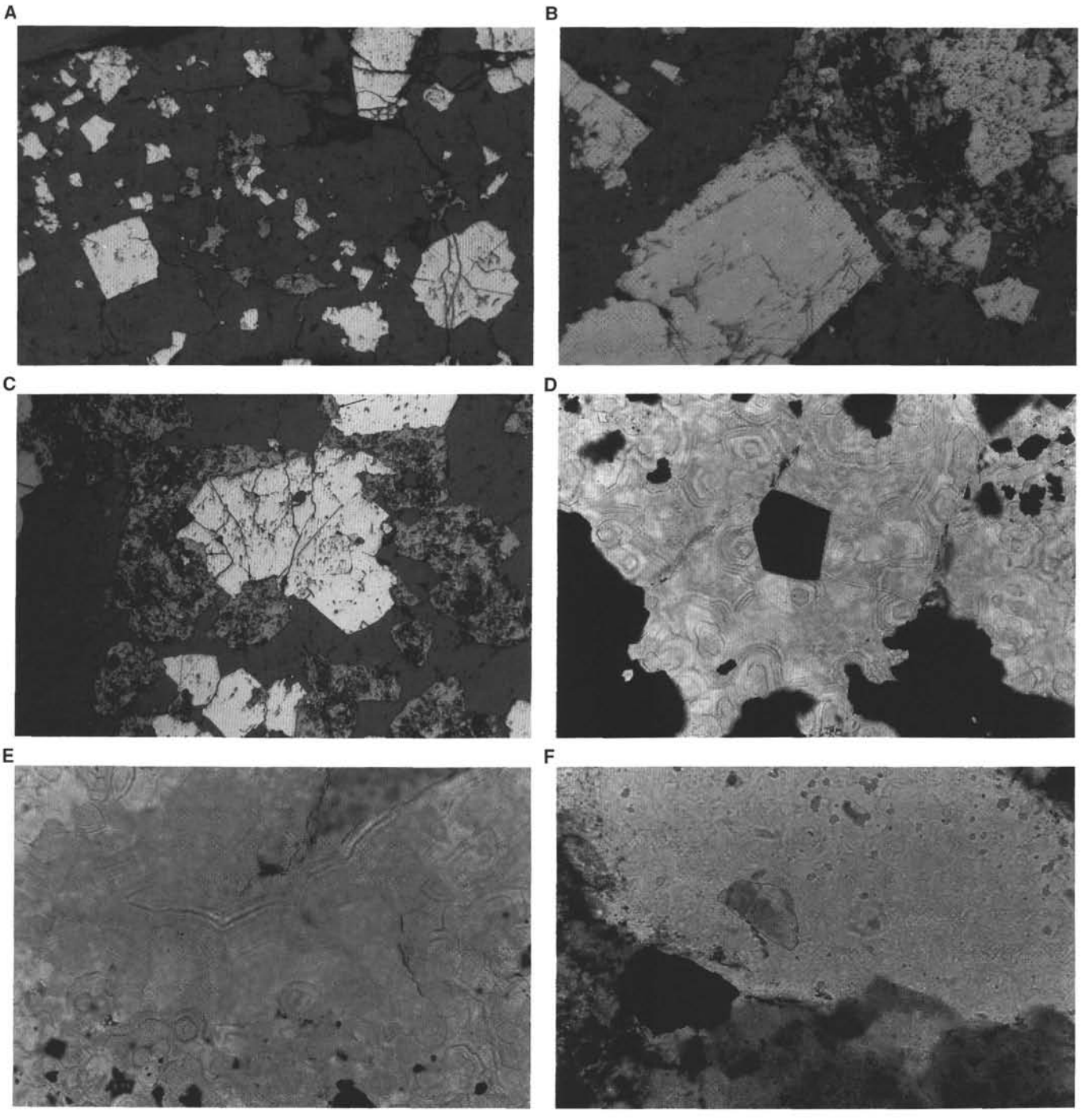

Figure 30. Thin-section photomicrographs of pyrite-silica breccias. **A.** Pyrite (white) as euhedral crystals and aggregates disseminated in quartz (dark gray). Chalcopyrite (medium gray) occurs as anhedral grains interstitial to quartz. Reflected light, field of view = 1.5 mm. Sample 158-957M-3R-1 (Piece 30, thin section from 134 to 136 cm). **B.** Two generations of euhedral pyrite growth (white) intergrown with quartz (dark gray) and chalcopyrite (medium gray, poor polish). Contacts between pyrite and quartz are corroded. Chalcopyrite (medium gray, pitted surface) occurs as inclusions in pyrite or interstitial to quartz and pyrite. Reflected light, field of view = 1.5 mm. Sample 158-957M-3R-1 (Piece 30, thin section from 134 to 136 cm). **C.** Intergrowth of pyrite, quartz, and chalcopyrite, with chalcopyrite replacing pyrite (arrows). Reflected light, field of view = 1.5 mm. Sample 158-957M-3R-1 (Piece 30, thin section from 134 to 136 cm). **D.** Euhedral pyrite (black) in a matrix of zoned euhedral quartz (light gray), microcrystalline quartz, and chalcedony. Transmitted light, field of view = 750 µm. Sample 158-957M-3R-1 (Piece 30, thin section from 134 to 136 cm). **E.** Closeup of silica textures. Very fine banding in chalcedony and microcrystalline quartz filling open spaces (central part of photo) after deposition of euhedral quartz with pyrite inclusions (black, lower part of photo). Transmitted light, field of view = 750 µm. Sample 158-957M-3R-1 (Piece 30, thin section from 134 to 136 cm). **F.** Inclusion of corroded, high-birefringence mineral (anhydrite?) in coarse-grained quartz. Transmitted light, field of view = 750 µm. Sample 158-957M-1R-2 (Piece 7, thin section from 34 to 36 cm).

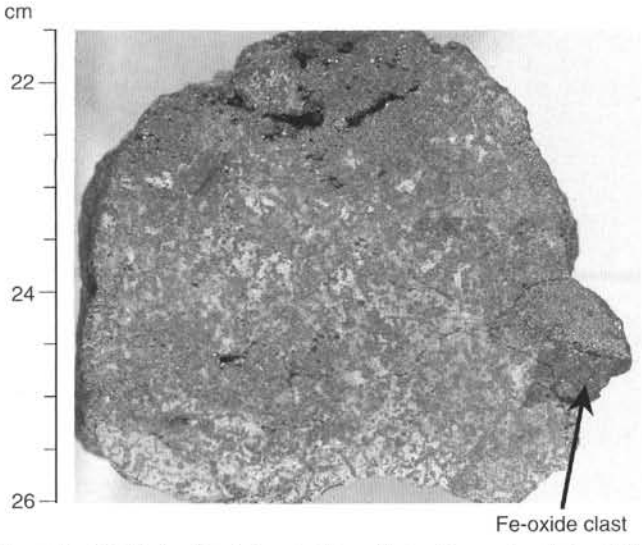

Figure 31. Silicified wallrock breccia (Type 10a), with angular, dark red, Fe-oxide clast, probably representing interpillow chert. Sample 158-957M-8R-1 (Piece 5, 21–26 cm).

in Hole 957M (Fig. 25). One 2-cm piece of massive granular pyrite contains interstitial white phyllosilicate; it could be either a nearly totally pyritized basalt fragment or possibly a fragment of a vein of massive pyrite (see below).

The siliceous wallrock breccias are cut by several generations of quartz and pyrite veins. Pyrite veins (0.1–0.5 mm in size) are abundant in the silicified clasts and, in many cases, form interconnecting networks. Other 0.1- to 1-mm-thick pyrite veins are commonly rimmed by 0.1- to 0.5-mm-wide bands of quartz, which may be replacing the adjacent basalt wallrock, as was observed in thin sections from other cores drilled from the TAG mound (see "Hydrothermal Alteration" sections, Chapters 7 and 8, this volume). White quartz veins, 0.1–2 mm in thickness, are common and, in at least one case, have cut earlier fine pyrite veins (Fig. 37). Slightly larger, 2- to 3-mm-thick quartz plus pyrite (± rare white phyllosilicate) veins are also common, in some cases with millimeter-wide silicification halos (e.g., Sample 158-957M-7R-1, Piece 5). Commonly vuggy, pyrite veins (1–7 mm wide) are present in many clasts; in many cases, the pyrite replaces the basaltic wallrock selvages (Fig. 37; Samples 158-957M-5R-1, Pieces 8, 9, and 13; 6R-1, Piece 6; 7R-1, Piece 3; 8R-1, Pieces 4, 5, and 8; and 9R-1, Pieces 3 and 4). Pyrite also commonly forms 1- to 3-mm-thick rims on silicified basalt clasts, partly replacing the clast margins (Fig. 38; Samples 158-957M-4R-1, Piece 12;

Table 3. AAS and CHNS analyses of rock samples from Holes 957I, 957K, and 957M in the TAG-4 area.

Core, section, interval (cm)	Size fraction or piece no.	Depth (mbsf)	Type	Rock type	S (wt%)	Fe (wt%)	Zn (wt%)	Cu (wt%)	Pb (ppm)	Ag (ppm)	Cd (ppm)
158-957I-											
1N-1, 33–41	6	9.33	5a	Porous massive pyrite	49.7	45.7	3.54	0.13	107	18	46
158-957K-											
1X-1, 24–29	4	0.21	5a	Porous massive pyrite	45.8	39.5	3.00	0.05	218	21	57
2N-1, 37–41	9	10.37	5	Massive pyrite	50.8	42.6	0.76	1.11	123	19	14
3X-1, 36–38	7	14.82	5	Massive pyrite	49.5	42.6	3.74	0.08	170	17	167
158-957M-											
1R-1, 16–47	>420 µm	0.16	1	Drill cuttings, Fe-oxides	0.9	51.7	0.06	0.09	46	9	<0.1
1R-1, 16–47	420–63 µm	0.16	1	Drill cuttings, Fe-oxides	1.2	52.4	0.07	0.19	101	5	0.5
1R-1, 16–47	<63 µm	0.16	1	Drill cuttings, Fe-oxides	4.7	51.5	0.28	0.29	132	12	5
3R-1, 57–60	14	14.87	9a	Pyrite-silica breccia	49.8	40.5	4.30	0.37	98	26	43
3R-1, 123–125	28	15.49	9a	Pyrite-silica breccia	40.2	34.0	0.87	1.61	35	47	22
5R-1, 90–92	15	25.18	9a	Pyrite-silica breccia	26.1	23.7	0.04	1.35	14	14	<0.1
8R-1, 0–4	1	38.30	5c	Massive granular pyrite	41.0	38.4	0.71	1.84	61	9	10

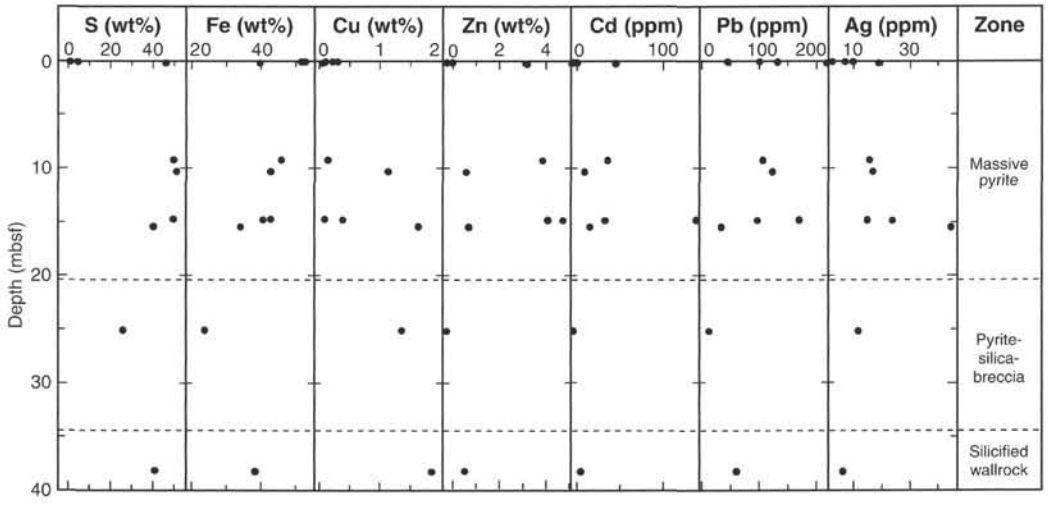

Figure 32. Variations in S, Fe, Cu, Zn, Cd, Pb, and Ag down a stratigraphic profile of the TAG-4 area. The stratigraphy is based on cores recovered from Holes 957I, 957K, and 957M. The data are summarized in Table 3.

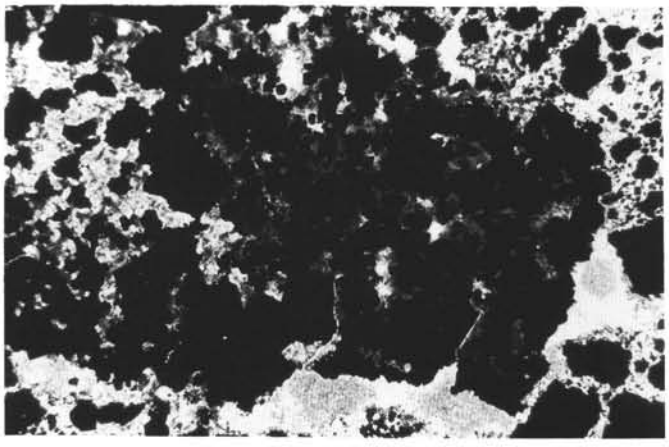

Figure 33. Overall view of an argillized, silicified, and pyritized basaltic clast, with an unidentified clay mineral, quartz, and disseminated pyrite replacing the basalt. Field of view = 6 mm. Sample 158-957I-1N-1 (Piece 12, 75–76 cm).

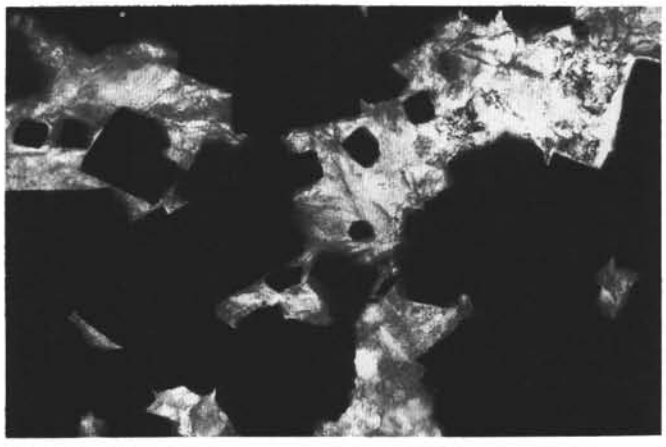

Figure 34. Closeup view of the silicified part of the basaltic clast showing platy phyllosilicates, and the "dirty" quartz (i.e., anhedral quartz crystals commonly with aligned submicroscopic inclusions), platy phyllosilicates and euhedral pyrite crystals. Field of view = 1.5 mm. Sample 158-957I-1N-1 (Piece 12, 75–76 cm).

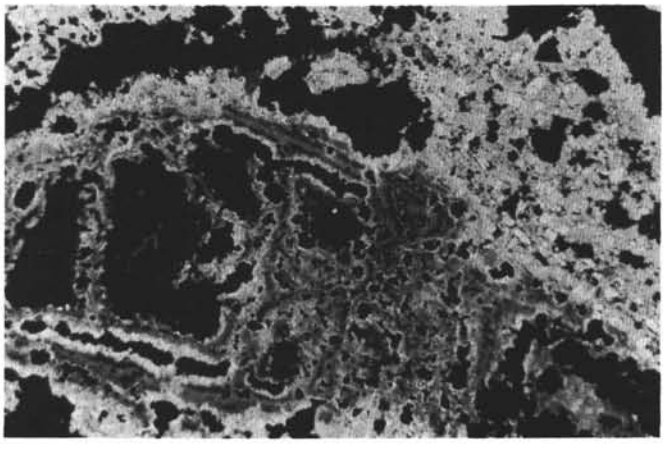

Figure 35. A silicified and pyritized glass clast, about 7.5 mm in length, exhibiting concentric pyrite and quartz bands, the latter with numerous clay mineral inclusions. Field of view = 6 mm. Sample 158-957M-1R-2 (Piece 7, 34–36 cm).

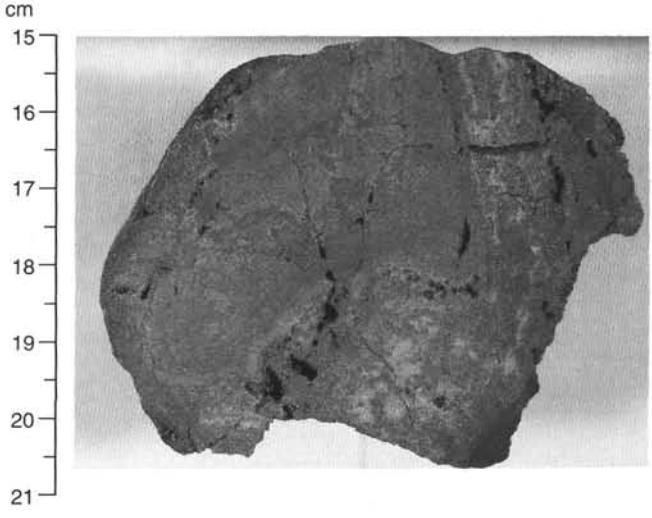

Figure 36. Silicified basalt clast in white quartz plus pyrite matrix from a pyrite-silica breccia. A 3-mm-wide vuggy pyrite vein (top) cuts the quartz plus pyrite matrix, and clast is rimmed and partly replaced by a 1- to 3-mm-wide band of pyrite (bottom). Sample 158-957M-6R-1 (Piece 4, 15–21 cm).

5R-1, Pieces 2, 6, and 14; 6R-1, Piece 4; and 7R-1, Piece 6). In one case, a 3-mm-thick pyrite plus quartz vein is cut by a vuggy 5-mm-thick pyrite vein, which also partly replaces wallrock along the pyrite vein (Fig. 38). In another case, a vuggy 1- to 3-mm-thick pyrite vein cuts the quartz plus pyrite breccia matrix (Fig. 36). Chalcopyrite appears to be a late phase, as observed in thin section and in hand specimen of at least one sample, where a 1-mm-thick chalcopyrite vein cuts across and fills the center of a 1-cm-wide pyrite vein (Sample 158-957M-8R-1, Piece 7).

The vein sequence in Hole 957M cores is generally similar to that observed in Holes 957C and 957E (see "Hydrothermal Alteration" section, Chapter 7, this volume). In cores from Hole 957M, three general stages were observed:

1. Early fine pyrite veins formed in the rocks, and chloritization of the rocks may have occurred at this time.
2. Quartz veins and quartz plus pyrite veins formed in the rocks, cutting earlier fine pyrite veins. Silicification halos formed along some veins, and chloritization of the rocks may have proceeded associated with this veining. The quartz plus pyrite breccia matrix may also have formed at this time.
3. Vuggy pyrite veins cut earlier veins, cut across the quartz plus pyrite matrix, and the wallrocks of the vuggy pyrite veins were pyritized. Late chalcopyrite may also have formed during the latter part of this vein stage. The late chalcopyrite veins may be similar to the late anhydrite-chalcopyrite-pyrite veins from the TAG-1 and TAG-2 areas, but no anhydrite is associated with the late chalcopyrite veins from Hole 957M.

The above sequence of veins was derived from combined crosscutting relationships of veins observed in many samples; however, many veins show no relationship to other veins, so multiple stages of pyrite and quartz veining could have occurred. For example, some brecciated basalts are cemented by pyrite, but others are clearly cemented by quartz plus pyrite. At the scale of observation in the

Figure 37. Silicified wallrock breccia, showing angular silicified basalt clasts in matrix of pyrite and quartz veins. White quartz vein at bottom cuts earlier vuggy pyrite veins. Pyrite replaces wallrock along the vuggy pyrite veins. Sample 158-957M-5R-1 (Piece 13, 73–79 cm).

drill core, it is difficult in many cases to distinguish between matrix and veins.

Mostly dark gray basalt, with variously colored, 1- to 15-mm-wide alteration halos, occurs from 42 mbsf to the bottom of Hole 957M at 51.2 mbsf (Cores 158-957M-9R and 10R; see Fig. 2). The mainly dark gray basalt occurs in Section 158-957M-9R-1 (Pieces 5–20) and throughout most of Core 158-957M-10R (except for two pieces), comprising about 95% of the basalt in this interval. In hand specimen, the dark gray basalt is slightly to moderately altered (~20%), with a light green smectite filling vesicles. Uniformly dark gray fragments are present (Samples 158-957M-9R-1, Pieces 8, 13, 15, 17, and 18; 10R-1, Pieces 2, 3, 5, and 14; and 10R-2, Piece 8), but some of these have <1-mm-thick red Fe-oxide/oxyhydroxide coatings on their outer surfaces. Other dark gray basalt fragments in Cores 158-957M-9R and 10R display various combinations of 1- to 5-mm-wide red, black, and green alteration halos around central portions of dark gray basalt (Figs. 39–41).

Red alteration halos, 2 mm wide, occur around dark gray basalt in several pieces (Fig. 39; Samples 158-957M-10R-1, Pieces 6, 7, 9, 10, 16, and 18). The outer surfaces of some of these have <1-mm-thick red to orange to slightly green coatings, which may be the remnants of veins. Several pieces exhibit 1- to 3-mm-wide, dark gray to black, alteration halos along exposed surfaces (Samples 158-957M-9R-1, Pieces 7 and 9; and 10R-1, Piece 13), and in one case, along a 0.5-mm-wide vein filled with chlorite, pyrite, amorphous silica, and quartz (Fig. 40). Still other pieces exhibit combined red and black halos, with a 2-mm-wide inner black halo surrounding dark gray basalt, and a 1- to 2-mm-wide outer red halo along the exposed surfaces (Samples 158-957M-9R-1, Pieces 19, 20; and 10R-1, Pieces 1, 8). Green halos also occur in one sample with a 3-mm-wide green halo alone (Sample 158-957M-10R-1, Piece 2); in other samples, however, 2- to 5-mm-wide inner green halos surround dark gray basalt and are bounded on the outside by 1-mm-wide external red halos (Samples 158-957M-9R-1, Pieces 10, 11, 14; and 10R-1, Pieces 11, 15, 20, 21). In several pieces, dark gray basalt is enclosed by 2- to 3-mm-wide black halos, which grade outward through diffuse contacts into

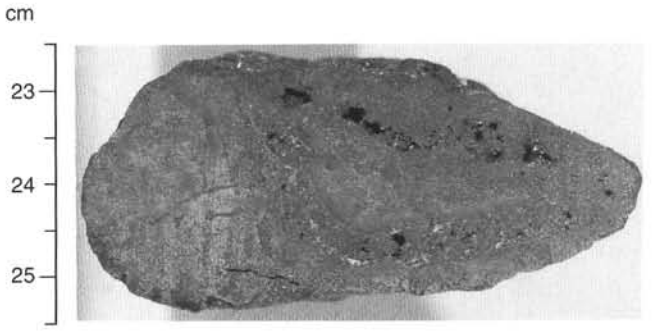

Figure 38. Pyrite plus white quartz vein (center) through basalt clast. Vuggy pyrite vein (3 mm wide) at top cuts earlier quartz plus pyrite vein, and pyrite replaces silicified basalt wallrock along vuggy pyrite vein. Sample 158-957M-7R-1 (Piece 5, 19.5–22.5 cm).

2- to 3-mm-wide outer green halos (Fig. 41; Samples 158-957M-9R-1, Pieces 10, 11, 14; and 10R-1, Pieces 11, 15, 20, 21). In some cases, these black halos contain traces of disseminated red Fe-oxides/oxyhydroxides, whereas the outer green halos contain disseminated pyrite. One piece displays a slightly different combination of halos, with dark gray basalt surrounded by a 3-mm-wide black halo that grades outward into a 5-mm-wide green halo, which is then surrounded on the outer edges of the piece by a 2-mm-wide red halo (Sample 158-957M-10R-2, Piece 5). Several pieces display multiple black and green alteration halos (Samples 158-957M-9R-1, Pieces 5, 6, 15, 16; and 10R-2, Piece 3), which consist of four to six bands, 1–2 mm wide, of alternating black and green halos.

In thin section, the dark gray basalts are partly altered (~20%). Vesicles are filled with colorless to pale green to tan smectite (saponite?), and olivine is partly altered to the same minerals, rarely with small amounts of accompanying red iron oxyhydroxide. Small (10 µm thick) veinlets of tan smectite are also present in some samples. Disseminated pyrite is common, and chalcopyrite rare, both occurring as 1- to 20-µm-diameter grains and rare globules in interstitial areas, along micrometer-sized fractures, and rarely lining vesicles.

The millimeter-wide red halos are partly (20%–50%) altered in thin section, with vesicles filled and olivine partly to totally replaced by colorless to tan smectite. Red iron oxyhydroxides are also common with smectite replacing olivine in micrometer-sized fractures, and disseminated in the groundmass, imparting the red color to the rock. Sulfide minerals are absent in the red halo, probably as the result of oxidation to iron oxyhydroxides.

A 300- to 400-µm-wide vein of chlorite (or mixed-layer chlorite-smectite), plus amorphous silica overgrown by quartz, and pyrite is bounded by a 1- to 2-mm-wide dark green to black alteration halo in Sample 158-957M-9R-1 (Piece 12, 76–79 cm) (Figs. 42–44). The vein appears to have been filled first with chlorite, then reopened and filled with amorphous silica, pyrite, and quartz, with the quartz occurring as overgrowths on the amorphous silica. The black halo around the vein is more intensively altered (30%–50% altered) than the dark gray host rock. The phyllosilicate in the black halo may be mixed-layer chlorite-smectite, rather than smectite, as observed in the host rock. Disseminated 10- to 100-µm pyrite is common in interstitial areas and replacing groundmass in the black halo.

The green alteration halo of Sample 158-957M-9R-1 (Piece 12, 76–79 cm) (similar to that in Fig. 41) ranges from less altered (30%–50%) in the inner portion toward the basalt to more intensively altered toward the outer margins of the halo, ranging to 100% altered in the outermost 1–2 mm. Plagioclase is partly to totally replaced by colorless to green chlorite, and olivine is totally replaced by chlorite (or mixed-layer chlorite-smectite), iron oxyhydroxides, and pyrite. Vesicles are commonly zoned, with an outer rim of brown smectite and inner core of green chlorite. Pyrite and lesser chalcopyrite are

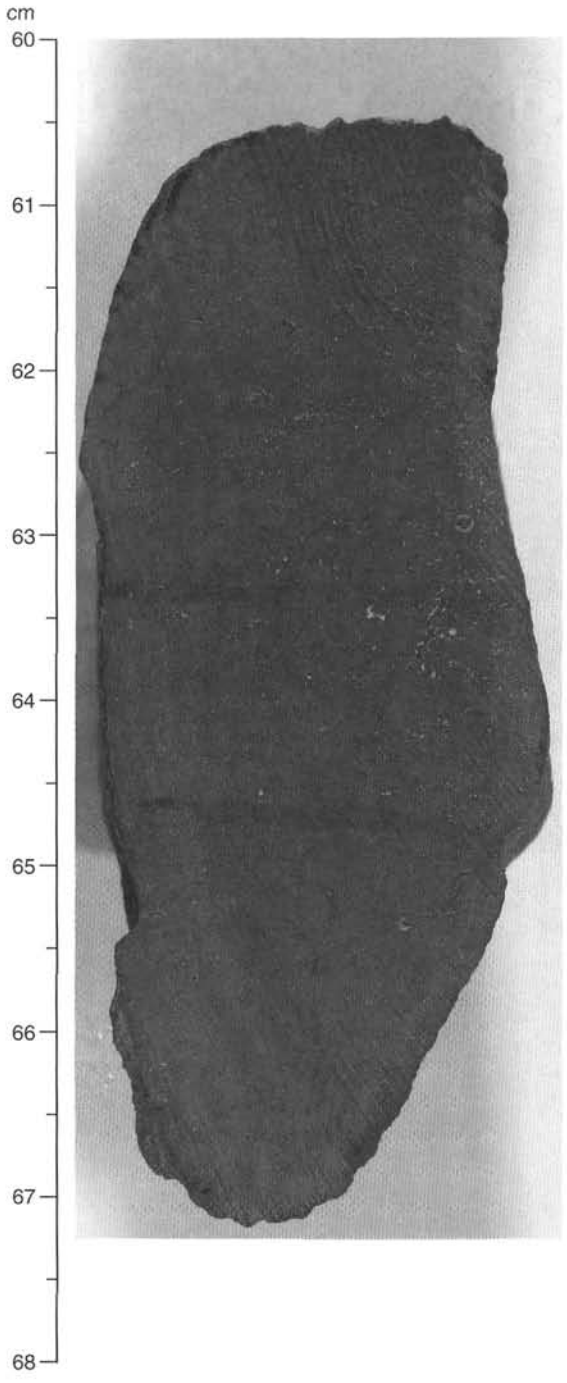

Figure 39. Dark gray, partly altered basalt rimmed by 1- to 3-mm-wide, red alteration halo (lighter gray) along exposed outer surfaces of basalt fragment. Sample 158-957M-10R-1 (Piece 9, 60–68 cm).

common as 5- to 100-µm-diameter grains disseminated in interstitial areas and replacing groundmass and olivine.

Other hydrothermally altered basalts were also recovered from the base of Hole 957M. A chloritized variolitic to holohyaline pillow rim is shown in Figures 45, 46, and 47. A 1 × 2 cm piece of light green, totally chloritized basalt in Section 158-957M-10R-2 (Piece 7) contains abundant disseminated pyrite and is cut by a 2- to 3-mm-wide quartz + pyrite vein (Fig. 48). Sample 158-957M-10R-1 (Piece 17) is a 3 × 4 cm clast of gray granular quartz with disseminated pyrite that

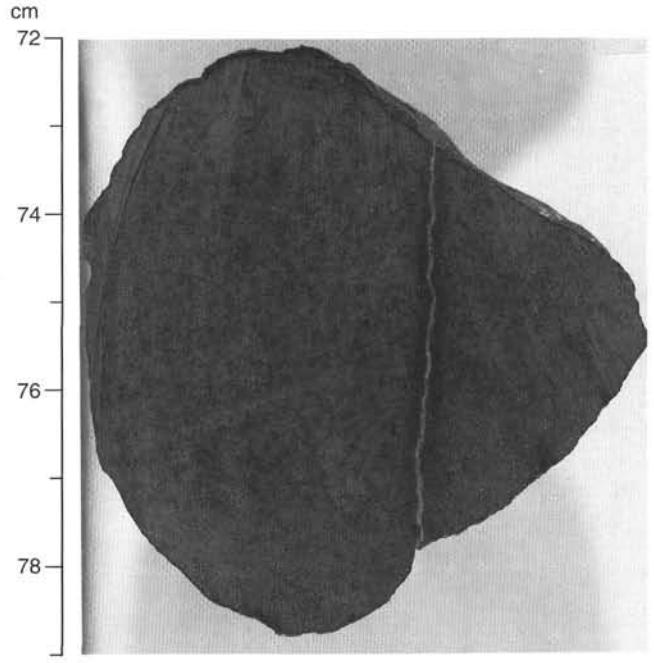

Figure 40. Dark gray, partly altered basalt cut by 1-mm-thick vein of chlorite, pyrite, amorphous silica, and quartz. A 1-mm-wide, black, chloritic alteration halo is present along both sides of the vein. Sample 158-957M-9R-1 (Piece 12, 72–79 cm).

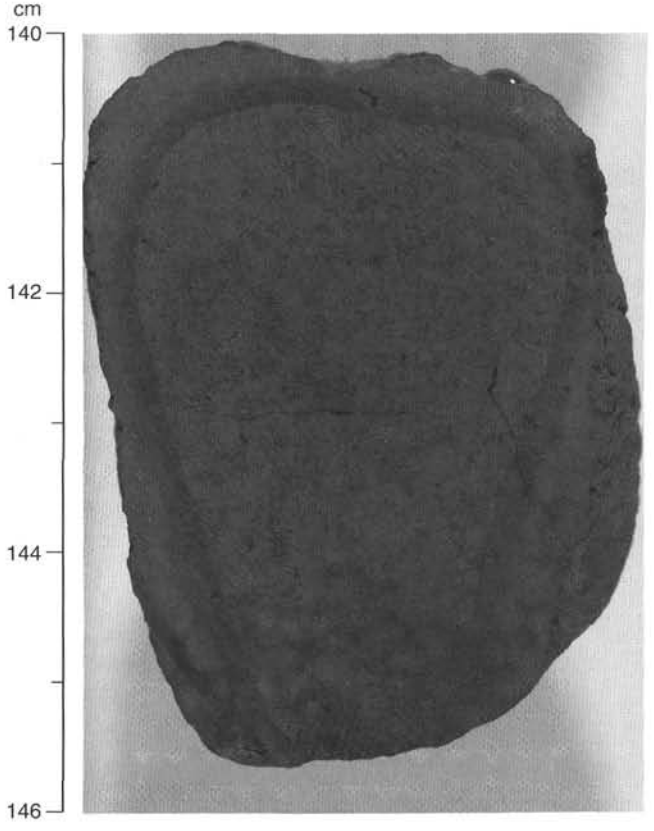

Figure 41. Dark gray, partly altered basalt, with 1- to 2-mm-wide, black alteration halo grading outward into a 2- to 3-mm-wide, green, chloritic alteration halo (see text for further description). Sample 158-957M-10R-1 (Piece 21, 140–146 cm).

Figure 42. Chloritized subvariolitic basalt with a 200- to 500-µm-thick vein of chlorite (or mixed-layer chlorite-smectite phase), with later amorphous silica, pyrite, and quartz. Both sides of the vein are bordered by 2.5-mm-thick, chloritized halos with disseminated pyrite. A vesicle at center is filled with chlorite. Field of view = 6 mm. Sample 158-957M-9R-1 (Piece 12, 72–79 cm).

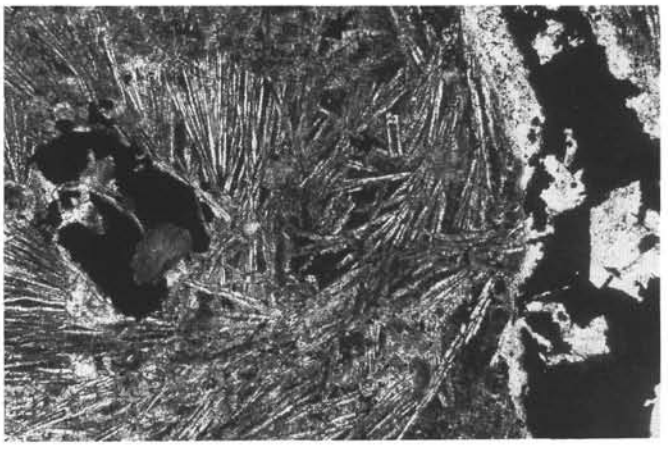

Figure 43. Close-up of the vein shown in Figure 42. On the left side, in the chloritized halo adjacent to the vein, a 300-µm olivine phenocryst is replaced by pyrite and chlorite. Field of view = 1.5 mm. Sample 158-957M-9R-1 (Piece 12, 72–79 cm).

has been locally stained red by iron oxide/oxyhydroxide. The quartz cements several 3- to 5-mm angular clasts of blue gray chloritized glass. This piece may be hydrothermally altered, recrystallized interpillow material, possibly with hydrothermal quartz and pyrite cement.

Interpretations

Altered basaltic material occurs approximately 20 m shallower in cores drilled from the TAG-4 area on the western side of the Black Smoker Complex than elsewhere on the mound (see "Stratigraphy" section, this chapter). The lowermost cores from Hole 957M record the effects of hydrothermal alteration beneath the margins of the mound, with chloritization of basalt along the edges of basalt fragments. Presumably, this is analogous to the earliest stages of alteration beneath the mound, as evidenced from the deeper cores from Hole 957E (TAG-1 area), where green chloritized rocks occur (see "Hydrothermal Alteration" section, Chapter 7, this volume). Based on the presence of chlorite, alteration temperatures were likely to have been at least 200°–250°C, and some magnesium must have been present, either from seawater or mobilized from basalts, to provide Mg for chlorite formation in veins and alteration halos. The presence of one totally chloritized basalt fragment as well as coarsely crystalline hydrothermal quartz in the deepest cores from Hole 957M indicate that hydrothermal circulation and alteration beneath the edges of the mound are highly variable locally. This is consistent with similar observations of basement alteration from Hole 957B (see "Hydrothermal Alteration" section, Chapter 8, this volume). More intensive chloritization and formation of gray to buff chlorite, as well as pyrite and perhaps some quartz veins in the overlying breccias, were probably related to upwelling high-temperature hydrothermal fluids (at temperatures up to ~350°C?). The formation of quartz plus sulfide veins and the concomitant silicification of the brecciated rocks may be related to the cooling and waning of circulation in this portion of the mound. The general decrease in hardness of the silicified basalt clasts downward in Hole 957M may be similar to the transition from silicified to chloritized basalts with depth in Hole 957E (see "Hydrothermal Alteration" section, Chapter 7, this volume). The smectitic alteration in the dark gray portions of the deepest basalts could be related to low-temperature alteration before chloritization or to later

Figure 44. Euhedral olivine phenocrysts are altered to colorless smectite (or talc?) along crystal outlines and cracks, in the dark gray portion of the rock, away from the vein of Figure 42. The olivine skeletal crystals are totally replaced by smectite. Field of view = 1.5 mm. Sample 158-957M-9R-1 (Piece 12, 72–79 cm).

stages. The red alteration halos around basalt fragments from the bottom of Hole 957M are probably lower temperature, seawater overprints on the higher temperature, vein-related, hydrothermal chloritization of the rocks, resulting in the oxidation of disseminated pyrite.

IGNEOUS PETROLOGY AND GEOCHEMISTRY

Hole 957M, on the western side of the Black Smoker Complex, intersected dark gray basalt at depths from 42 to 51.2 mbsf. The samples appear to be fragments of basalt pillows, as several of the pieces are rimmed by glassy rinds or are holohyaline. Texturally, these fragments are sparsely olivine phyric basalt and variably altered pillow basalt. A piece-by-piece description of these samples is given in Table 4. Although some fresh cut surfaces occur, many of the pieces do not appear to have been cored but, instead, to have been gathered into the core barrel as fragments. Some pieces have thin, green, alteration

Figure 45. Chloritized and silicified glassy pillow rim with holohyaline and variolitic textures, at right and left, respectively. The interstitial glass is totally replaced by phyllosilicate. Two elliptical vesicles (the largest one is 2.4 mm in length) are filled with a 25-µm-thick layer of colloform brown phyllosilicate along the walls, followed by chalcedony, and again brown phyllosilicate at the center. The glass surrounding the vesicles displays dark concentric alteration bands. Notice several fissures converging toward the largest vesicle, crossing through the altered glass bands, and opening into the vesicles. Some of these "feeders" initiated from the right side of the outer holohyaline rim of the pillow (i.e., out of the clast); the others are connected to a main fissure, which also initiated outside of the clast. Field of view = 6 mm wide. Sample 158-957M-10R-1 (Piece 19, 129–132 cm).

Figure 47. Chloritized glassy pillow rim with holohyaline texture. A few isolated varioles and one large (2.4-mm-long) vesicle are visible. The edge of the pillow rim and of the sample is at top. The altered glass displays finely zoned concentric alteration banding reminiscent of Liesegang rings. The smaller varioles are about 800 µm in diameter. A phyllosilicate-filled fissure runs down through the glassy rim to the right of the vesicle. Field of view = 6 mm. Sample 158-957M-10R-1 (Piece 19, 129–132 cm).

halos along exposed surfaces; in some cases, an intense alteration rind permeates the outer few millimeters of the core (see "Hydrothermal Alteration" section and Fig. 49).

Several of the basalt pieces recovered have less altered interiors (Fig. 49) and, on freshly broken surfaces, small (0.5 to 1 mm) pale green, translucent olivine crystals can be seen. Altered variolitic structures are common in several samples (Fig. 50) and are particularly visible in the silicified, chloritized, and pyritized basalt samples

Figure 46. Close-up of Figure 45, showing a "feeder" fissure crossing the altered interstitial glass with concentric alteration fronts (at left), then crossing the dark altered glass around the vesicle (at center), and finally opening into the vesicle. The fissure stops at the vesicle wall (i.e., under the first dark, colloform phyllosilicate layer). Field of view = 1.5 mm wide. Sample 158-957M-10R-1 (Piece 19, 129–132 cm).

(e.g., Samples 158-957M-9R-1, Piece 3; 10R-1, Piece 19; and 10R-2, Piece 7). Only a few small, round vesicles are present (<1 to 2 vol%, most <1 mm in diameter). These are commonly filled with a green phyllosilicate and are rarely encrusted with crystalline calcite.

Thin-section observations demonstrate that textures range from intergranular (Sample 158-957M-9R-1, Piece 5) to subvariolitic (Samples 158-957M-9R-1, Piece 12, and 10R-1, Piece 6) and variolitic (Sample 158-957M-10R-1, Piece 9). Plagioclase microlites are acicular to lath shaped, with some very rare hopper-shaped crystals. These crystals are fresh, more so in samples from the interiors of pieces. Olivine phenocrysts are significantly more altered than plagioclase microlites, although fresh olivine crystal cores are not uncommon. The groundmass of the sparsely phyric samples is primarily a mixture of microcrystalline to cryptocrystalline plagioclase, clinopyroxene, small interstices or pools of variably altered glass, and granular, fine-grained titanomagnetite. Rare, coarser, spinel grains were identified in hand specimen, but none were observed in thin section. Trace amounts of sulfide minerals (primarily pyrite) are present; these appear to be mainly related to alteration features, however, and are concentrated in the alteration halos. Groundmass in the holohyaline pillow rinds is pervasively altered basaltic glass, with rare plagioclase microlites.

The major and trace element composition of Sample 158-957M-10R-1 (Piece 6) is listed in Table 5. This basalt has a Mg# of 60.8 and contains 1.67 wt% TiO_2 and 2.42 wt% Na_2O. This composition is virtually identical to the basalt sample analyzed from Hole 957B. These values are indicative of N-type mid-ocean-ridge basalts (Basaltic Volcanism Study Project, 1981) with low Zr abundances of 80 to 109 ppm and high K to Ba ratios of 51 to 76.

PHYSICAL PROPERTIES

Introduction

From 4 holes (Holes 957I, 957J, 957K, and 957M) drilled at the TAG-4 site, 12 fragmentary samples and 2 minicores recovered from 14 sections (Table 6) have provided us with information on the index properties of rocks on the western side of the Black Smoker Complex. In addition, measurements of electrical resistivity and compressional (*P*-wave) velocity were made on 2 minicores extracted from altered basalt pieces from Hole 957M.

Holes 957I, 957J, and 957K

A sample of red and gray chert rimmed by sulfide (Sample 158-957J-1X-1, 1–3 cm) is characterized by relatively low bulk density (2.48 g/cm^3) and high porosity (9.02%). The remaining four samples from Holes 957I and 957K are composed of porous massive pyrite and show a narrow range of high values of bulk density (4.34–4.50 g/cm^3), combined with a range of high values of porosity (8.22% to 11.53%) (Figs. 51, 52).

Hole 957M

Seven sulfide fragments were analyzed from Hole 957M: four pyrite-silica breccia samples taken from 9.70 to 25.34 mbsf, and three silicified wallrock breccia samples taken from 29.40 to 38.68 mbsf. With the exception of the top sample from Hole 957M (Sample 158-957M-2R-1, 40–42 cm), the bulk and grain densities of the pyrite-silica breccia samples decrease with depth, whereas the silicified wallrock breccia samples show an increase of densities with depth (Fig. 51).

Figure 52 shows the relation between bulk density and porosity values for samples from the TAG-4 area. An increase in bulk densities of the pyrite-silica breccia samples is associated with an increase in total porosity, probably because of textural differences. Two of the silicified wallrock breccia samples (Samples 158-957M-7R-1, 19–21 cm, and 8R-1, 38–40 cm) recovered at 34.49 and 38.68 mbsf have bulk densities greater than 4.2 g/cm^3 and relatively high values of porosity (7.3% and 6.5%) (Table 6 and Fig. 52).

Moderately altered basalts encountered at about 43 mbsf in Hole 957M exhibit properties typical of this rock type, based on measurements on two minicores (Samples 158-957M-9R-1, 61–63 cm, and 10R-1, 35–37 cm): bulk densities are 2.88 and 2.90 g/cm^3, porosity values are 1.2% and 1.3%, resistivities are 4.1 and 5.8 Ωm, and compressional (*P*-wave) velocities are 6.09 and 6.13 km/s (Tables 6, 7).

Summary

The four holes drilled at the TAG-4 area on the western side of the Black Smoker Complex recovered sulfide types characterized by unique physical properties, as compared with sulfide-anhydrite-bearing rocks sampled from other parts of the mound. The rocks recovered from the eastern side of the mound are characterized by generally lower values of density and porosity and variable density/porosity relations (see Table 11, Chapter 7, and Table 9, Chapter 8, both in this volume). The differences in density-porosity relations observed between the rock types from the western side of the mound and those from the eastern side of the mound are attributed to textural differences. The shallow sulfide samples of the TAG-4 area exhibit mineralogies and textures that are consistent with primary deposition as porous massive sulfide crusts precipitated in situ (see "Sulfide Petrology and Geochemistry" section). These samples have a nearly constant bulk density despite a 4% range in porosity. The sulfides of the TAG-1 and TAG-2 area, as well as the rocks sampled from deeper in the mound in the TAG-4 area, exhibit predominantly clastic textures consistent with an accumulation of broken chimney material, and show somewhat more variable density-porosity relationships.

PALEOMAGNETISM

At Hole 957M in the TAG-4 area, paleomagnetic results were obtained from two minicore basalt samples taken from Sections 158-957M-9R-1 and 10R-1, respectively. We measured a number of standard magnetic properties, including the NRM intensity and direction, the initial volume magnetic susceptibility, the Koenigsberger ratio, and the anisotropy of magnetic susceptibility (AMS). The two samples were then demagnetized in progressive steps of increasing AF field, up to 80 mT to allow some inferences to be made about the

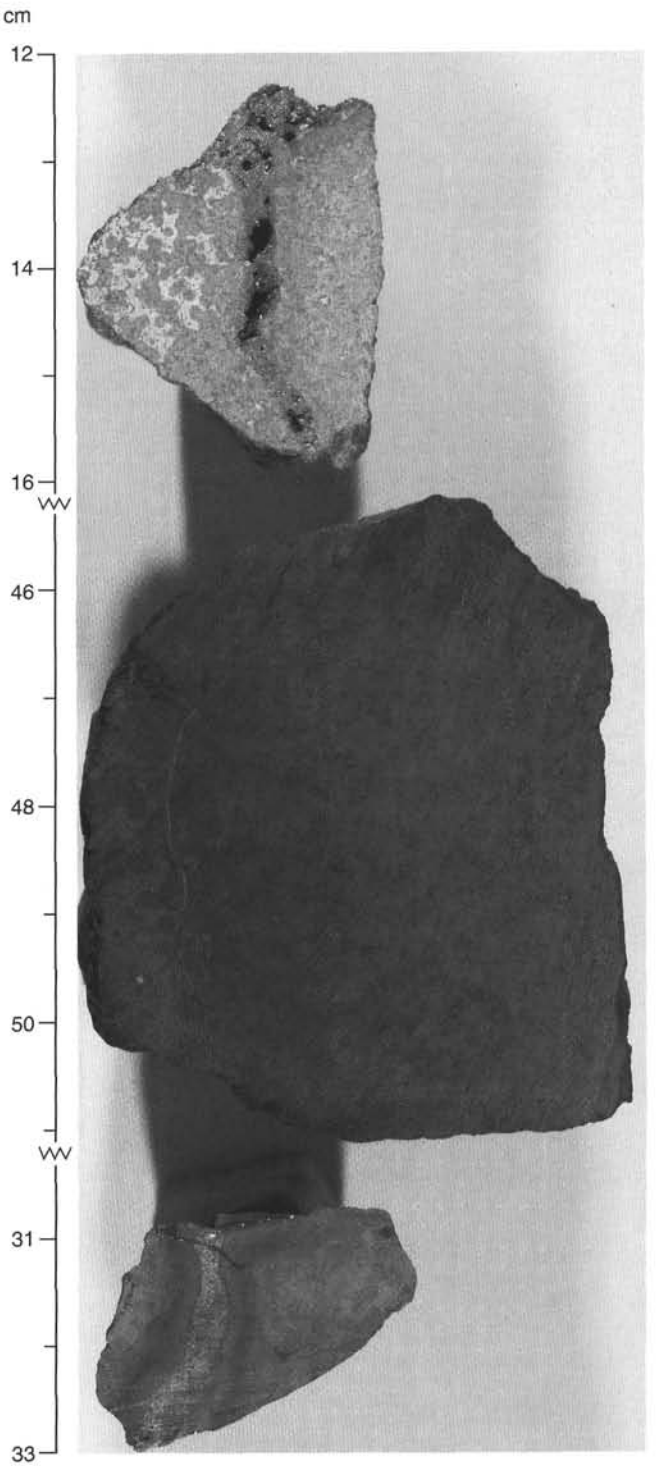

Figure 48. Various types of altered variolitic and glassy pillow rims encountered in the lowermost portion of Hole 957M. In the top sample, the round varioles are clearly visible to the left, where the crystalline varioles and basalt are replaced by chlorite and pyrite (gray), and the formerly glassy material is now replaced by a white phyllosilicate. The altered basalt in this sample is cut by a 2-mm-wide vuggy pyrite vein (Sample 158-957M-9R-1, Piece 3, 12–17 cm). The middle piece is a dark gray basalt, partly altered to smectite (see text), with round varioles (black) in an altered glassy matrix (gray) at left (Sample 158-957M-9R-1, Piece 8, 45–52 cm). The bottom sample is a totally chloritized pillow rim cut by a 2- to 3-mm-thick quartz plus pyrite vein bordered by double light-dark halos. Relict texture of round varioles (darker gray) in a chloritized glassy matrix (lighter gray) is just visible in the right half of the specimen (Sample 158-957M-10R-2, Piece 7, 30.5–33.5 cm).

Table 4. Igneous lithology log for Hole 957M.

Core, section, interval (cm)	Piece no.	Piece depth (mbsf)	Lithology	Contact	Plagioclase Min. (%)	Plagioclase Max. (%)	Average gs–ph (mm)	Average gs–gm (mm)	Phenocryst habit
158-957M-									
9R-1, 12–17	3	42.30	Silicified basalt clasts	No contact observed					
9R-1, 17–24	4	42.35	Silicified basalt blasts						
9R-1, 24–30.5	5	42.42	Sparsely phyric olivine basalt	No contact observed				0.5	
9R-1, 30.5–37	6	42.49	Sparsely phyric olivine basalt					0.5	
9R-1, 37–45	7	42.55	Sparsely phyric olivine basalt					0.5	
9R-1, 45–52	8	42.63	Sparsely phyric olivine basalt					0.5	
9R-1, 52–58	9	42.70	Sparsely phyric olivine basalt					0.5	
9R-1, 58–66	10	42.76	Sparsely phyric olivine basalt					0.5	
9R-1, 66–72	11	42.84	Sparsely phyric olivine basalt					0.5	
9R-1, 72–79	12	42.90	Sparsely phyric olivine basalt					0.5	
9R-1, 79–84	13	42.97	Sparsely phyric olivine basalt					0.5	
9R-1, 84–90	14	43.02	Sparsely phyric olivine basalt					0.5	
9R-1, 90–94.5	15	43.08	Sparsely phyric olivine basalt					0.5	
9R-1, 94.5–100	16	43.13	Sparsely phyric olivine basalt					0.5	
9R-1, 100–104	17	43.18	Sparsely phyric olivine basalt					0.5	
9R-1, 104–110	18	43.22	Sparsely phyric olivine basalt					0.5	
9R-1, 110–117	19	43.28	Sparsely phyric olivine basalt					0.5	
9R-1, 117–122	20	43.35	Sparsely phyric olivine basalt					0.5	
10R-1, 0–5	1	46.20	Sparsely phyric olivine basalt					0.5	
10R-1, 5–11	2	46.25	Sparsely phyric olivine basalt					0.5	
10R-1, 11–18	3	46.31	Sparsely phyric olivine basalt		0	2	1	0.5	Lath
10R-1, 18–23	4	46.38	Sparsely phyric olivine basalt		0	2	1	0.5	Lath
10R-1, 23–32	5	46.43	Sparsely phyric olivine basalt		0	2	1	0.5	Lath
10R-1, 32–43	6	46.52	Sparsely phyric olivine basalt		0	2	1	0.5	Lath
10R-1, 43–51	7	46.63	Sparsely phyric olivine basalt		0	2	1	0.5	Lath
10R-1, 51–60	8	46.71	Sparsely phyric olivine basalt		0	2	1	0.5	Lath
10R-1, 60–68	9	46.80	Sparsely phyric olivine basalt		0	2	1	0.5	Lath
10R-1, 68–76	10	46.88	Sparsely phyric olivine basalt		0	2	1	0.5	Lath
10R-1, 76–83	11	46.96	Sparsely phyric olivine basalt		0	2	1	0.5	Lath
10R-1, 83–95	12A	47.03	Sparsely phyric olivine basalt		0	2	1	0.5	Lath
10R-1, 83–95	12B	47.15	Sparsely phyric olivine basalt		0	2	1	0.5	Lath
10R-1, 95–106	13	47.27	Moderately phyric olivine basalt		0	2	1	0.5	Lath
10R-1, 106–112	14	47.38	Sparsely phyric olivine basalt		0	2	1	0.5	Lath
10R-1, 112–117	15	47.44	Sparsely phyric olivine basalt		0	2	1	0.5	Lath
10R-1, 117–121	16	47.49	Sparsely phyric olivine basalt		0	2	1	0.5	Lath
10R-1, 121–126	17	47.53	Silicified basalt	No contact observed					
10R-1, 126–129	18	47.58	Sparsely phyric olivine basalt	No contact observed	0	2	1	0.5	Lath
10R-1, 129–132	19	47.61	Altered pillow rim basalt	No contact observed					
10R-1, 132–140	20	47.64	Sparsely phyric olivine basalt	No contact observed	0	2	1	0.5	Lath
10R-1, 140–146	21	47.72	Sparsely phyric olivine basalt		0	2	1	0.5	Lath
10R-2, 0–10	1	47.78	Sparsely phyric olivine basalt		0	2	1	0.5	Lath
10R-2, 10–15	2	47.88	Sparsely phyric olivine basalt		0	2	1	0.5	Lath
10R-2, 15–19.5	3	47.93	Sparsely phyric olivine basalt		0	2	1	0.5	Lath
10R-2, 19.5–23.5	4	47.98	Sparsely phyric olivine basalt		0	2	1	0.5	Lath
10R-2, 23.5–27.5	5	48.02	Sparsely phyric olivine basalt		0	2	1	0.5	Lath
10R-2, 27.5–30.5	6	48.06	Sparsely phyric olivine basalt		0	2	1	0.5	Lath
10R-2, 30.5–33.5	7	48.09	Altered pillow rim basalt	No contact observed					
10R-2, 33.5–39	8	48.12	Sparsely phyric olivine basalt	No contact observed	0	2	1	0.5	Lath

magnetization stability and history of the sample (Fig. 53). Table 8 summarizes the magnetic properties of these two samples. The NRM intensities of these two samples are very strong (on the order of 10^4 mA/m), much stronger than those (about 4×10^3 mA/m) of typical dredged and drilled oceanic basalts in the Atlantic (Lowrie, 1977). The Koenigsberger ratio and the initial magnetic susceptibility of these two samples are also much higher than those of the sulfides recovered during Leg 158, which is expected as they are known to have very different magnetic mineralogy. Based on the magnetic behavior during AF demagnetization (Fig. 53), we infer that the magnetic carrier is titanomagnetite. More accurate identification of the magnetic carrier awaits shore-based thermomagnetic analyses and mineralogic study. Similar to the sulfide samples recovered from the TAG-1 and TAG-2 areas, these two basalt samples show that there is virtually no anisotropy of magnetic susceptibility (AMS) is in these samples.

As with samples recovered from elsewhere within the mound, vertically directed, drilling-induced magnetization overprints the primary magnetization of the rocks. Both samples exhibited signs of this drilling-induced magnetization, as evidenced by the almost vertical inclinations in the NRM measurements. Fortunately, AF demagnetization to 10 mT can effectively remove this relatively "soft" overprint and isolate the stable component of magnetization (Fig. 53). Although only two samples were measured, it seems reasonable to conclude that drilling has had a lesser effect on the NRM of these basalt samples as compared with that of sulfide cores from the TAG-1 area. In Sample 158-957M-9R-1, 61–63 cm, a second component of magnetization (with inclination = 41.5°) was also removed during AF demagnetization. This component has a low coercivity and probably represents a relatively recent field overprint caused by viscous processes. The demagnetization curves for both samples (Fig. 53) reveal the stable component of magnetization. The stable component for both samples has a much shallower inclination (14°) compared to the expected inclination (55°) at this site, suggesting that the basalt fragments are rubble or that the section has been rotated. More representative sampling and detailed rock magnetic measurements including thermomagnetic characterization are needed to determine the relationship of magnetic properties to the nature of the alteration regime.

Table 4 (continued).

Olivine Min. (%)	Olivine Max (%)	Average gs–ph (mm)	Average gs–gm (mm)	Phenocryst habit	Color	Groundmass	Vesicle (%)	Glass (%)	Alteration (%)
					Light gray				100
					Light gray				100
	1	2	<1	Euhderal	Dark gray with blue green rim	Microcrystalline	1	0	50
	1	2	<1	Euhderal	Dark gray with blue green rim	Microcrystalline	1	0	50
	1	<2	<1	Euhderal	Dark gray	Microcrystalline	1	0	50
	1	2	<1	Euhderal	Dark gray	Microcrystalline	1	10	50
	1	2	<1	Euhderal	Dark gray	Microcrystalline	1	0	50
	1	2	<1	Euhderal	Dark gray	Microcrystalline	1	0	50
	1	2	<1	Euhderal	Dark gray	Microcrystalline	1	0	50
	1	2	<1	Euhderal	Dark gray	Microcrystalline	1	0	50
	1	2	<1	Euhderal	Dark gray	Microcrystalline	<1	0	50
	1	2	<1	Euhderal	Dark gray	Microcrystalline	1	0	50
	1	2	<1	Euhderal	Dark gray	Microcrystalline	1	0	50
	1	2	<1	Euhderal	Dark gray with blue green rim	Microcrystalline	2	0	50
	1	2	<1	Euhderal	Dark gray	Microcrystalline	1	0	50
	1	2	<1	Euhderal	Dark gray	Microcrystalline	1	0	50
	1	2	<1	Euhderal	Dark gray	Microcrystalline	1	0	50
	1	2	<1	Euhderal	Dark gray	Microcrystalline	1	0	50
	1	2	<1	Euhedral	Dark gray	Microcrystalline	<1	0	50
	1	2	<1	Euhedral	Dark gray	Microcrystalline	<1	0	50
	1	2	<1	Euhedral	Dark gray	Microcrystalline	<1	0	50
	1	2	<1	Euhedral	Dark gray	Microcrystalline	<1	0	50
	1	2	<1	Euhedral	Dark gray	Microcrystalline	<1	0	50
	1	2	<1	Euhedral	Dark gray with red brown rim	Microcrystalline	<1	0	50
	1	2	<1	Euhedral	Dark gray with red brown rim	Microcrystalline	<1	0	50
	1	2	<1	Euhedral	Dark gray with red brown rim	Microcrystalline	<1	0	50
	1	2	<1	Euhedral	Dark gray with red brown rim	Microcrystalline	<1	0	50
	1	2	<1	Euhedral	Dark gray with red brown rim	Microcrystalline	<1	0	50
	1	2	<1	Euhedral	Dark gray with green gray rim	Microcrystalline	<1	0	50
	1	2	<1	Euhedral	Dark gray with green gray rim	Microcrystalline	<1	0	70
	1	2	<1	Euhedral	Dark gray with green gray rim	Microcrystalline	<1	0	70
	1	5	<1	Euhedral	Dark gray	Microcrystalline	<1	0	50
	1	2	<1	Euhedral	Dark gray	Microcrystalline	<1	0	50
	1	2	<1	Euhedral	Dark gray with green gray rim	Microcrystalline	<1	0	50
	1	2	<1	Euhedral	Dark gray with red brown rim	Microcrystalline	<1	0	50
					Light gray		<1	0	100
	1	2	<1	Euhedral	Dark gray with red brown rim	Microcrystalline	<1	0	60
					Red brown to green gray		<1	0	100
	1	2	<1	Euhedral	Dark gray with green gray rim	Microcrystalline	<1	0	50
	1	2	<1	Euhedral	Dark gray with green gray rim	Microcrystalline	<1	0	50
	1	2	<1	Euhedral	Dark gray with green gray rim	Microcrystalline	<1	0	50
	1	2	<1	Euhedral	Dark gray with green gray rim	Microcrystalline	<1	0	50
	1	2	<1	Euhedral	Dark gray with green gray rim	Microcrystalline	<1	0	50
	1	2	<1	Euhedral	Dark gray with green gray rim	Microcrystalline	<1	0	50
	1	2	<1	Euhedral	Dark gray with green gray rim	Microcrystalline	<1	0	50
	1	2	<1	Euhedral	Dark gray with green gray rim	Microcrystalline	<1	0	50
					Light green		<1	0	100
	1	2	<1	Euhedral	Dark gray	Microcrystalline	<1	0	50

REFERENCES

Basaltic Volcanism Study Project, 1981. *Basaltic Volcanism on the Terrestrial Planets:* New York (Pergamon Press).

Lowrie, W., 1977. Intensity and direction of magnetisation in oceanic basalts. *J. Geol. Soc. London,* 133:61–82.

Tivey, M.K., Humphris, S.E., Thompson, G., Hannington, M.D., and Rona, P.A., 1995. Deducing patterns of fluid flow and mixing within the TAG active hydrothermal mound using mineralogical and geochemical data. *J. Geophys. Res.,* 100:12527–12555.

Ms 158IR-110

NOTE: For all sites drilled, core-description forms ("barrel sheets") and core photographs can be found in Section 3, beginning on page 227. Thin-section data are given in Section 4, beginning on page 345.

Table 4 (continued).

Core, section, interval (cm)	Piece no.	Comments
158-957M-		
9R-1, 12–17	3	
9R-1, 17–24	4	
9R-1, 24–30.5	5	Plagioclase microlites appear fresh; olivine replaced by chlorite and Fe oxyhydroxides
9R-1, 30.5–37	6	Olivine replaced by Fe oxyhydroxides, pyrite, and white mineral; vesicles filled with smectite and chlorite
9R-1, 37–45	7	Olivine replaced by chlorite and surrounded by disseminated pyrite; vesicles filled by chlorite and white clay mineral
9R-1, 45–52	8	Partial variolitic dark gray rim (0.5–3 mm diameter) in a light gray alteration matrix; olivine replaced by chlorite
9R-1, 52–58	9	Olivine replaced by and vesicles filled with chlorite; one vesicle filled with pyrite (0.5 mm diameter)
9R-1, 58–66	10	Olivine replaced by Fe oxyhydroxides
9R-1, 66–72	11	Vesicles filled with chlorite
9R-1, 72–79	12	Olivine replaced by Fe oxyhydroxides; vesicles filled with light green mineral
9R-1, 79–84	13	Olivine replaced by and vesicles filled with light green clay mineral
9R-1, 84–90	14	Olivine replaced by and vesicles filled with light green clay mineral
9R-1, 90–94.5	15	Olivine replaced by and vesicles filled with light green clay mineral
9R-1, 94.5–100	16	Olivine replaced by Fe oxyhydroxides; vesicles filled with light green mineral
9R-1, 100–104	17	Olivine replaced by and vesicles filled with light green clay mineral
9R-1, 104–110	18	Olivine replaced by and vesicles filled with light green clay mineral
9R-1, 110–117	19	Olivine replaced by and vesicles filled with light green clay mineral
9R-1, 117–122	20	Olivine replaced by and vesicles filled with light green clay mineral
10R-1, 0–5	1	Plagioclase appears fresh; olivine replaced by chlorite in sample interiors; vesicles filled by light green mineral
10R-1, 5–11	2	Plagioclase appears fresh; olivine replaced by chlorite in sample interiors; vesicles filled by light green mineral
10R-1, 11–18	3	Plagioclase appears fresh; olivine replaced by chlorite in sample interiors; vesicles filled by light green mineral
10R-1, 18–23	4	Plagioclase appears fresh; olivine replaced by chlorite in sample interiors; vesicles filled by light green mineral
10R-1, 23–32	5	Plagioclase appears fresh; olivine replaced by chlorite in sample interiors; vesicles filled by light green mineral
10R-1, 32–43	6	Plagioclase appears fresh; olivine replaced by chlorite in sample interiors; vesicles filled by light green mineral
10R-1, 43–51	7	Plagioclase appears fresh; olivine replaced by chlorite in sample interiors; vesicles filled by light green mineral
10R-1, 51–60	8	Plagioclase appears fresh; olivine replaced by chlorite in sample interiors; vesicles filled by light green mineral
10R-1, 60–68	9	Subvariolitic texture with varioles present along the edges
10R-1, 68–76	10	Subvariolitic to variolitic texture
10R-1, 76–83	11	Olivine replaced by chlorite in sample interiors and Fe oxyhydroxides; vesicles filled by light green mineral
10R-1, 83–95	12A	Subvariolitic texture; plagioclase appears fresh; olivine replaced by chlorite; vesicles filled by light green mineral
10R-1, 83–95	12B	Subvariolitic texture; plagioclase appears fresh; olivine replaced by chlorite; vesicles filled by light green mineral
10R-1, 95–106	13	Plagioclase appears fresh; olivine replaced by chlorite in sample interiors; vesicles filled by light green mineral
10R-1, 106–112	14	Plagioclase appears fresh; olivine replaced by chlorite in sample interiors; vesicles filled by light green mineral
10R-1, 112–117	15	Plagioclase appears fresh; olivine replaced by chlorite and Fe oxyhydroxides; vesicles filled by light green mineral
10R-1, 117–121	16	Variolitic texture; plagioclase appears fresh; olivine replaced by chlorite in sample interiors
10R-1, 121–126	17	
10R-1, 126–129	18	Subvariolitic texture; plagioclase appears fresh; olivine replaced by chlorite; vesicles filled by light green mineral
10R-1, 129–132	19	Variolitic basalt with glassy rim that has been altered to chlorite; varioles are replaced by Fe oxyhydroxides
10R-1, 132–140	20	Plagioclase appears fresh; olivine replaced by chlorite in sample interiors; vesicles filled by light green mineral
10R-1, 140–146	21	Subvariolitic texture; plagioclase appears fresh; olivine replaced by chlorite; vesicles filled by light green mineral
10R-2, 0–10	1	Plagioclase appears fresh; olivine replaced by chlorite in sample interiors; vesicles filled by light green mineral
10R-2, 10–15	2	Plagioclase appears fresh; olivine replaced by chlorite in sample interiors; vesicles filled by light green mineral
10R-2, 15–19.5	3	Plagioclase appears fresh; olivine replaced by chlorite in sample interiors; vesicles filled by light green mineral
10R-2, 19.5–23.5	4	Plagioclase appears fresh; olivine replaced by chlorite in sample interiors; vesicles filled by light green mineral
10R-2, 23.5–27.5	5	Plagioclase appears fresh; olivine replaced by chlorite in sample interiors; vesicles filled by light green mineral
10R-2, 27.5–30.5	6	Plagioclase appears fresh; olivine replaced by chlorite in sample interiors; vesicles filled by light green mineral
10R-2, 30.5–33.5	7	Subvariolitic texture
10R-2, 33.5–39	8	Plagioclase appears fresh; olivine replaced by chlorite in sample interiors; vesicles filled by light green mineral

Table 5. Whole-rock XRF basalt chemistry of Sample 158-957M-10R-1 (Piece 6).

	Average	1 SD		Average
Major elements (wt%):			Trace elements (ppm):	
SiO_2	50.47	0.16	V	272
TiO_2	1.67	0.02	Cr	335
Al_2O_3	14.96	0.07	Ni	167
Fe_2O_3	11.15	0.15	Cu	70
MnO	0.19	0.00	Zn	85
MgO	8.72	0.02	Rb	2
CaO	10.85	0.04	Sr	123
Na_2O	2.41	0.04	Y	36
K_2O	0.16	0.01	Zr	109
P_2O_5	0.15	0.00	Nb	1
			Ba	18
Total	100.70		Ce	10
LOI	0.88			
FeO**	10.03			
Mg#	60.77	0.38		
FeO/MgO	1.15	0.02		
CaO/Al_2O_3	0.72	0.00		

Notes: Major element composition represents average of two replicate analyses. FeO** = total iron as FeO. Mg# = 100 × (Mg/[Mg+ΣFe]). SD = standard deviation, and LOI = loss on ignition.

Table 4 (continued).

Additional alteration comments
Silicified variolitic rim; pyrite on outside of clasts and lining vug
Silicified (chloritized?) basalt clasts; pyrite coating on clasts and lining vugs
Rim alteration (1 cm wide) of concentric halos of light to dark green/gray with disseminated pyrite; microfracture filled with chlorite and white clay mineral
Thin veins filled with chlorite, pyrite, or Fe oxyhydroxides; concentric alteration halo (1 cm wide) of outer green and gray zones with disseminated pyrite to red inner zone
No alteration halo present
No alteration halo present; vesicles and vein (borders variolitic rim) filled with chlorite and yellow green mineral; the vein is 1 cm from edge
No alteration halo present
Outer light gray halo (5 mm wide) and inner dark gray halo (5 mm wide) are present
Outer light gray halo and inner dark gray halo (5 mm wide) are present
No outer halo; 1 mm thick vein with 1.5 mm thick chlorite halo; vein has pyrite, chlorite, and white clay mineral present
No halo present
No halo present
No halo present
Outer light gray halo, dark gray halo, and inner red brown halo are present and ~5 mm wide; disseminated pyrite in the outer light gray zone
No halo present
Dark green gray outer halo of chlorite and disseminated pyrite
Outer Fe oxyhydroxide halo (<1 mm wide), green gray halo (1–2 mm wide), and inner red brown halo are present
No halo present
No halo present
No halo present
No halo present
No halo present
No halo present
Red alteration halo (2 mm wide) is present in which olivines and matrix are replaced by Fe oxyhydroxides
Red alteration halo (2 mm wide) is present in which olivines and matrix are replaced by Fe oxyhydroxides
Red alteration halo (2 mm wide) is present in which olivines and matrix are replaced by Fe oxyhydroxides
Red to yellow alteration rim is present in which olivines and matrix are replaced by Fe oxyhydroxides
Red brown alteration rim is present in which olivines and matrix are replaced by Fe oxyhydroxides
Light green gray alteration halo (2 mm wide) of chlorite with disseminated pyrite; pyrite is oxidized
Green alteration halo consists of chlorite with disseminated pyrite
Outer red halo (<1 mm wide) and inner dark green halo (1 mm wide) are present. Inner halo consists of chlorite with disseminated pyrite
No halo present
No halo present
Outer green halo (5 mm wide) with disseminated pyrite and inner dark green halo (2–3 mm wide) of chlorite are present
2 large vesicles (2 and 3 mm in diameter) filled with white clay mineral; red Fe oxyhydroxide halo present
Silicified basalt with disseminated pyrite and a chlorite clast
Red Fe oxyhydroxide halo (1 mm thick) has replaced all olivines and matrix
Outer green halo with pyrite and inner dark green halo are present; olivine replaced by Fe oxyhydroxides near inner halo; chlorite vein (<1 mm thick) cuts across sample
Alteration halo up to 5 mm thick; olivines replaced by Fe oxyhydroxides near halo; varioles are oxidized; fracture (< .5 mm wide) filled with pyrite
Green halo of chlorite with disseminated pyrite is present; fracture filled with chlorite and pyrite; olivine replaced by Fe oxyhydroxides near halo
Outer light green halo of chlorite and disseminated pyrite and inner dark green halo are present
Outer green halo (5 mm wide), light gray halo (1–2 mm wide), red halo (1 mm wide), and green halo (1 mm wide) are present. Green halos consist of chlorite with disseminated pyrite
Light gray halo (3–4 mm wide) consists of chlorite (without pyrite); olivine is replaced by Fe oxyhydroxides near halo
Alternating green and brown halos (total of 1 cm wide) and inner red halo are present
Alternating green and brown halos (total of 1 cm wide) and inner red halo are present; olivine is replaced by Fe oxyhydroxides near halo
Disseminated pyrite is present; vein is 1–3 mm wide and filled with pyrite, quartz and chlorite; vein has green, light gray, dark gray halos (3 cm wide) present
No halo present

Table 6. Index properties of samples recovered from Holes 957I, 957J, 957K, and 957M.

Core, section, interval (cm)	Depth (mbsf)	Bulk water content (%)	Bulk density [B] (g/cm^3)	Bulk density [C] (g/cm^3)	Grain density [B] (g/cm^3)	Grain density [C] (g/cm^3)	Porosity [B] (%)	Porosity [C] (%)	Rock type (F = fragment, M = minicore)
158-957I-									
1N-1, 33–35	9.33	2.19	4.80	4.43	5.23	4.79	10.28	9.48	Porous massive pyrite (F)
158-957J-									
1X-1, 1–3	0.01	3.72	2.68	2.48	2.86	2.63	9.75	9.02	Red and gray chert (F)
158-957K-									
1X-1, 14–16	0.14	1.90	4.76	4.44	5.12	4.75	8.81	8.22	Porous massive pyrite (F)
2N-1, 37–39	10.37	1.96	4.84	4.50	5.23	4.83	9.24	8.60	Porous massive pyrite (F)
3X-1, 8–10	14.58	2.72	4.86	4.34	5.43	4.77	12.90	11.53	Porous massive pyrite (F)
158-957M-									
2R-1, 40–42	9.70	1.76	3.61	3.51	3.78	3.67	6.22	6.04	Pyrite-silica breccia (F)
3R-1, 57–59	14.87	2.13	4.70	4.38	5.10	4.72	9.75	9.09	Pyrite-silica breccia (F)
4R-1, 31–33	19.61	1.59	4.53	4.29	4.79	4.52	7.03	6.66	Pyrite-silica breccia (F)
5R-1, 104–106	25.34	0.85	3.55	3.46	3.62	3.54	2.93	2.86	Pyrite-silica breccia (F)
6R-1, 10–12	29.40	1.07	3.64	3.51	3.75	3.61	3.82	3.68	Silicified wallrock breccia (F)
7R-1, 19–21	34.49	1.77	4.38	4.24	4.65	4.50	7.55	7.32	Silicified wallrock breccia (F)
8R-1, 38–40	38.68	1.43	4.39	4.65	4.61	4.90	6.11	6.47	Silicified wallrock breccia (F)
9R-1, 61–63	42.91	0.42	2.91	2.88	2.94	2.90	1.18	1.17	Altered basalt (M)
10R-1, 35–37	46.55	0.45	2.93	2.90	2.96	2.92	1.29	1.28	Altered basalt (M)

Note: [B] and [C] refer to the method used to calculate bulk and grain density (see "Index Properties" section, "Explanatory Notes" chapter, this volume).

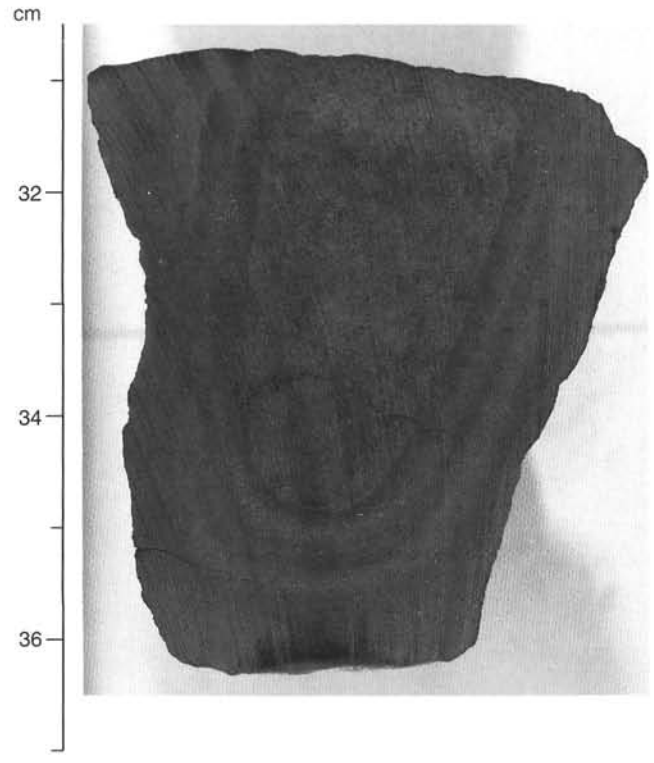

Figure 49. Sample 158-957M-9R-1 (Piece 6, 30.5–37 cm) exhibits a complex, concentric alteration halo (~1 cm wide) of chloritized basalt and a less altered interior of sparsely olivine phyric basalt.

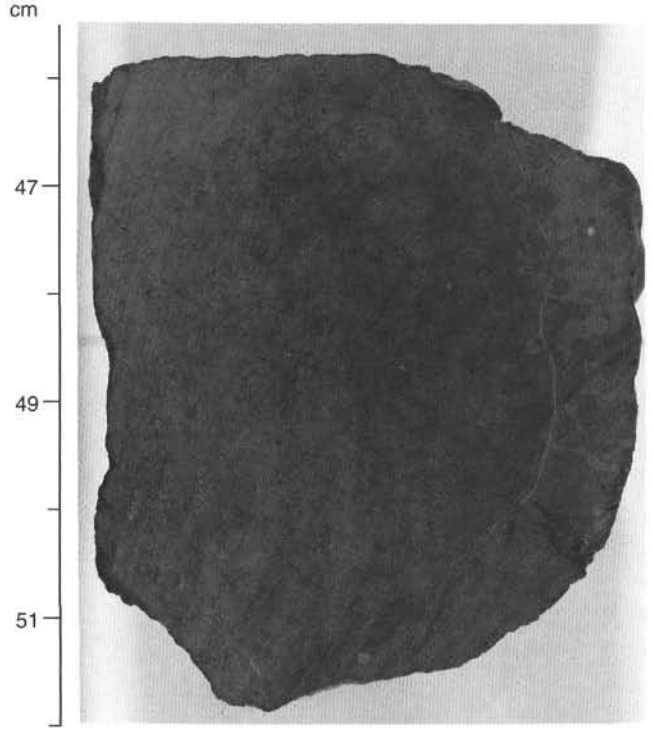

Figure 50. Working half of Sample 158-957M-9R-1 (Piece 8, 45.5–52 cm). This sample exhibits a well-developed variolitic texture along one side (top).

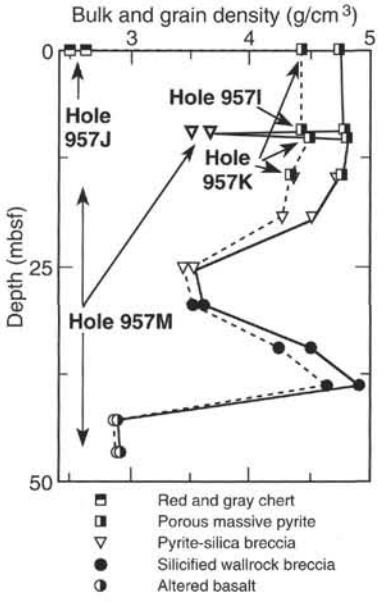

Figure 51. Bulk (dashed line) and grain (solid line) density values of samples identified by rock type vs. depth, Holes 957I, 957J, 957K, and 957M.

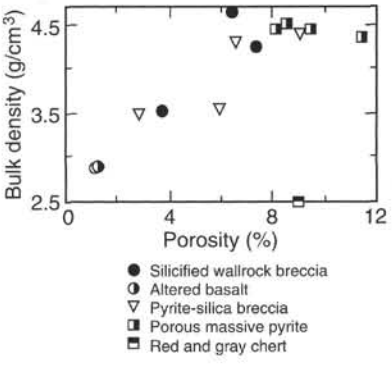

Figure 52. Bulk density vs. porosity for samples identified by rock type, Holes 957I, 957J, 957K, and 957M. Symbols same as in Figure 51.

Table 7. Electrical resistance, *P*-wave velocity, and related properties measured in minicores recovered from Holes 957I, 957J, 957K, and 957M.

Core, section, interval (cm)	Depth (mbsf)	Length (mm)	Diameter (mm)	Resistance (Ω)	Resistivity (Ωm)	Formation factor	*P*-wave velocity (km/s)	Rock type
158-957M-								
9R-1, 61–63	42.91	25.27	25.26	208	4.125	20.625	6.085	Altered basalt
10R-1, 35–37	46.55	21.63	25.25	250	5.788	28.938	6.132	Altered basalt

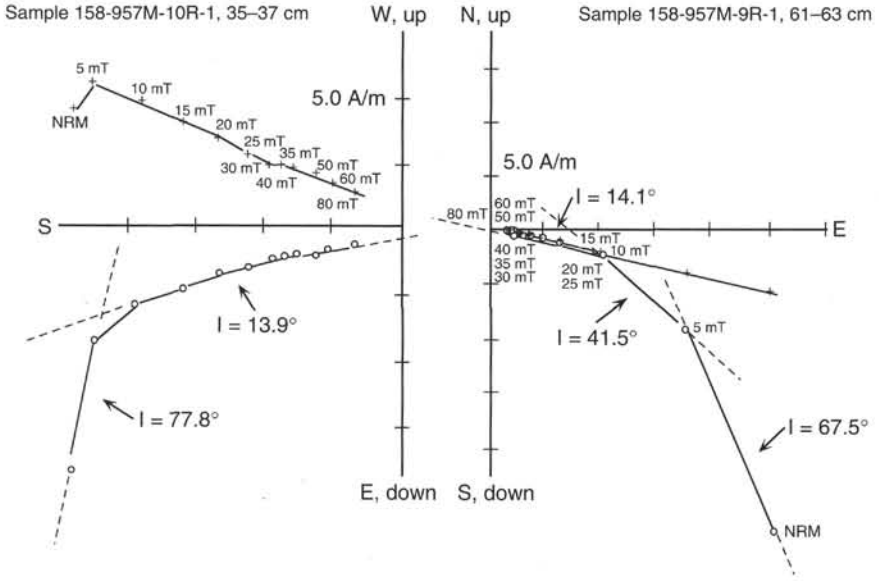

Figure 53. Vector endpoint diagram showing the results of alternating-field demagnetization for discrete samples from Cores 158-957M-9R and 10R. The magnetic component is shown by a straight dashed line fitting the data points, and the corresponding inclination (I) is indicated. Open circles and crosses represent vector endpoints projected onto the vertical and horizontal planes, respectively.

Table 8. Magnetic properties of minicore samples from Hole 957M.

Core, section, interval (cm)	Depth (mbsf)	NRM intensity (10^4 mA/m)	Declination (degrees)	Inclination (degrees)	K (10^{-6} SI)	Q ratio	$P = K_1/K_3$
158-957M-							
9R-1, 61–63	42.91	3.82	103.9	14.1	24940	45.92	1.012
10R-1, 35–37	46.55	1.59	204.2	13.9	18030	26.37	1.052

Notes: Inclination = stable inclination after demagnetization; K = magnetic susceptibility in 10^{-6} SI units; Q ratio = Koenigsberger ratio; P = anisotropy factor; K_1 and K_3 = maximum and minimum principal axes of suceptibility.